EXTRATROPICAL FORCING OF TROPICAL ATLANTIC VARIABILITY

by

Dimitry Smirnov

A dissertation submitted in partial fulfillment of

the requirements for the degree of

Doctor of Philosophy

(Atmospheric Science)

at the

UNIVERSITY OF WISCONSIN-MADISON

2011

ProQuest LLC
789 East Eisenhower Parkway
P.O. Box 1346
Ann Arbor, MI 48106-1346

EXTRATROPICAL FORCING OF TROPICAL ATLANTIC VARIABILITY

submitted to the Graduate School of the
University of Wisconsin-Madison
in partial fulfillment of the requirements for the
degree of Doctor of Philosophy

By

DIMITRY SMIRNOV

Date of final oral examination: October 3, 2011

Month and year degree to be awarded: December 2011

The dissertation is approved by the following members of the Final Oral Committee:

Daniel J. Vimont, Associate Professor, Department of Atmospheric Science
Zhengyu Liu, Professor, Department of Atmospheric Science
Matthew Hitchman, Professor, Department of Atmospheric Science
Ankur Desai, Associate Professor, Department of Atmospheric Science
James P. Kossin, Atmospheric Scientist, NOAA

ABSTRACT

The dominant mode of coupled ocean-atmosphere variability in the Tropical Atlantic, the Atlantic Meridional Mode (AMM), responds strongly to seasonally dependent remote forcing. Previous studies have focused on AMM during boreal spring, when it is readily excited by ENSO and the NAO forcing. However, relatively little is known about AMM variability during boreal fall, when it strongly regulates Atlantic hurricane activity and thus commands important societal impacts. A recent finding using a linear inverse model (LIM) of near-global SST anomalies suggests that the boreal fall AMM is forced by extratropical Atlantic SST anomalies and shows remarkable predictability with lead times approaching one year.

To investigate the validity and mechanism of the LIM, a set of ensemble simulations are designed using an AGCM coupled to a slab-ocean. By initializing the GCM with LIM-derived SST anomalies, the main result of this research is the confirmation of the LIM result using an alternate physical framework. Excitation of the AMM is found to involve at least two processes: one is the thermodynamic, wind-evaporation-SST (WES) feedback, and the other is a low-cloud/SST feedback. The WES feedback is found to amplify the AMM-like response by a factor of three compared to when it is absent. However, SST anomalies are still found in the tropics when the WES feedback is suppressed. Meanwhile, the low-cloud-SST feedback is found to be locally important in the north tropical Atlantic stratocumulus region during boreal summer, but is unlikely to affect the large-scale AMM-like response. Additionally, we find that the GCM response depends strongly on the season of forcing (consistent with the LIM and some past studies), and also exhibits modest non-linearity initially, but progresses towards a more linear response later in the simulation. Another notable conclusion is that oceanic dynamics are not needed to explain the LIM result, as can be partly expected from

the relatively short, interseasonal time-scales that are considered. This manuscript focuses on a mechanistic diagnosis of the GCM result, highlighting relevance to previous, similar studies, as well as offering several avenues for future research.

ACKNOWLEDGEMENTS

I would like to thank my advisor, Daniel Vimont, for giving me as much leeway as a student could want, but also, always pointing me in the right direction when the research got tough. I would also like to thank my committee members, Professors Zhengyu Liu, Matt Hitchman and Ankur Desai and Dr. Jim Kossin.

Thanks to the members of the Precious Roy Fiasco for forgetting science for a bit to enjoy music. Thanks to die-hard storm chasers Croix Christenson and Daniel Henz for the hours of time spent being passionate weather nerds. Finally, thanks to Katie and my family in supporting me to see this through.

ACRONYMS & ABBREVIATIONS

AMM	Atlantic Meridional Mode
AMO	Atlantic Multidecadal Oscillation
CAM	NCAR's Community Atmosphere Model, Version 3.1, part of CCSM
CCSM	NCAR's Community Climate System Model, Version 3
DOM	Data-ocean model (prescribed SST)
ENSO	El-Nino Southern Oscillation
EOF	Empirical Orthogonal Function
GCM	Global Climate Model
ITCZ	Inter-tropical Convergence Zone
LIM	Linear inverse model
MCA	Maximum Covariance Analysis
MDR	Main Development Region [for Atlantic tropical cyclone formation]
NAO	North Atlantic Oscillation
OPT	"Optimal" SST anomaly structure (see Fig. 2.1)
SLP	Sea-level Pressure
SOM	Slab-ocean model
SST	Sea surface Temperature
SVD	Singular Value Decomposition

TABLE OF CONTENTS

LIST OF FIGURES

LIST OF TABLES

1 INTRODUCTION

This chapter summarizes key findings in past literature regarding air-sea interaction in the Atlantic basin. Due to the different mechanisms involved, section 1.1.1 discusses the tropical Atlantic, while section 1.1.2 describes the extratropical Atlantic. For reference, "extratropical" denotes regions poleward of roughly 30°. In Section 1.2, literature discussing the extratropical-tropical connection is reviewed, with an emphasis on the role played by the former in forcing the latter. Finally, section 1.3 highlights outstanding questions regarding extratropical-tropical interaction and introduces the motivation for this research.

1.1 Climatology

1.1.1 Tropical Atlantic

The main feature in the climate of the tropical Atlantic basin is the meridional movement of the inter-tropical convergence zone (ITCZ) that slightly lags the seasonal cycle of solar insolation (Mitchell and Wallace, 1992). In addition to the seasonal cycle, there exist two dominant forms of coupled ocean-atmosphere variability in the tropical Atlantic basin (see Xie and Carton (2004) for a review). The most dominant form, the Atlantic Meridional Mode (hereafter, AMM from Chiang and Vimont (2004); hereafter, CV04) is a thermodynamically coupled process that involves the interaction of low-level winds, sea-level pressure (hereafter, SLP) and SST. The spatial structure of the AMM is shown in Fig. 1.1 by regressing SST, SLP and low-level wind anomalies (obtained from NCEP-NCAR Reanalysis over the period 1950-2008, Kalnay and co authors (1996)) onto the normalized AMM index (here I use the SST time series from CV04). Also shown is the time series from 1950 onwards. From here on, we refer to this as the "positive" phase of the AMM, or simply the AMM, with the negative

phase being of opposite polarity. The secondary mode, the Atlantic Nino, dominates SST variance during boreal summer when the thermocline shoals in the Gulf of Guinea (Merle, 1980). For this reason, the Atlantic Nino is characterized by a dynamical ocean-atmosphere interaction very similar to, albeit much weaker than El Nino-Southern Oscillation (ENSO; Zebiak (1993); Carton and Huang (1994)). The spatial pattern of the Atlantic Nino is a monopole region of SST anomalies in the equatorial Tropical Atlantic and Gulf of Guinea (not shown). The AMM has been associated with many societal impacts including the Nordeste and Sahel rainfall variability (Namias (1972); Hastenrath (1976)), and more recently, anomalies in the Atlantic hurricane activity (Kossin and Vimont (2007); hereafter, KV07).

The AMM has been discussed in scientific literature since the 1970's and a brief history is appropriate here. Namias (1972) and Hastenrath and Heller (1977) were intrigued by recurring periods of drought in northeast Brazil, and related rainfall anomalies in the "Nordeste" (an agriculturally intensive region of northeast Brazil) to larger-scale atmospheric circulation anomalies. There was large spatial coherence in the anomalous atmospheric fields when times of drought and deluge were observed. Both the aforementioned studies found that a slackening (intensification) of the persistent easterly trade winds, or concomitantly a weakening (strengthening) of the subtropical anticyclone circulation, resulted in decreased (increased) rainfall during the Nordeste's rainy season, which is boreal spring. Positive SST anomalies in the northern Tropical Atlantic correspond to a (+) AMM, shown in Fig. 1.1 and vice versa. Due to the long, oceanic fetch that modulates Nordeste rainfall, Hastenrath (1978) suggested concurrent patterns of atmospheric (e.g. SLP) and SST anomalies indicative a coupled air-sea process.

Hastenrath and Heller (1977) observed that when the Nordeste experiences drought, the entire Atlantic Inter-tropical Convergence Zone (ITCZ) is displaced anomalously

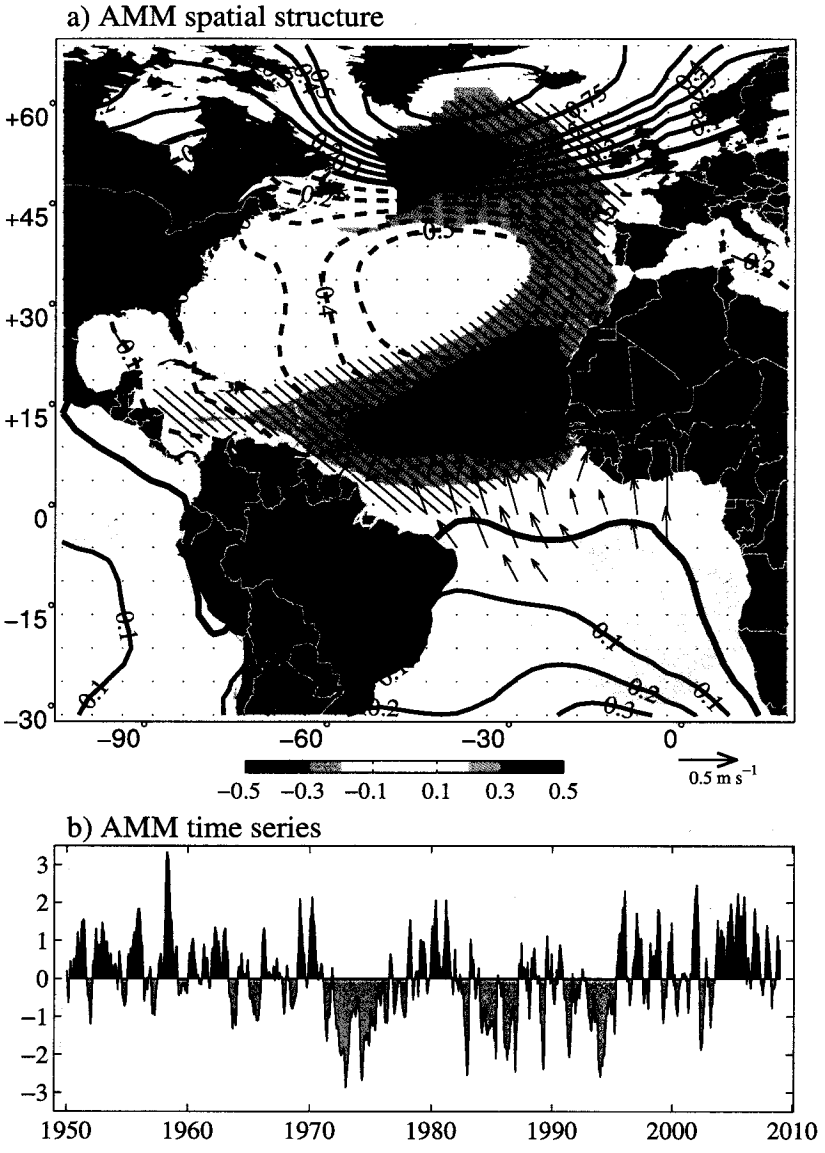

Figure 1.1: a) Regressions of SST (shaded), SLP (contoured) and low-level horizontal wind (vectors) onto the AMM index of CV04 using monthly data. The hatching denotes regions of SST anomalies that exceed the 98% confidence level. Wind vectors are shown only if significant at the 95% level. All values represent anomalies per one standard deviation of the AMM index. b) Normalized AMM time series from the SST component of the MCA.

northward in association with a decrease (increase) of SLP to the north (south) of the equator. This suggests that the AMM is not merely a boundary-layer process but linked to the Atlantic portion of the Hadley cell through its connection with the ITCZ. Substantial evidence of this has been shown both in observations and in modeling studies of the AMM (Moura and Shukla (1981); Smirnov and Vimont (2011)). Since the 1970's, the AMM has had several names including the "dipole mode" due to a seemingly concurrent dipole of SST anomalies north and south of the ITCZ (Moura and Shukla (1981); Servain (1991); Rajagopalan et al. (1998)) and the interhemispheric mode due to the anomalous meridional position of the ITCZ (Ruiz-Barradas et al. (2000)). Due to the rich history of literature that exists on the AMM, scientists have also defined the mode using several different techniques ranging from an index of Nordeste rainfall anomalies (Hastenrath and Heller (1977)) to a four-variable maximum covariance analysis (hereafter, MCA) of SST, oceanic heat content, wind stress and diabatic heating anomalies (Ruiz-Barradas et al. (2000)). For the purpose of this work, the AMM is defined by singular value decomposition (SVD) of the covariance matrix of SST and horizontal wind (both U and V components) anomalies over the Atlantic basin, from 30°S to 30°N, as in CV04. It is notable that use of the term "dipole mode" has been controversial because it is not entirely evident that SST anomalies to the north and south of the ITCZ vary in an anti-correlated fashion. As first discussed by Houghton and Tourre (1992) and later by Enfield et al. (1999), it appears that the SST anomalies associated with the AMM may or may not feature a dipole, which makes the "dipole mode" term inappropriate. Indeed, Fig. 1.1 shows a very weak signal in the tropical south Atlantic.

Figure 1.1 provides several important observations that are a central theme to the research herein. First, note that the structure of significant SST anomalies (denoted by hatching) is not just limited to the tropical Atlantic, even though the AMM

index is based on data limited to 30°N. This raises the issue of whether there is extratropical-tropical interaction to lead to such a pattern, or is this coincidental. The structure of SLP anomalies extends well into the extratropical regions and strongly resembles a (-) NAO. Because causality cannot be deduced on the basis of a simultaneous regression, we can only conclude that the (-) NAO coincides with the (+) AMM. Second, from Fig. 1.1, it is seen that the positive SST anomalies north of the equator coexist with anomalously weak easterly trade winds. Because weaker winds result in a decrease in the latent heat flux, which is the dominant forcing term of the surface energy budget (Cayan (1992)), one may conclude that the anomalies in wind speed force the SST anomalies. Another possibility is the existence of a wind-evaporation-SST (WES) feedback (Liu and Xie (1994); Xie and Philander (1994)) that can maintain SST and wind anomalies *once one or the other is already present.* For example, coupled GCM simulations initialized with AMM-like tropical SST anomalies can re-create the anomalous atmospheric circulation seen in the subtropical portion of Fig. 1.1 (Smirnov and Vimont (2011)). However, this does not answer how the SST anomalies initially appeared; thus, once again, the causality is not intuitive and needs further exploration.

Although it is thought that the AMM requires external forcing for its existence, many studies have shown that the mode is destabilized (or at least made less stable) through the WES feedback that can maintain elevated SSTs after external forcing has subsided (Liu and Xie (1994); Chang et al. (1997); Xie (1999); Vimont (2010)). The WES feedback seems to be confined to the tropics (Chang et al. (2000)) and occurs when SST anomalies force an atmospheric response that reinforces the original SST anomalies through wind-induced latent heat flux (hereafter, F_{LH}) changes. Liu and Xie (1994) show that the WES feedback induces an equatorward and westward propagation of coupled disturbances in the tropics, which can be described as a transient response to an anomalous vorticity source in a linearized β-plane vorticity budget (Hoskins and

Karoly (1981); Vimont (2010)). In theory, a thermodynamic mode like the AMM can exist in an atmosphere coupled to a static ocean. However, Servain et al. (1999) showed significant coherence between the time series of the meridional Atlantic ITCZ position (a proxy for the AMM) and the thermocline slope along the equator (a proxy for the Atlantic Nino), suggesting oceanic processes may be significant. Two other key issues that remain to be resolved are: i) the northern extent of the WES feedback phenomenon and ii) the importance (relative to remote effects) of the WES feedback in sustaining and propagating SST anomalies into the deep tropics.

1.1.2 Extratropical Atlantic

In the mid-latitudes, most SST variability, from timescales of several days to months, is forced by the atmosphere through surface latent and sensible heat fluxes (Frankignoul and Hasselmann (1977); Frankignoul (1985); Cayan (1992); Deser and Blackmon (1993)). The extratropical atmospheric forcing "engine" can be described by SLP or surface heat flux anomalies around a mean state, which represents the collective activity of internal processes that arise from baroclinic and barotropic instabilities of the fluid atmosphere (Smagorinsky (1953); Hoskins and Karoly (1981)). Implicit in the term "internal process" is the notion that the underlying SST does not influence the atmospheric processes due to the large heat capacity that limits SST variability during high-frequency forcing. In fact, this discrepancy in the atmospheric forcing / oceanic response time scales was the basis of the simple, yet encompassing early model of mid-latitude SST variability that includes two components: a random, white-noise forcing and a Newtonian-like damping (Frankignoul and Hasselmann (1977); hereafter FH77), as shown below:

$$\frac{dT'}{dt} = N - \lambda T' \tag{1}$$

where T' is the SST anomaly and N is the atmospheric forcing and λ is a damping time-scale, which can take on units of time^{-1}. N is the effect on SST by atmospheric forcing, which is dominated by the turbulent, and largely unpredictable, heat flux components (Alexander (1992b); Cayan (1992)).

Several additional findings have built on the foundation established by the FH77 paradigm. An important assumption for eqn. 1 is that N can be described by a random, "white-noise" process. Taking the Fourier transform of eqn. 1, followed by multiplying each Fourier harmonic by its complex conjugate, yields the relation $\tilde{T}'^2 = \tilde{N}^2(\omega^2 + \lambda^2)^{-1}$, where the tilde indicates the amplitude of each Fourier series and the ω is the frequency. Given $\tilde{N} \neq \tilde{N}(\omega)$, $\tilde{T}'$ is expected to increase for a decrease in ω, producing a "red-noise" power spectrum (Frankignoul (1985); Alexander and Penland (1996), Alexander (2010)). However, it has been shown that the leading mode of atmospheric variability in the Atlantic sector, the NAO, which can be used as a proxy of N in eqn. 1, has significant low-frequency variations (Hurrell (1995)) suggesting an active response in slowly-varying media such as SST, sea-ice (Battisti et al. (1995); Sutton and Allen (1997); Rodwell et al. (1999); Hurrell et al. (2006)) and soil moisture anomalies (Bhatt et al. (2003)).

The paradigm of FH77 is useful when considering observational data, and eqn. 1 can be related to a simplified mixed-layer ocean heat budget with atmospheric forcing (Alexander (1992a); Alexander et al. (2000)), as such:

$$\rho_w C_w H \frac{dT}{dt} = F_{NET} + Q \tag{2}$$

where ρ_w is the ocean water density (1026 kg m^{-3}), C_w is the heat capacity of ocean water (3930 J kg^{-1} K^{-1}), H is the mixed-layer depth and T is the mixed layer temperature. Thus, the left hand side represents the time tendency of the oceanic heat

content. F_{NET} can be decomposed as:

$$F_{NET} = F_{SW} - F_{LW} - F_{LH} - F_{SH} \tag{3}$$

where the terms on the right-hand side represent the net shortwave, longwave, sensible and latent heat fluxes at the surface, respectively. Hereafter, positive surface fluxes imply a transfer of heat from the ocean to the atmosphere. In eqn. 3, Q represents the contribution of all oceanic processes including Ekman advection and pumping, mean advection by currents and entrainment below the mixed layer (Frankignoul (1985)). The similarities between eqn. 2 and eqn. 1 make it convenient to model air-sea interaction as the oceanic mixed-layer forced by stochastic atmospheric forcing, characterized by F_{NET}. However, the role of the damping (or feedback) term, λ, in eqn. 1 is not intuitive and several approaches have been hypothesized, as discussed next.

Barsugli and Battisti (1998) separated the λ term into two components: a portion that is coupled to the ocean and a portion that is purely stochastic. The main finding was that, in a coupled system, the SST responds to atmospheric forcing by decreasing F_{NET}, thus reddening the low-frequency portion of the SST spectrum. In turn, this constrains the amount of atmospheric variability that can be reproduced in an uncoupled (prescribed SST) simulation. This idea was also expanded on by Bretherton and Battisti (2000), who concluded that even when incorporating the atmospheric response to SST anomalies, the amount of NAO variance explained by SST anomalies is only 15%, which is certainly of questionable use in forecasting applications. Furthermore, Bretherton and Battisti (2000) proposed two important caveats with using prescribed SST anomalies: (i) when averaging over multiple realizations, the AGCM only reproduced less than 50% of the observed atmospheric variability (Manabe and Stouffer (1996)), and more importantly (ii) the AGCMs suggested that the atmosphere acts to

dampen the imposed SST anomalies, whereas all available evidence clearly shows that the atmosphere *forces* the observed SST anomalies (Saravanan (1998)).

Several additional experiments have been done by extending on the basic principles of eqn. 1. Sura et al. (2006) argued that λ depends on the air-sea contrast, and thus decomposed λ into a mean and anomalous part, arguing that the product $T'\lambda'$ results in a so-called "multiplicative" noise that actually *increases* the persistence time of SST anomalies. This was confirmed by comparing daily SST and net surface heat flux anomalies at an Ocean Weather Ship in the North Pacific. Finally, Lee et al. (2008) clarified that the idea of decomposing λ as in Barsugli and Battisti (1998) is merited, but is more complex than a simple feedback involving a "static" air-sea thermal gradient. Instead, they argued that the "dynamic" wind-induced forcing of SST (through Ekman advection) can be much more important than the "static" component in Barsugli and Battisti (1998), especially in mid-latitude zones of large SST gradients. However, the main point is that while eqn. 1 is an good null hypothesis for mid-latitude air-sea interaction, other processes such as the influence of SSTs on the atmosphere as well as internal oceanic processes are required to successfully describe observations.

In terms of modeling air-sea interaction, several approaches have been taken. By prescribing observed SST anomalies in an AGCM, Sutton and Allen (1997), Rodwell et al. (1999), Mehta et al. (2000) have shown that the low-frequency component of the NAO can be well recreated. These studies concluded that SST anomalies exert a significant signal on low-frequency atmospheric variability, and thus, due to the relatively long decorrelation times, raise hope for predictability. Another important conclusion was that using ensemble experiments allows one to determine the SST feedback onto N because the intrinsic variability cancels out when averaging over multiple realizations of the stochastic forcing. For example, Mehta et al. (2000) showed that using 16 AGCM ensembles, one can obtain a correlation of 0.75 between the model simulated

and observed low-frequency NAO time series. However, as a counterpoint, Bretherton and Battisti (2000) showed that an equally accurate recreation of the NAO can be seen using a simplified, coupled model forced by a purely stochastic (white-noise) atmosphere that offers little predictability. Yet, in a different physical framework, Wu and Gordon (2002) used a fully-coupled GCM with subsurface damping of mixed layer temperature anomalies with the aim of reducing low-frequency SST variability. The main finding was a substantial decrease in the low frequency portion of the NAO power spectrum. Unaddressed issues still remain due to the wide range of hypotheses of the SST response to the atmosphere, from purely passive (FH77) to strongly coupled (Latif and Barnett (1996)).

Collectively, idealized and GCM modeling studies since the 1970's have developed a base of evidence showing that the extratropical atmosphere, both in the Pacific and Atlantic basins, responds to SST anomalies at a rate of 10-50 m K^{-1} for 500-mb geopotential heights, and 1-5 hPa K^{-1} for SLP (Chervin et al. (1980); Webster (1981); Ferranti et al. (1994); Peng et al. (1995); Kushnir and Held (1996); Peng and Robinson (2001); Liu and Wu (2004)), though the type of atmospheric response (baroclinic versus barotropic) is unclear because of sensitivities to seasonality (Peng et al. (1997)), linearity (Deser et al. (2004)) and even the GCM (see Table 1 in Kushnir et al. (2002), for overview). Apart from the Gulf Stream region, where the atmosphere responds strongly to the large oceanic heat flux convergence (Minobe et al. (2008); Kwon et al. (2010)), significant uncertainty regarding extratropical Atlantic air-sea interaction stills begs the question: given that extratropical SST anomalies exert a non-negligible influence on the atmosphere, is the signal strong enough to have use for predictability? Several observational studies of the North Atlantic have found that there is a statistically significant correlation when SST leads SLP (e.g. Czaja and Frankignoul (1999); Czaja and Frankignoul (2002); Cassou et al. (2004); Frankignoul

and Kestenare (2005)). However, it appears that this interaction is restricted to the late summer through early winter time period when the ocean leads by several months. Unfortunately, reproducing these results consistently using GCMs has seen limited success thus far.

1.2 Extratropical-Tropical Interaction

Many prior studies have investigated sources of tropical Atlantic variability and predictability and have shown the important roles of external forcing from ENSO (Curtis and Hastenrath (1995); Chang et al. (1997); Enfield and Mayer (1997); Penland and Matrosova (1998); Chang et al. (1998); Ruiz-Barradas et al. (2000); Liu et al. (2004); Repelli and Nobre (2004)) and the NAO (Czaja et al. (2002); Kushnir et al. (2006)). CV04 showed that SST variance in the northern tropical Atlantic (the AMM region) has a strong seasonal cycle with a boreal spring peak. Czaja (2004) explained this by showing that ENSO- and NAO-induced wind variability peaks during boreal winter, with a lagged effect on SST. Figure 1.2 examines the seasonality by showing the variance of the standardized AMM index based on separate months. Although the overall variance when using all months is unity, there is a clear seasonal cycle with almost twice as much variability during the boreal spring (defined as March-May, MAM) compared to late boreal summer and fall (August-October, ASO). Czaja et al. (2002) showed that it is the wind-induced component of the latent heat flux that causes SST anomalies 1-2 months after the forcing, due to the lagged response by the tropical Atlantic mixed layer. Another secondary reason for the boreal spring maximum in AMM variance is due to the proximity of the ITCZ to the equator at that time, allowing for a more efficient WES feedback. This occurs due to the β term in a linearized, shallow-water β-plane model (Gill (1980); Liu (1996); Vimont (2010)) which displaces the SLP response to tropical SST anomalies slightly poleward, allowing for a much more efficient

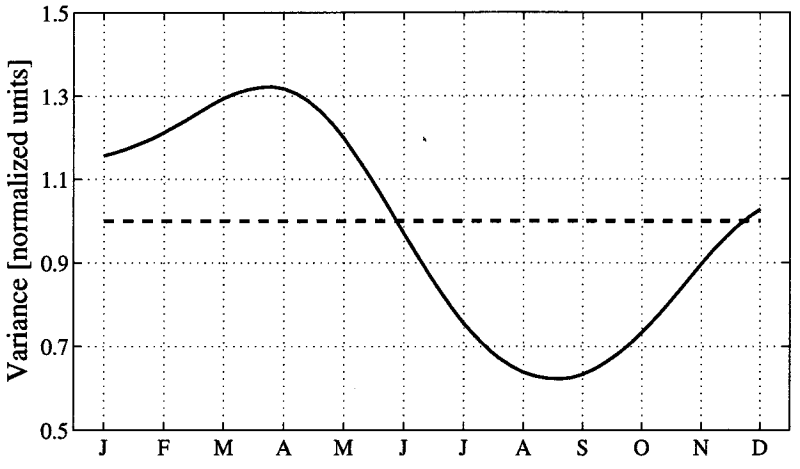

Figure 1.2: Variance of the normalized AMM index using monthly stratified data. For reference, the dashed line is equal to 1, which is the variance when using all months.

coupling between wind and SST anomalies. Because $\beta > 0$ and f changes sign at the equator, this effect is most prominent when a dipole in SST anomalies straddles the equator.

Because ENSO and NAO are only weakly correlated (Riviere and Orlanski (2007); Muller et al. (2008)), their forcing of the AMM can be decomposed into separate components. This is seen in Table 1.1, which shows the lagged correlations between the boreal spring AMM index (AMM_{MAM}) and the previous winter's NAO and ENSO indices (obtained from NOAA's Climate Prediction Center; the Nino34 Index was used as a proxy for ENSO). Note that all indices have been temporally smoothed with a 3-month running mean, which is consistent with the AMM index. The results in Table 1.1 are consistent with Ruiz-Barradas et al. (2000) and show that NAO_{DJF} and $ENSO_{DJF}$ each explains roughly 20% of the springtime AMM variance. Two additional variables were included as predictors: the wintertime AMM (AMM_{DJF}) and the wintertime SST anomaly over the entire North Atlantic basin (labeled NATL), excluding the domain of the AMM (i.e. north of 30°N). The inclusion of the wintertime AMM was based on

Table 1.1: Correlations with AMM_{MAM}

	$\mathbf{AMM_{MAM}}$	$\mathbf{AMM_{MAM-HP}}$	$\mathbf{AMM_{MAM-LP}}$
$\mathbf{AMM_{DJF}}(1)$	**0.53**	0.19	**0.75**
$\mathbf{NAO_{DJF}}(2)$	**-0.38**	**-0.37**	-0.21
$\mathbf{NINO_{DJF}}(3)$	**0.44**	**0.56**	0.04
$\mathbf{NATL_{DJF}}$	**0.27**	-0.14	**0.72**
(2) + (3)	**0.55**	**0.63**	**0.16**
(1) + (2) + (3)	**0.80**	**0.63**	**0.66**

evidence suggesting that remote forcing is not essential to AMM variability (Wu and Liu (2002)). The inclusion of the North Atlantic SST anomaly is based on VK07 who find that the extratropical portion of the Atlantic Multi-decadal Oscillation (AMO) is well correlated with the AMM *when the former leads the latter.* This is discussed in more detail shortly. Table 1.1 shows that the AMM_{DJF} explains 25% of the AMM_{MAM} variance, only slightly more than either ENSO or the NAO. Surprisingly, the $NATL_{DJF}$ only explains $< 10\%$ of the AMM_{MAM} variance.

Several additional tests are shown in Table 1.1. First, the AMM_{MAM} was decomposed into a high-frequency (subscript HP) and low-frequency (subscript LP) components. The LP component was calculated by successive application of a 37 and 25-month running mean, which approximately retains variance at periods greater than 5 years. The HP component was the residual between the (AMM_{MAM}) and the (AMM_{MAM-LP}). As intuition suggests, the aforementioned correlations of ENSO and the NAO mainly arise from the high-frequency forcing of the AMM_{AMM}. Meanwhile, most of the predictive skill between the AMM_{DJF} and AMM_{MAM} is from low-frequency persistence. It is also found that adding NAO_{DJF}, $ENSO_{DJF}$ and the AMM_{DJF} as predictors into a multivariate regression onto the AMM_{MAM} produces a increasingly better fit with each predictor. This is due to the minimal redundancy of shared information between the various predictors. In fact, there is no statistically significant

correlation between any combination of the three predictors. Using all three predictors and minimizing the least-squares error term results in a correlation of r=**0.80** between the predicted and actual AMM_{MAM} with comparable skill at both the lower-frequency (r=**0.63**) and higher-frequency (r=**0.66**) components, as shown in Table 1.1. Lastly, a scatter plot between the predicted and observed AMM_{MAM} is shown in Fig. 1.3. Note from the residuals of the fit (Fig. 1.3b) that there is significantly more unexplained variance at higher values of AMM_{MAM}. Also note that the multivariate regression has been cross-validated by using only the first 30 years of the dataset, and by predicting the latter 29 years. There was very little difference between the training data fit and the skill when applied to the independent data set.

The large seasonal cycle of AMM variance (Fig. 1.2) due to the associated seasonality of ENSO and NAO warrants a more detailed look at AMM variability during other seasons. Figure 1.4 shows the same regression of SST and winds onto the AMM as in Fig. 1.1 except for March-May (MAM, panel [a]) and August-October (ASO, panel [b]), which corresponds to the maximum and minimum in AMM variance from Fig. 1.2, respectively. To first order, the two patterns are qualitatively similar in the northern Tropical Atlantic, yet several important differences are seen. First, note that during MAM, there is a robust dipole of SST anomalies and cross-equatorial wind anomalies over the tropical Atlantic, which is not seen during ASO. This is consistent with a WES-feedback SST structure and was briefly described by Enfield and Mayer (1997) and attributed to the symmetry of the ITCZ with respect to the equator. Second, the position and amplitude of the positive SST anomalies in the northern Tropical Atlantic is weaker and farther north during ASO, compared to MAM. The difference in meridional positions is likely associated with seasonal shift of the subtropical high and ITCZ, which are both climatologically farthest north during ASO (Xie and Carton (2004). The reduction in amplitude is well explained by a substantial decrease in

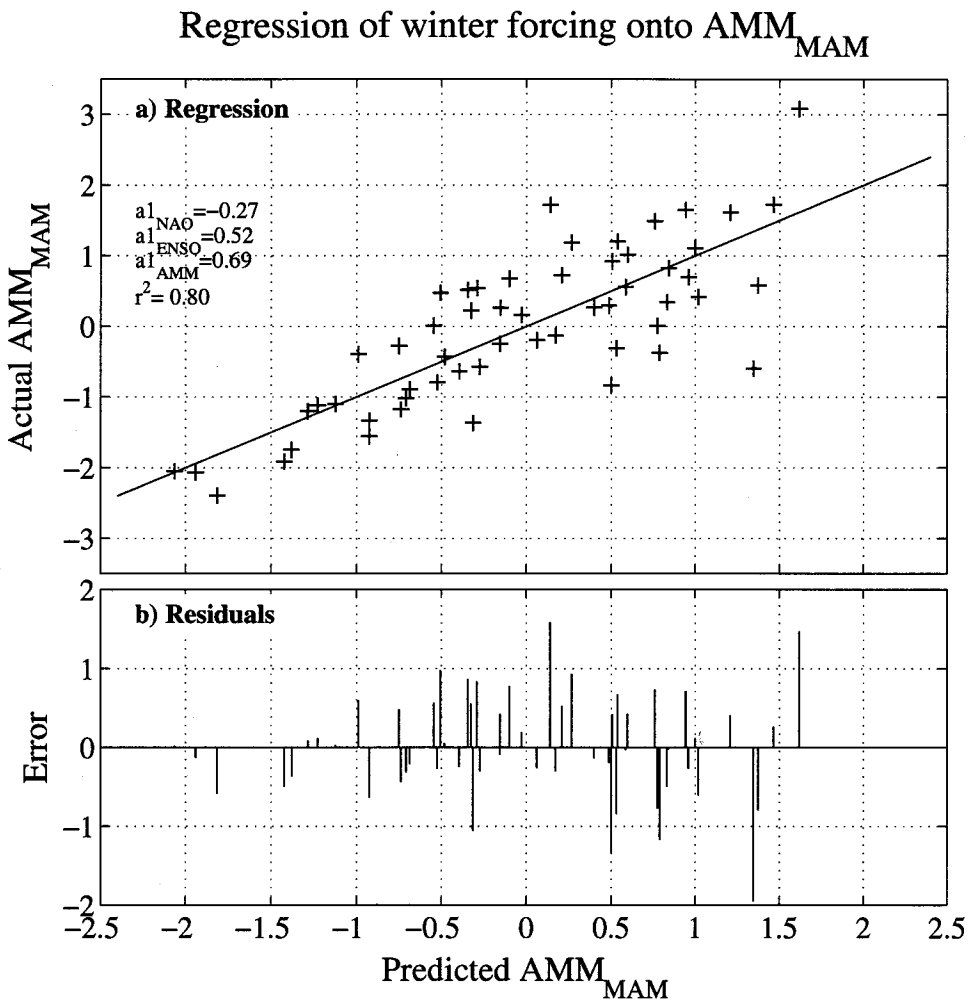

Figure 1.3: (a) Winter forcing of springtime AMM from a multivariate regression using AMM_{DJF}, NAO_{DJF} and $ENSO_{DJF}$ as predictors. (b) Residuals (actual-predicted) from the best-fit line in (a).

forcing by ENSO and NAO (Czaja (2004)). Third, there is the lack of SST anomalies around Bermuda during ASO, while substantial (-) SST anomalies are seen during MAM. Similarly, there are very large differences in the structure of extratropical SST anomalies. Figure 1.4a resembles the pan-Atlantic SST tripole anomaly pattern (Tanimoto and Xie (1999); Czaja and Frankignoul (2002); Kushnir et al. (2006)) whereas, Fig. 1.4b is markedly weaker in amplitude and resembles the North Atlantic Horseshoe (Czaja and Frankignoul (2002)).

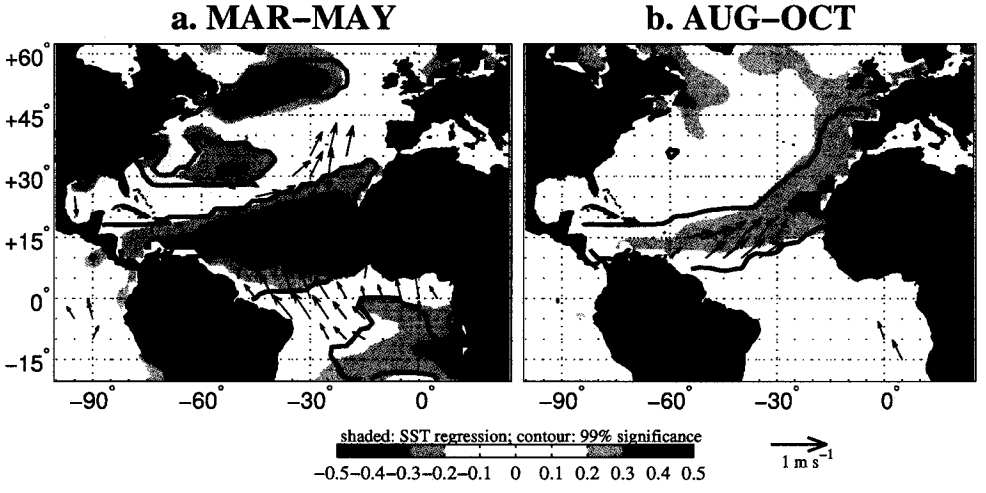

Figure 1.4: Similar to 1.1 but only for SST (shaded) and low-level horizontal wind (vectors) for (a) March to May and (b) August to October. Note that the AMM index was re-standardized for each season to ensure a standard deviation of unity.

To investigate the atmospheric circulation, Fig. 1.5 shows regressions of SLP anomalies onto the AMM during MAM and ASO. The differences in SST anomalies between MAM and ASO are also consistent in the SLP patterns. During MAM, a (+) AMM coexists with a (-) NAO, while during ASO, the resemblance to a preferred NAO phase is very subtle or non-existent, partially accounting for the differences in SST patterns seen in Fig. 1.4. Even though the amplitude of AMM variability during boreal fall is substantially weaker than during the spring, KV07, VK07 and Vimont

(2011) provide two compelling reasons to investigate the AMM during this time. First is the strong link between the AMM and Atlantic hurricane activity (both frequency and strength of storms), where the (+) AMM (i.e. warmer SST) corresponds to more storms and more stronger storms. This occurs due to the large air-sea coupling that collectively unites the (+) SST anomalies with (-) wind, (+) humidity and (-) wind shear anomalies over the Atlantic main development region (Goldenberg et al. (2001); KV07, Wang et al. (2008); Smirnov and Vimont (2011)). This is in stark contrast to typhoon activity in western Pacific, which is dominated by ENSO variability and *negatively* correlates with local SST anomalies (Chan and Liu (2004)). Second, VK07 suggest that the AMM may be forced through extratropical SST anomalies. This was based on a lagged correlation between the AMM and NATL SST anomalies (the NATL is essentially the Atlantic Multidecadal Oscillation without the tropical Atlantic portion). Though the simultaneous correlation between NATL and AMM is fairly high, even higher correlations occur when the NATL leads the AMM by roughly one year. Vimont (2011) showed that this connection is strongly dependent on season and peaks when the extratropics force during boreal fall.

To investigate the role of external forcing of the AMM_{ASO}, Table 1.2 presents correlations between the same predictors as in Table 1.1. Unlike the boreal spring AMM, there is no substantial correlation between the previous season's (MJJ) ENSO or NAO indices, even when decomposing the AMM_{ASO} into high- and low-frequency components as before. Persistence of the AMM (AMM_{MJJ}) explains more variance during AMM_{ASO} (40%) compared to AMM_{MAM} (28%), which can result from either a heightened role of local variability during this time or a substantial decrease in variance (reducing the denominator in the correlation equation). However, by far the biggest difference between the boreal spring and fall seasons is the role of extratropical Atlantic SST anomalies (NATL). Table 1.2 shows that $NATL_{MJJ}$ explains 29% of AMM_{ASO}

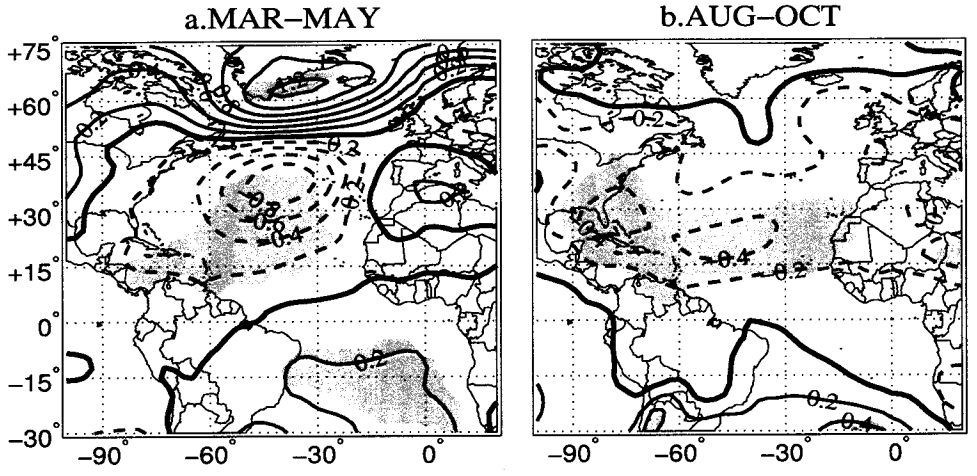

Figure 1.5: Regression (contoured) and correlations (shaded) of SLP anomalies onto AMM index for (a) March to May and (b) August to October. Positive (negative) values are denoted by the solid (dashed) contours and the zero-contour is thickened. Shaded regions are significant at the 95% confidence level.

Table 1.2: Correlations with $\mathrm{AMM_{ASO}}$

	$\mathbf{AMM_{ASO}}$	$\mathbf{AMM_{ASO-HP}}$	$\mathbf{AMM_{ASO-LP}}$
$\mathbf{AMM_{MJJ}}$	**0.64**	0.25	**0.63**
$\mathbf{NAO_{MJJ}}$	-0.22	-0.08	-0.22
$\mathbf{NINO_{MJJ}}$	-0.16	**-0.29**	0.07
$\mathbf{NATL_{MJJ}}$	**0.54**	0.22	**0.52**
$\mathbf{NATL_{SON}(-1)}$	**0.61**	0.14	**0.69**

variance, which is four times greater than during $\mathrm{AMM_{MAM}}$. Nearly all of this explained variance is from the predictability of the low-frequency component of $\mathrm{AMM_{ASO}}$. One other predictor is included, the state of NATL during the previous fall [$\mathrm{NATL_{SON}}(-1)$], which explains a substantial 40% of variance of $\mathrm{AMM_{ASO}}$, as was highlighted by Vimont (2011).

A separate body of literature exists that suggests the extratropics can force tropical SST anomalies on longer timescales. For example, paleoclimatic evidence shows that glacial periods in the Northern Hemisphere are associated with a change in the ITCZ position. Chiang and Bitz (2005) and Broccoli et al. (2006) confirmed this by

forcing an AGCM coupled to a slab ocean with Arctic sea and land-ice anomalies, noting a *southward* movement of the ITCZ. Because a slab ocean cannot produce anomalous oceanic dynamics, a thermodynamic pathway (for example, through the WES feedback) is responsible for the tropical circulation changes. In both these studies, the tropical atmosphere is forced to cool by enhanced evaporation due to the ice-induced drying in the extratropics. Because the moisture gradient is only one portion of the latent heat flux equation, it is not intuitive that the WES feedback argument explicitly involves changes in the moisture gradient. However, in a similar experiment as Chiang and Bitz (2005), Mahajan (2008) prescribed the climatological surface wind speed in the calculation of turbulent fluxes and showed that eliminating the WES feedback greatly reduced the magnitude of the tropical response to extratropical cooling. Yet, Mahajan et al. (2011) conclude that the WES feedback is not essential in generating tropical SST anomalies. Similarly, using a fully coupled GCM, Dong and Sutton (2002) and Zhang and Delworth (2005) show that a large pulse of freshwater in the northern Atlantic Ocean (inducing a slowing of the thermohaline circulation) leads to a southward shift in the ITCZ within a decade. These studies conclude that the steady state (equilibrium) response has large contributions from oceanic processes, but in the short-term (within the first few years), the atmosphere acts as the main signal carrier. Dahl et al. (2005) conclude that the tropical response to a slowdown of the MOC increases the strength of the northern hemisphere Hadley cell due to an increased pole-to-equator temperature gradient. However, by varying the efficiency of a GCM's convective parameterization scheme, Kang et al. (2008) showed large sensitivity of the ITCZ displacement to radiative changes in the hemisphere of thermal forcing, which, in the extreme case, can completely damp the extratropical thermal anomalies locally.

Although the focus of this research is to investigate the impact of extratropical forcing of tropical Atlantic variability, the latter can also force the former. Marshall

et al. (2001), Okumura et al. (2001) and Cassou et al. (2004) all document how tropical Atlantic variability can impact NAO variability from lagged Rossby-wave teleconnections, where the Rossby wave source is anomalous diabatic heating within the Atlantic ITCZ. A similar phenomenon has been documented involving ENSO and it's impact on remote areas through the so-called "atmospheric bridge" (Lau (1997); Trenberth et al. (1998); Alexander et al. (2002). Although the amount of remote forcing by the tropics is undoubtedly higher in the Pacific due to ENSO, the main point is that Atlantic extratropical-tropical interaction is a coupled system, even though here we focus only on the response forced by the extratropics.

1.3 Approach

The foundation of this research comes from a recent finding by Vimont (2011), who used a linear inverse model (LIM) based on SST observations to investigate the predictability of SST in the tropical Atlantic sector, with a particular interest in the AMM. Extratropical Atlantic SST anomalies were found to be an important precursor to boreal fall AMM variability. However, because the LIM offers little in the way of a mechanism, it is important to investigate how the AMM excitation occurs, and to make sure the LIM result is not a statistical artifact. A coupled ocean-atmosphere model provides a good framework to test this hypothesis, while simultaneously exploring questions such as: (i) how can the extratropics force tropical variability on the short time scales suggested by the LIM?, (ii) how important is the WES feedback, as highlighted by previous studies, (iii) why does the LIM forecast skill have such large seasonality? This rest of the manuscript seeks to answer these questions and is organized as follows: Section 2 introduces the experimental methods, namely the LIM and the GCM. Section 3 provides the main findings of the GCM simulation based on the LIM results of Vimont (2011) and proposes a physical mechanism of how the tropics respond to

extratropical forcing. Section 4 explores key sensitivity tests based on the initial GCM results including the role of seasonality and linearity. Also in section 4 is an analysis of feedback processes thought to be key factors in the LIM result, including the WES feedback and a secondary, radiative-SST feedback. Section 5 provides conclusions and finally, Section 6 explores further avenues of research including an preliminary analysis into the origin of the LIM initial condition.

2 EXPERIMENTAL DESIGN & MODEL SETUP

2.1 Setting up the experiment: Linear Inverse Model

Although the LIM is not the primary focus of this research, it is important to develop a background to help put the results in context. The LIM provides an alternate framework (compared to GCMs) for investigating the evolution of SST anomalies. In LIM, one assumes that the evolution of SST anomalies is a Markov process forced by stochastic "noise", much like eqn. 1. To introduce the LIM framework, start with a prognostic equation for the evolution of a state vector, $\overrightarrow{X}$, for a Markov process (Penland and Sardeshmukh (1995b):

$$\frac{d\overrightarrow{X}}{dt} = \mathbf{B}\overrightarrow{X} + N(\overrightarrow{X}) + \zeta \tag{4}$$

where $\mathbf{B}$ is the "deterministic feedback" matrix, or linear operator mentioned above, N represents the non-linear processes that contribute to the growth of $\overrightarrow{X}$ and ζ is the stochastic noise. For our purposes, the state vector $(\overrightarrow{X})$ represents SST anomalies at any given time. Note that it is possible to add additional state vectors such as thermocline depth (to account for oceanic dynamics) or geopotential height anomalies, but using the simplest hypothesis, one can assume that both of those additional state vectors are to some degree already represented by SST anomalies. Also note that although ζ is regarded as noise, it needs to have either spatial or temporal coherence in order to explain the growth of $\overrightarrow{X}$, making it only quasi-random (Penland and Sardeshmukh (1995b).

Given a set of observations, we can parameterize N as linear processes (Sardeshmukh and Sura (2009)), set ζ in eqn. 4 to 0, and eqn. 4 becomes a homogeneous differential equation with solution $\overrightarrow{X}_f = \overrightarrow{X}_i e^{\mathbf{B}\Delta\mathbf{t}}$. The "i" and "f" denote the initial and final states, and Δt is the duration over which the prediction is made, hereafter

τ. Using the Fokker-Planck equation that seeks to maximize the probability of a transition to $\vec{X}_f$ given $\vec{X}_i$ (Penland (1989)), the homogeneous portion of eqn. 4 can be solved using:

$$C(\tau) = e^{\mathbf{B}\tau} C(0) \tag{5}$$

where $C(0)$ and $C(\tau)$ are the simultaneous and lagged covariance matrices of the state vector, respectively:

$$C(0) = \vec{X}(t)\vec{X}(t)^T \tag{6}$$

$$C(\tau) = \vec{X}(t+\tau)\vec{X}(t)^T. \tag{7}$$

Thus, $\mathbf{B}$ is normally found as a second step after finding the system's Green function, $\mathbf{G}$ (also termed propagator matrix), as such:

$$\mathbf{G} = e^{\mathbf{B}\tau} = C(\tau)C(0)^{-1} \tag{8}$$

$$\mathbf{B} = \tau^{-1} ln[C(\tau)C(0)^{-1}]. \tag{9}$$

Finally, SVD can be applied to $\mathbf{G}$, as such (Penland, 1989):

$$\mathbf{G} = \mathbf{U} e^{\mathbf{B}\tau} \mathbf{V}^{\mathbf{T}}. \tag{10}$$

To clarify terminology, the eigenvectors of $\mathbf{B}$ are usually termed Empirical Normal Modes (ENM) or Principal Oscillation Patterns (POP) as in von Storch et al. (1988), Hasselmann (1988), Penland (1989) and Penland and Sardeshmukh (1995b). Unlike

EOFs, which are constrained to represent patterns that contain the most simultaneous variance and are essentially "static", ENMs are "dynamic" and can thus be used for predictive purposes Brunet and Vautard (1996).

The LIM has already been shown to be useful in the prediction of ENSO (Penland and Sardeshmukh (1995b)), tropical Atlantic SST anomalies (Penland and Matrosova (1998); Vimont (2011)), mid-latitude 500-hPa height anomalies (Newman et al. (2003)) and the Pacific Decadal Oscillation (Alexander et al. (2008)). The variety of successful applications suggests that the LIM is an effective, complementary tool to numerical prediction. In order to ensure that a particular LIM result is robust and useful, it is typical to test for the stability of $\mathbf{B}$ at various lags, as well as to make sure that the growth (singular values of $\mathbf{G}$) is greater than the growth of the noise that is present in eqn. 4 (Penland and Sardeshmukh (1995a)).

2.2 GCM experiments based on the LIM

2.2.1 LIM Results

The LIM analysis herein is prepared using two monthly-averaged SST data sets (NCEP-Reanalysis from Kalnay and co authors (1996); Hadley from Rayner et al. (2003)) and closely follows the method of Vimont (2011) except that (i) the SST data includes the North Pacific domain, and (ii) $\tau = 11$ mo. in eqn 8. These changes had little effect on the outcome of the LIM for the Atlantic basin (D. Vimont, personal correspondence). To conduct the LIM analysis, monthly SST anomalies over the period 1950-2005 are found by removing the annual cycle, smoothing temporally with a 3-month running mean and spatially with a 2-dimensional 1-4-6-4-1 smoother. As in Penland and Sardeshmukh (1995b), the SST anomalies are transformed into EOF space through an eigenanalysis, and the top 18 EOFs (roughly explaining 80% of the domain-wide variance) make up the state vector $\vec{X}$ in eqn. 6 and 7. After performing

SVD on the Green's function (eqn. 10) with $\tau = 11$ months, the first column of $\mathbf{U}$ and $\mathbf{V}$ correspond to the first "optimal" SST anomaly structure and evolution of that optimal over the course of τ.

The first optimal pattern evolves into a structure that resembles ENSO and has been extensively studied (e.g. Penland and Sardeshmukh, 1995). However, the second optimal pattern evolves into a structure that resembles the AMO (and AMM in the tropics). This second optimal pattern (hereafter referred to as OPT), when transformed back into a spatial structure is shown in Fig. 2.1a, c for the NCEP and Hadley SST datasets, respectively. The OPT transitions into the final structures shown in Fig. 2.1b, d for the NCEP and Hadley datasets. Although there are differences between the final structures depending on the dataset, both show an AMO-like "horseshoe" pattern of SST anomalies. The final structure is not very sensitive to the choice of τ between the range of 8 to 15 months. Meanwhile, the NCEP and Hadley OPT structures are similar over most of the domain, with some differences in the tropics.

Although the linear dynamical operator, $\mathbf{B}$, in the LIM is seasonally invariant, Vimont (2011) found that the 11-mo. predictive skill of the AMM has strong seasonality with a maximum in predictive skill during boreal fall (suggesting an initial condition during the previous fall). The correlation between the predicted and actual boreal fall AMM at a lag of 11 months is **0.6**, which raises the question of what is causing this skill (KV07). The physical mechanism of the transition from the OPT to AMM-like structure is hard to deduce from the LIM alone, and a coupled GCM provides a different physical basis and alternate framework from which to investigate the forcing of the AMM. The next section discusses the setup of GCM experiments that are conducted in order to validate the LIM.

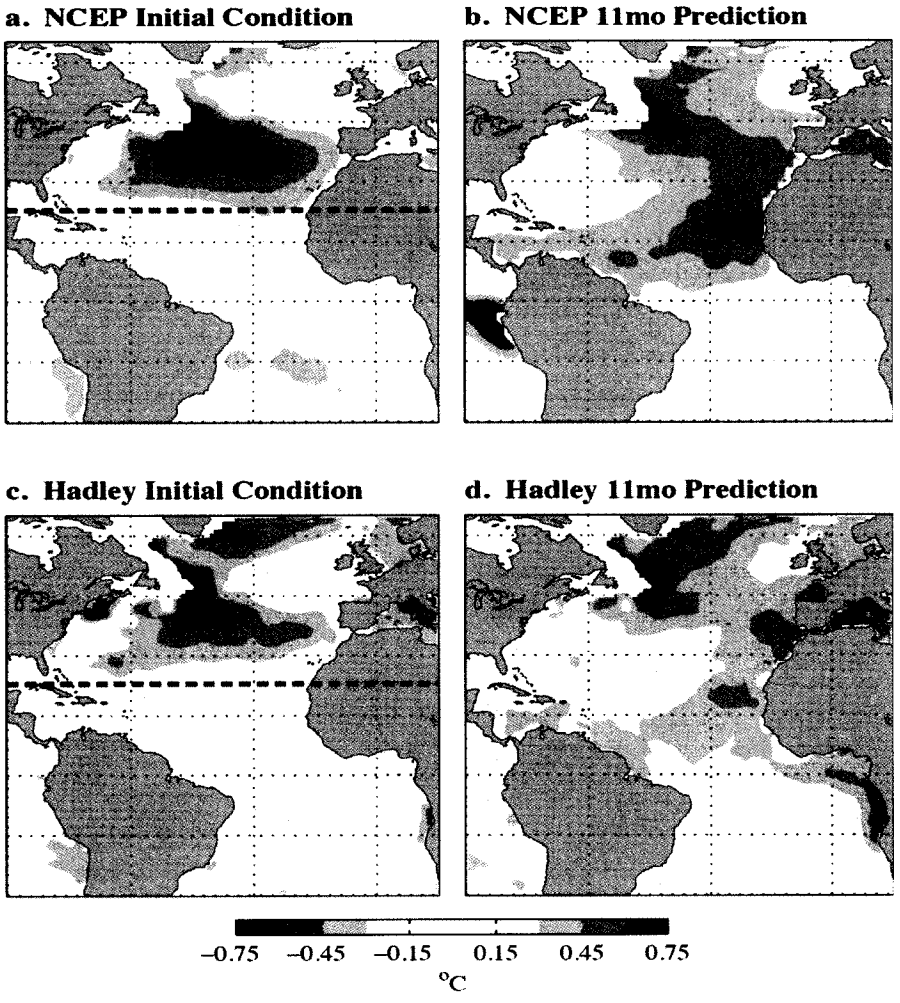

Figure 2.1: a) and c) "Optimal" initial conditions that evolve into b) and d) the final conditions based on using the NCEP (a,b) and Hadley (c,d) SST datasets in the LIM (eqn. 8 with $\tau = 11$ mo.).

2.2.2 NCAR CCSM3 GCM Overview

For all experiments, we use the Community Atmosphere Model (CAM), version 3.1, which is part of the coupled Community Climate System Model (CCSM; Collins et al. (2006)), version 3, developed at the National Center for Atmospheric Research (Boulder, Colorado). CAM is run using the default Eulerian dynamical core with T42 resolution (approximately 2.8^o resolution in physical space) with a 20-minute timestep and has 26 unequally spaced vertical levels (more levels within the boundary layer and in the tropopause) on a hybrid sigma-pressure vertical coordinate. For all simulations, CAM is coupled to an interactive land and sea-ice model with multiple options for representing the ocean. In the simplest ocean, a data-ocean model (hereafter, CAM+DOM), SST is prescribed, which makes this an uncoupled simulation where the atmosphere does not impact the ocean. To introduce coupling, a slab-ocean model (hereafter, CAM+SOM) is used where a 50-m constant depth, seasonally invariant mixed layer interacts with the atmosphere through a simplified surface energy budget (see eqn. 2). Because the ocean in SOM is "static", there are no internal oceanic dynamics, eliminating phenomena such as ENSO and the Atlantic Nino. Another consequence of the static ocean is the need to parameterize the oceanic heat flux convergence to maintain a closed energy budget and a drift-free long-term climate. This is done by solving for the difference between the net atmospheric energy flux and mixed layer heat tendency from an uncoupled simulation forced with climatological SST (see Appendix 7.1).

A 40-year long CAM+SOM control experiment (hereafter, SOM.CLIMO) shows that our GCM reproduces the salient features of the tropical and extratropical Atlantic climate well, including convective precipitation near the ITCZ and storm track variability (Collins et al. (2006)). Of particular importance is the latent heat flux (hereafter, F_{LH}), which is compared in Fig. 2.2 between SOM.CLIMO and NCEP-

Table 2.1: % Explained by top 2 EOFs of SST Anomalies in Tropical Atlantic

	SOM.CLIMO	NCEP(1951-)	NCEP(1979-)	MERRA	CFSR
$EOF1$	27	25	21	26	26
$EOF2$	24	16	17	22	21

Reanalysis. In the tropical Atlantic, SOM.CLIMO captures the annual mean F_{LH} of 100-150 W m^{-2} well, and also reproduces the correct magnitude and spatial variations of F_{LH} standard deviation with values of 15-20 W m^{-2}. Documented biases in CAM+SOM include a slightly exaggerated and southward displaced NAO, and excessive low-cloud cover off the northwest African coast (Alexander et al. (2006)). To compare variability, Fig. 2.3 shows the top two EOFs of tropical Atlantic (30°S – 30°N) SST anomalies between the last 30 years of SOM.CLIMO and 30-years of observations from the Modern Era Retrospective-Analysis for Research and Applications (MERRA; Rienecker and co authors (2011)). In observations, the dominant pattern is reminiscent of the AMM, though with some contamination from the Atlantic Nino along the equator from the Gulf of Guinea and westward. This seems to be the second dominant pattern from SOM.CLIMO, and there is no resemblance of the Atlantic Nino due to the static ocean. The second dominant pattern from observations also contains large SST anomalies in the Northern Tropical Atlantic, which is similar to the first EOF from SOM.CLIMO, though the GCM shows simultaneous warm SST anomalies in the southern hemisphere trade wind region. Regardless, the order of top two EOFs is statistically indistinguishable, as shown by overlap when considering the error in the amount of variance explained by each pattern (bottom panels). Table 2.1 shows that the amount of variance explained by the top two EOFs is comparable between SOM.CLIMO and three observational data sets.

Next, Fig. 2.4 compares the dominant EOFs of detrended North Atlantic SST variability between the SOM.CLIMO (left panel) and observations (right panel). Com-

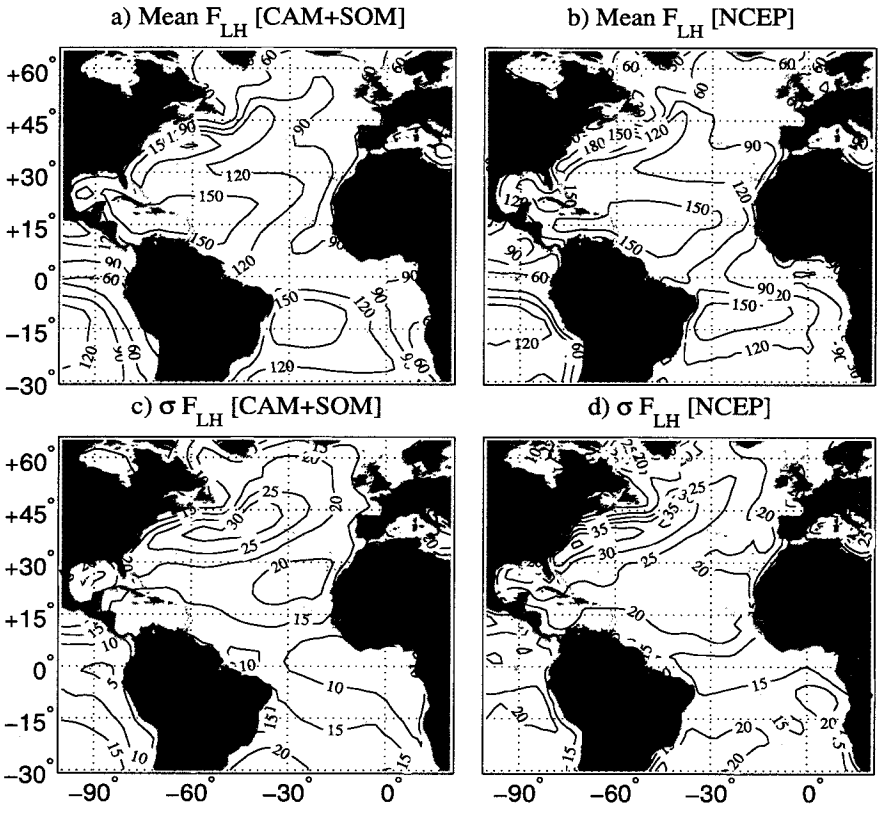

Figure 2.2: Annual mean F_{LH} from (a) SOM.CLIMO and (b) NCEP-Reanalysis. Contour interval is 30 W m^{-2}. Standard deviations of F_{LH} after removing the annual cycle from (c) SOM.CLIMO and (d) NCEP-Reanalysis. Contour interval is 5 W m^{-2}.

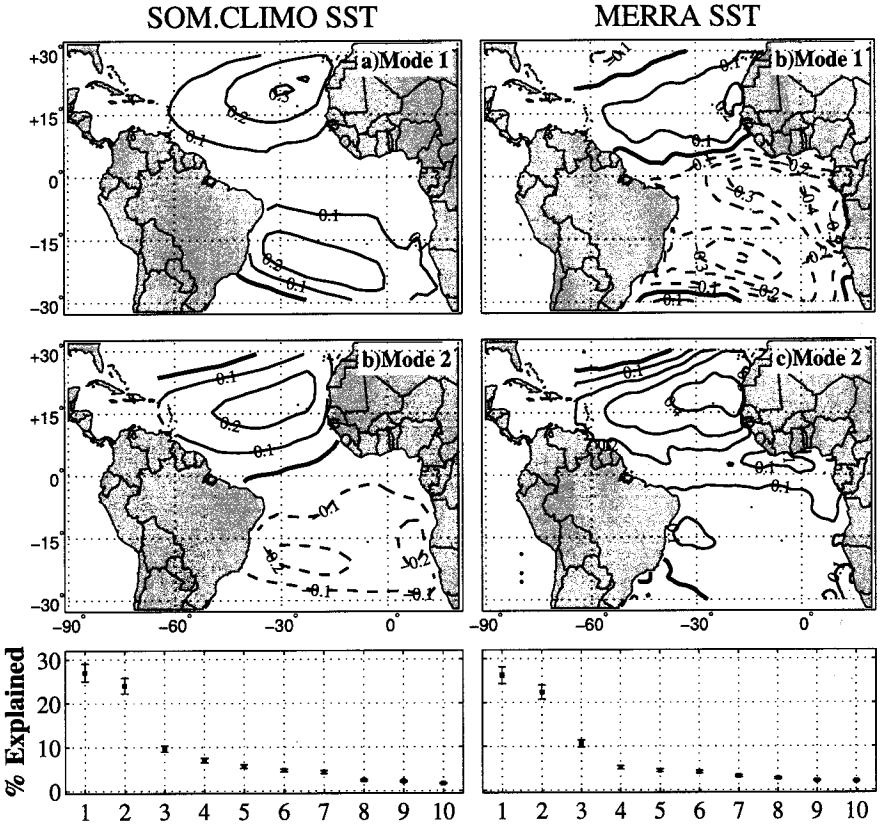

Figure 2.3: Comparison of dominant two EOFs of tropical Atlantic SST anomalies in SOM.CLIMO (left column) and MERRA observations (right column). The bottom row shows the percent variance explained by top 10 modes in each analysis, along with a measure of error suggested by North et al. (1982).

Table 2.2: % Explained by top 2 EOFs of SST Anomalies in North Atlantic

	SOM.CLIMO	NCEP(1951-)	NCEP(1979-)	MERRA	CFSR
$EOF1$	33	35	30	25	28
$EOF2$	20	14	12	13	10

pared to the tropical Atlantic, the GCM more accurately portrays SST variability over the entire North Atlantic basin. The dominant mode, which strongly resembles the AMO (e.g. Kerr (2000)) is slightly more active in SOM.CLIMO (33% variance explained) compared to MERRA (25%). Also, SOM.CLIMO has a more zonally symmetric tripole structure and neglects the anomalies off the west coast of Spain. There are also large discrepancies in the Gulf Stream region, as expected due to the absence of oceanic variability. The second mode is largely comparable between the GCM and observations, though it is overactive in the model (20% variance explained in SOM.CLIMO versus 13% in observations). Table 2.2 compares the top two modes using three different data sets and shows general agreement.

2.2.3 Experimental Design

The LIM result is intriguing and can be investigated using a coupled GCM by initializing the model with the LIM-based OPT SST anomaly shown in Fig 2.1. Note that all SST anomalies outside of the Atlantic basin have been zeroed out. To be consistent with the seasonality of AMM predictive skill shown by Vimont (2011), the SST anomaly was added on November 1st. Because the OPT SST anomaly contains loadings over both the tropical and extratropical Atlantic, three separate simulations are conducted: *(i)* one that initializes with the full OPT structure, hereafter SOM.TOTAL, *(ii)* one that initializes with only the extratropical portion of OPT (north of 23°), hereafter SOM.MID and *(iii)* one that initializes with only the tropical portion of OPT (south of 23°), hereafter SOM.LOW. Each of these three simulations is run with both NCEP-

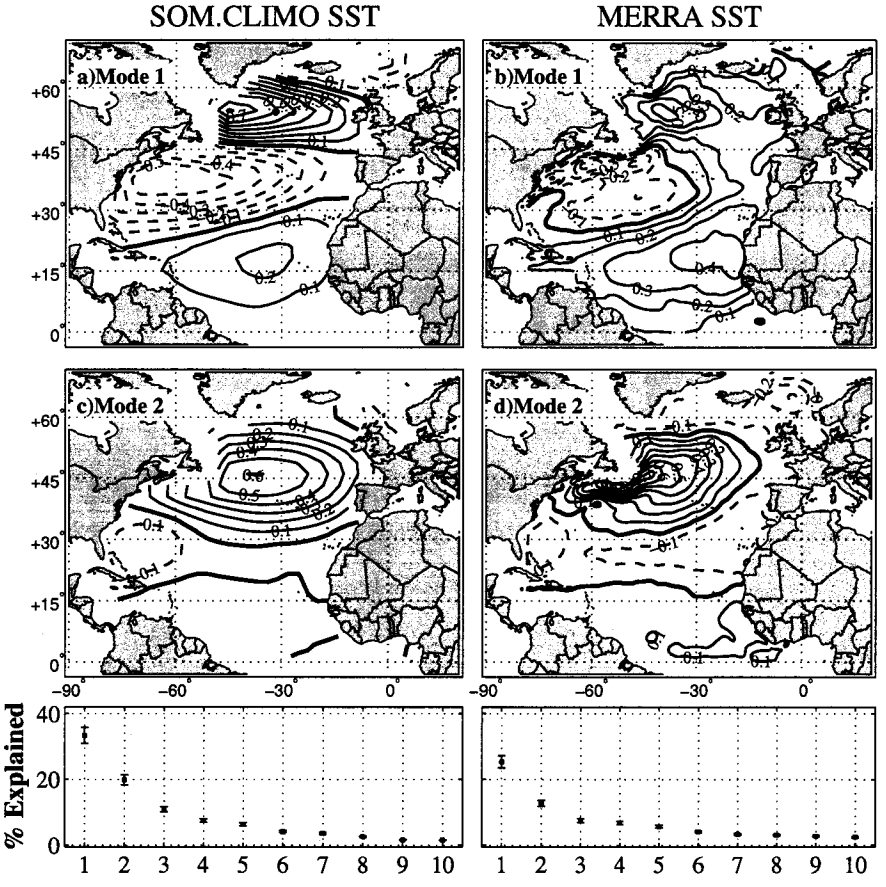

Figure 2.4: Comparison of dominant two EOFs of North Atlantic SST anomalies in SOM.CLIMO (left column) and MERRA observations (right column). The bottom row shows the percent variance explained by top 10 modes with a measure of error, as suggested by North et al. (1982).

based and Hadley-based OPT structures. Because a large portion of OPT is in the extratropics where the atmospheric response to SST anomalies is often difficult to access due to large internal atmospheric variability, an ensemble approach is used. Each November 1st land, ice, ocean and atmosphere history file from the last 30 years of the SOM.CLIMO simulation is used to initialize a separate ensemble member; thus, we have 30 ensembles. Linearity is investigated by initializing each ensemble with warm and cold OPT anomalies. These GCM experiments are outline in Table 2.3. Note that all remaining experiments in Table 2.3 are addressed in the manuscript in the sequence they are conducted.

To present results, the mean difference between the warm and cold ensembles is shown for SST, SLP and other fields, as necessary. Seasonally averaged differences are shown for November-January (NDJ), February-April (FMA), May-July (MJJ) and August-October (ASO). This conveniently coincides with the seasonality of SST over the tropical Atlantic, being warming (coolest) during ASO (FMA). To test for significance, the 95% confidence level is used based on a 2-sided Student's T-test with a null hypothesis of no difference between the warm and cold ensembles. For fields with large internal variability (e.g. SLP), the 90% confidence level is used. Because CAM uses a hybrid sigma-pressure vertical coordinate (i.e. actual height depends on the surface pressure), all atmospheric variables are interpolated in a log-linear fashion to constant pressure levels. The results of the SOM.TOTAL, SOM.MID and SOM.LOW experiments are presented in the following chapter.

Table 2.3: List of GCM Experiments

Run Name	**Model**	**Perturbation**	**Duration**
DOM.CLIMO	CAM+DOM	None	40 years
SOM.CLIMO	CAM+SOM	None	40 years
SOM.TOTAL#	CAM+SOM	2-σ anomaly from LIM (see Fig. 2.1)	30 13-mo. warm & cold ens. initialized Nov. 1st
SOM.MID#	CAM+SOM	Same as above but *north* of 23°N	Same as SOM. TOTAL
SOM.LOW#	CAM+SOM	Same as above but *south* of 23°N	20 13-mo. ens. initialized Nov. 1st
DOM.MID	CAM+DOM	Same as SOM.MID	10 years
DOM.WES-OFF	CAM+DOM with prescribed U over Atlantic	None	15 years
SOM.WES-OFF	CAM+SOM with prescribed U over Atlantic	Same as SOM.MID	Same as SOM.MID
SOM.SW-CLIM	CAM+SOM with prescribed SW over eastern Atlantic	Same as SOM.MID	Same as SOM.MID but 15 ens.

Used both NCEP and Hadley SST data for initial conditions

3 EXTRATROPICAL FORCING OF TROPICAL ATLANTIC VARIABILITY

This chapter provides the results of the initial GCM experiments that are designed based on the results of the LIM. Sections 3.1-3.3 shows the results of the SOM.TOTAL, SOM.LOW and SOM.MID experiments, respectively. Section 3.4 proposes a physical mechanism for extratropical forcing of the AMM, while section 3.5 investigates the role of linearity; a discussion is provided in section 3.6.

3.1 Full Condition: SOM.TOTAL

The evolution of SST anomalies for the NCEP- and Hadley-based SOM.TOTAL experiments is shown in Fig. 3.1 and 3.2, respectively. Contours are the mean difference between the warm and cold ensemble members and the shaded regions are significant at the 95% confidence interval. Both simulations show a steady, equatorward propagation of SST anomalies starting in NDJ that reach the tropics by FMA. Also, both simulations show a large attenuation of the mid-latitude SST anomaly within the first 3 months, especially north of 35°N mainly due to anomalous F_{LH}. By ASO, both simulations have SST anomalies near 15°N with a structure that weakly resembles the AMM (compare with Fig. 1.4), and reproduces the LIM result.

To investigate the atmospheric response to the SST anomalies, Fig. 3.3 and 3.4 show the SLP response for the NCEP- and Hadley-based SOM.TOTAL experiment, respectively. The evolution of the SLP difference is not as coherent or gradual as the propagation of SST anomalies seen in Fig. 3.1 and 3.2. Furthermore, there are large differences between the NCEP and Hadley-based simulations. For example, during FMA (Fig. 3.3a and 3.4a) there is a statistically significant, yet opposite response where the NCEP-based simulation projects onto the (-)NAO, while the Hadley-based simulation resembles a (+)NAO. The use of 30 ensemble members is thought to be an adequate

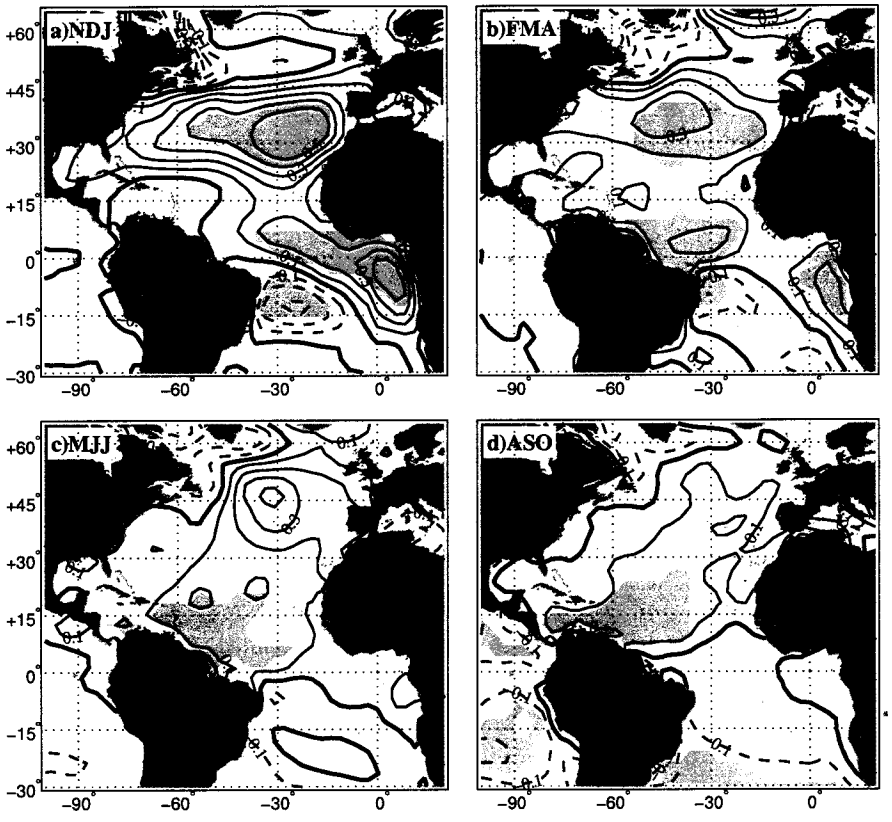

Figure 3.1: Mean difference in SST between the warm and cold ensembles of the NCEP-based SOM.TOTAL for (a) NDJ, (b) FMA, (c) MJJ, and (d) ASO. The contour interval is 0.1^0C, negative contours are dashed and the zero contour is thickened. Shading indicates areas that are significant at the 95% confidence level.

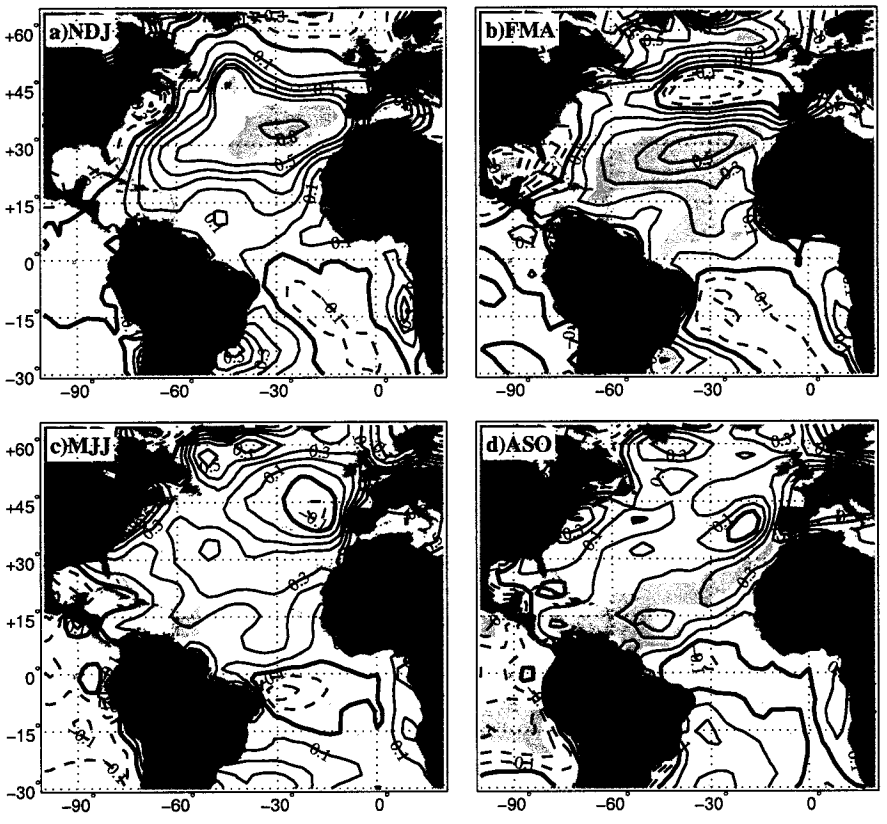

Figure 3.2: Same as 3.1 except for the Hadley-based SOM.TOTAL experiment.

sample size, yet the discrepancies between Fig. 3.3 and 3.4 suggests the use of more ensembles may have yielded substantial additional information. However, if focusing on the area in the immediate vicinity of the initial SST anomaly, near 30°N and 30°W, both runs show some consistency during FMA and MJJ when negative SLP anomalies are seen in the northern subtropical Atlantic (compare Fig. 3.3b,c with 3.4b,c). In fact, the local response may be more important that the large-scale response, such as the projection on the NAO, which has been the main focus of several past studies (Peng et al. (2002); Deser et al. (2004)). The relatively quick development of subtropical SLP anomalies is later shown to be critical in producing an AMM-like response.

One possible explanation regarding the inconsistencies in Fig. 3.3 and 3.4 is the large differences in SST loadings in the tropical Atlantic region. Though the difference in tropical SST anomalies between the NCEP- and Hadley-based OPT is only a few tenths of a degree, tropical SST variance is much lower than the mid-latitudes and the tropical atmosphere is much more sensitive to SST anomalies (Holton (2004)). Furthermore, several studies have shown that tropical Atlantic SST anomalies can produce an atmospheric response in the subtropics and even farther (Okumura and Xie (2006); Cassou et al. (2004)). In the next section, we investigate the significance of the tropical contribution to the SOM.TOTAL simulation.

3.2 Low-latitude Only: SOM.LOW

Figure 3.5 shows the evolution of SST anomalies from tropical portion of the NCEP-based OPT. Note that this simulation used 20 ensembles, unlike the 30 used in the SOM.TOTAL. The Hadley-based SOM.LOW simulation showed a very weak signal and is not discussed. The SST response in SOM.LOW is *opposite* to the SOM.TOTAL simulation and suggests that the tropics may be destructively interfering with the atmospheric response caused by the extratropical portion of the NCEP-based OPT.

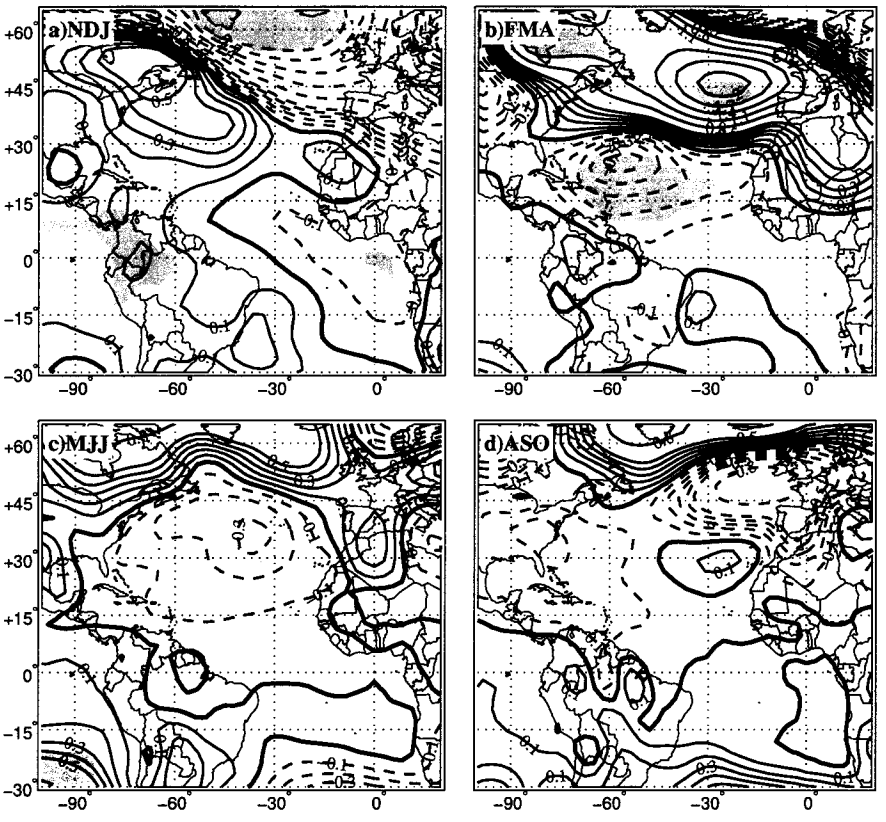

Figure 3.3: Mean SLP difference for the NCEP-based SOM.TOTAL. Shading denotes significance at the 90% confidence level and contours are capped at +/- 2-hPa.

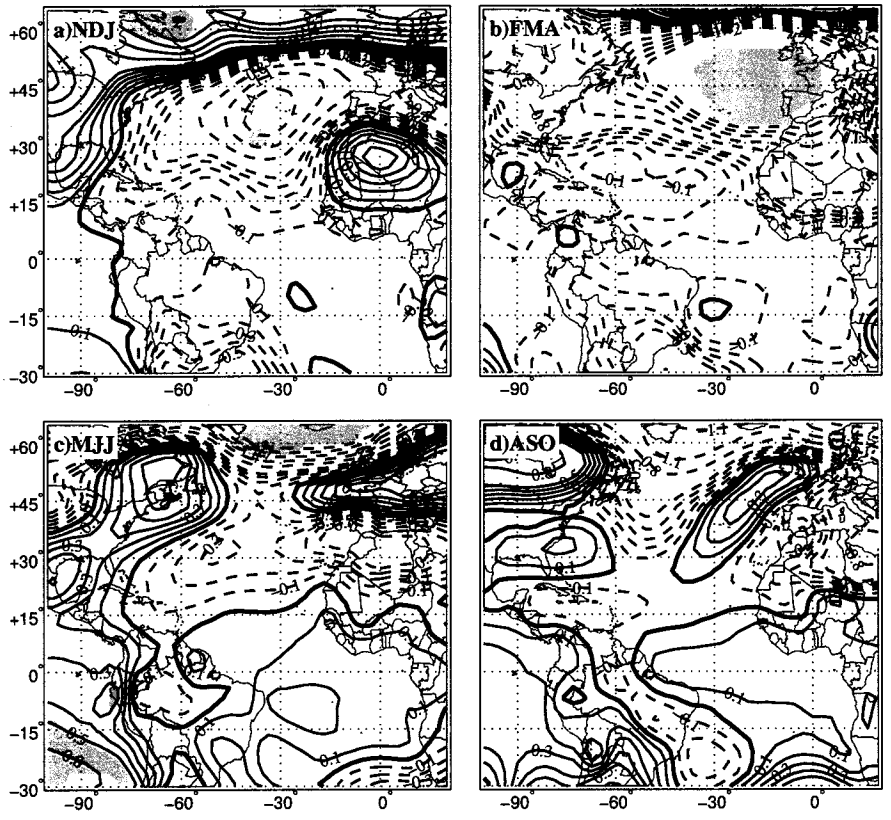

Figure 3.4: Mean SLP difference for the Hadley-based SOM.TOTAL. Shading denotes significance at the 90% confidence level and contours are capped at +/- 2-hPa.

The next section considers only the extratropical component in order to confirm this. In Fig. 3.6, which shows the SLP response in the SOM.LOW simulation, there is anomalously high SLP just north of colder SSTs, which signifies a coupled process and represents the (-) phase of the AMM. The SOM.LOW simulation also supports a previous finding that the Atlantic Nino can force AMM variability during boreal spring (Okumura and Xie (2006)). Also note that there are large, though insignificant, SLP differences in the high-latitudes, which may support previous findings of NAO forcing by the tropical Atlantic (Okumura et al. (2001); Cassou et al. (2004)).

Several complications induce uncertainty in the results of the SOM.LOW experiment and also, the tropical component of the NCEP-based OPT. First, the CAM+SOM framework does not include oceanic thermocline variability, making it significantly underestimate SST variance in the Atlantic Nino region (Gulf of Guinea and westward along the equator). To visualize this, Fig. 3.7 shows the ratio of SST variance (i.e. annual cycle removed) between the SOM.CLIMO simulation and NCEP-Reanalysis SST. Note that both data sets span 30 years (NCEP-Reanalysis data from 1979-2008), and the spatial pattern does not change appreciably if other 30-year segments of NCEP-Reanalysis data was used. Although the CAM+SOM framework slightly underestimates variance over most of the tropical Atlantic domain due to a fixed 50-m mixed layer depth (e.g. Saravanan and Chang (1999)), it grossly underestimates the variance in the Atlantic Nino region where only 20% of the observed SST variance is depicted. The second reason why the SOM.LOW simulation results are uncertain is due to the difference in the tropical portion of the NCEP- and Hadley-based OPT. The differences are mainly in the southern Tropical Atlantic and may be due to poor data sampling, especially before the establishment of the PIRATA buoy array (Servain et al. (1998); Servain et al. (1999); L. Matrosova, personal correspondence). Due to uncertainty in the tropical portion of the OPT, the tropical forcing on the atmosphere is not believed

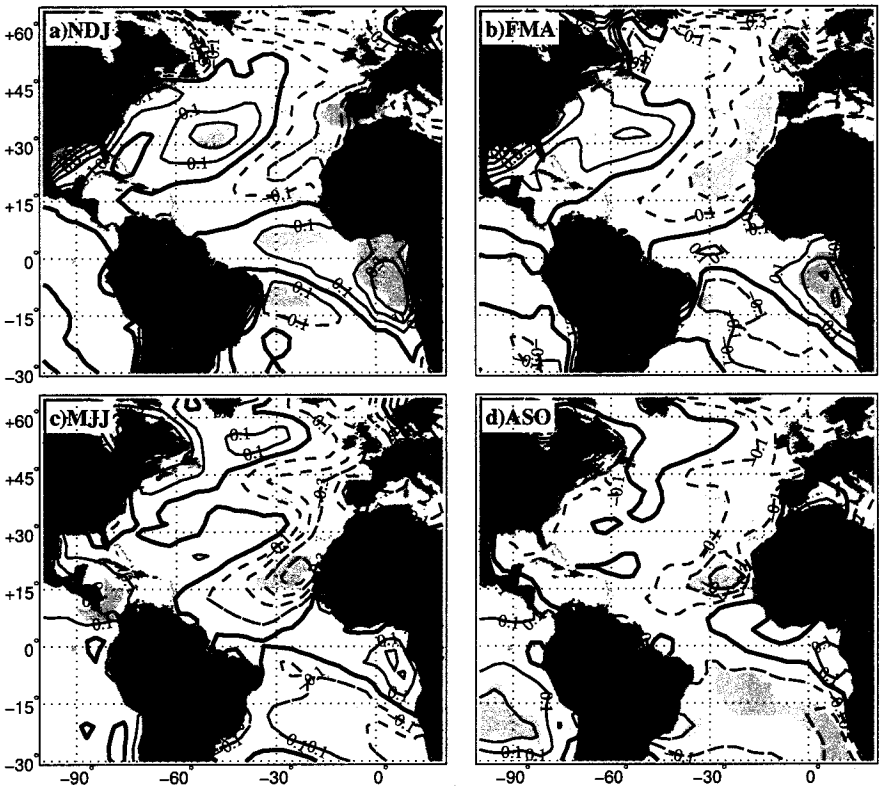

Figure 3.5: Mean SST difference for the NCEP-based SOM.LOW simulation. Shading denotes significance at the 95% confidence level, contour interval is 0.1 K.

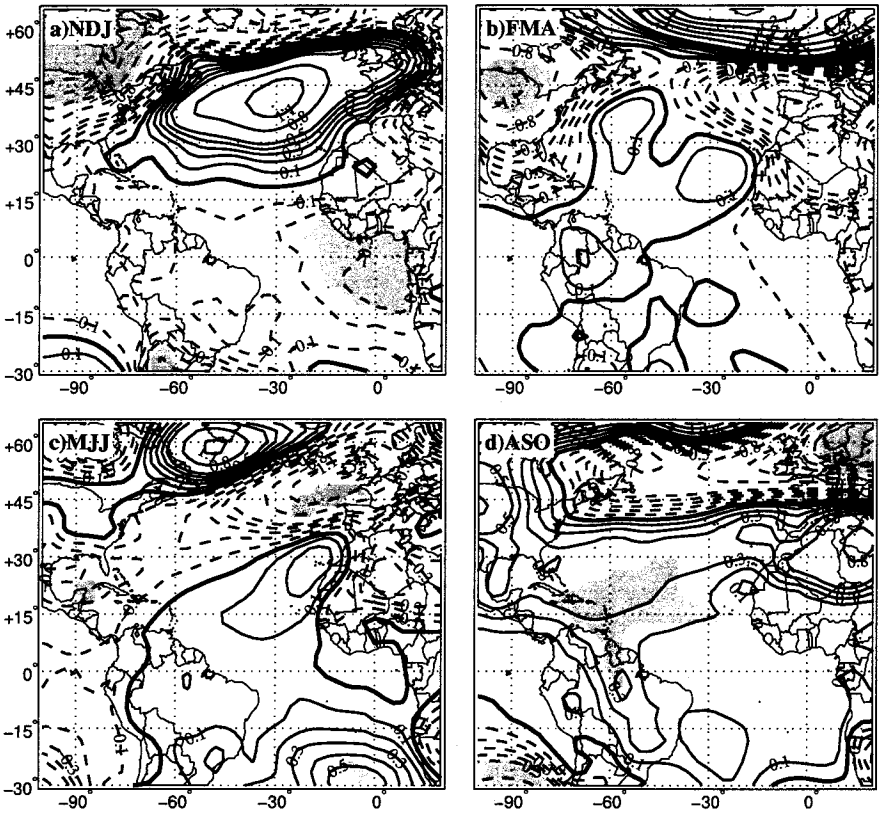

Figure 3.6: Mean SLP difference for the NCEP-based SOM.LOW simulation Shading denotes significance at the 90% confidence level, contour interval is 0.1-hPa.

to be a significant contributor to the LIM result. The next section analyzes the extra-tropical contribution to the results of SOM.TOTAL and shows a stark contrast with SOM.LOW.

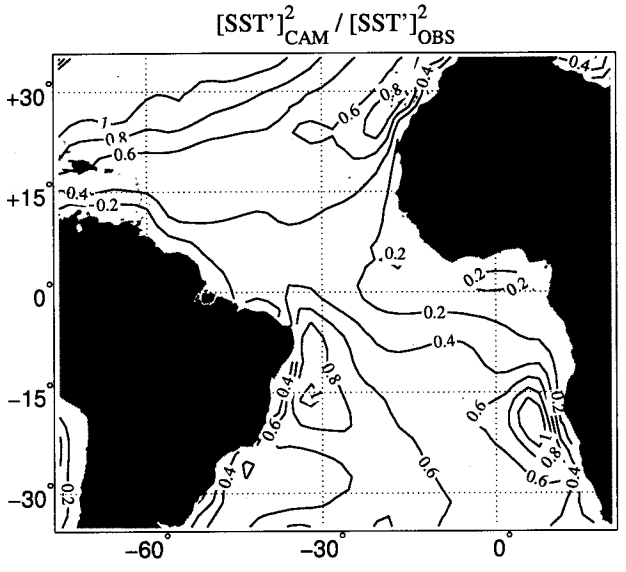

Figure 3.7: Ratio of SST variance between the SOM.CLIMO simulations and NCEP-Reanalysis SST (1979-2008). For consistency, both data sets are 30 years long.

3.3 Mid-latitude Only: SOM.MID

A set of CAM+SOM ensembles is run with just the mid-latitude portion of the OPT pattern (SOM.MID from Table 2.3). The results for the mean SST difference are shown in Fig. 3.8 and 3.9 for NCEP and Hadley-based OPT, respectively. Unlike in the SOM.TOTAL, both SOM.MID simulations show a large area of SST anomalies that propagate equatorward. By ASO, the resulting pattern looks strikingly similar to a (+) AMM. Furthermore, the NCEP and Hadley-based simulations are similar to each other, lending strong support that it is indeed the mid-latitude portion of OPT that is responsible for most of the skill in the LIM. In fact, the evolution of SST anomalies in the SOM.TOTAL experiment can be well approximated as the linear combination

of SOM.MID and SOM.LOW. However, due to the uncertainty in the tropical portion of the OPT and the lack of oceanic dynamics in the CAM+SOM, most discussion of results hereafter is based on the NCEP-based SOM.MID ensemble simulation (Fig. 3.8), as it highlights the excitation of the AMM most vividly and is consistent with both versions of the SOM.TOTAL and the Hadley-based SOM.MID.

The atmospheric response in the NCEP- and Hadley-based SOM.MID is shown in Fig. 3.10 and 3.11, respectively. The spatial pattern of SLP anomalies between the two simulations greatly differs through the NDJ and FMA periods. During NDJ, the NCEP based simulation (Fig. 3.10a) shows a very strong projection onto the (-) NAO pattern (recall that a (-) NAO implies a reduction (increase) in the Icelandic Low (Bermuda High); vice versa for a (+) NAO). In contrast, the Hadley-based SOM.MID (Fig. 3.11) projects onto the (+) NAO. Although past studies (e.g. Deser et al. (2004)) have focused on the projection of the atmospheric response to SST anomalies in the context of the large-scale quasi-stationary waves (e.g. NAO), in this case, it may be more important to consider the *local* atmospheric response. Based on Hoskins and Karoly (1981) and Kushnir et al. (2002), it is expected that a (+) SST anomaly in the mid-latitudes should produce a (-) SLP anomaly, as can be deduced through conservation of atmospheric vorticity for a shallow-heat source. Indeed, both the NCEP- and Hadley-based SOM.MID simulations show a (-) SLP on the eastern fringe of the initial SST anomaly (compare Fig. 3.10a and Fig. 3.11a in the region 25°W, 35°N).

Significant paleoclimatic evidence for Atlantic extratropical-tropical interaction has been found when comparing Greenland ice cores (a proxy for high-latitude climate) with sediment cores from freshwater runoff in the Cariaco basin (a proxy for the ITCZ strength and position) off the northeast coast of South America (Peterson et al. (2000)). This has motivated past GCM experiments that have shown a southward shift of the ITCZ when imposing cooling in the high-latitudes (Chiang et al.

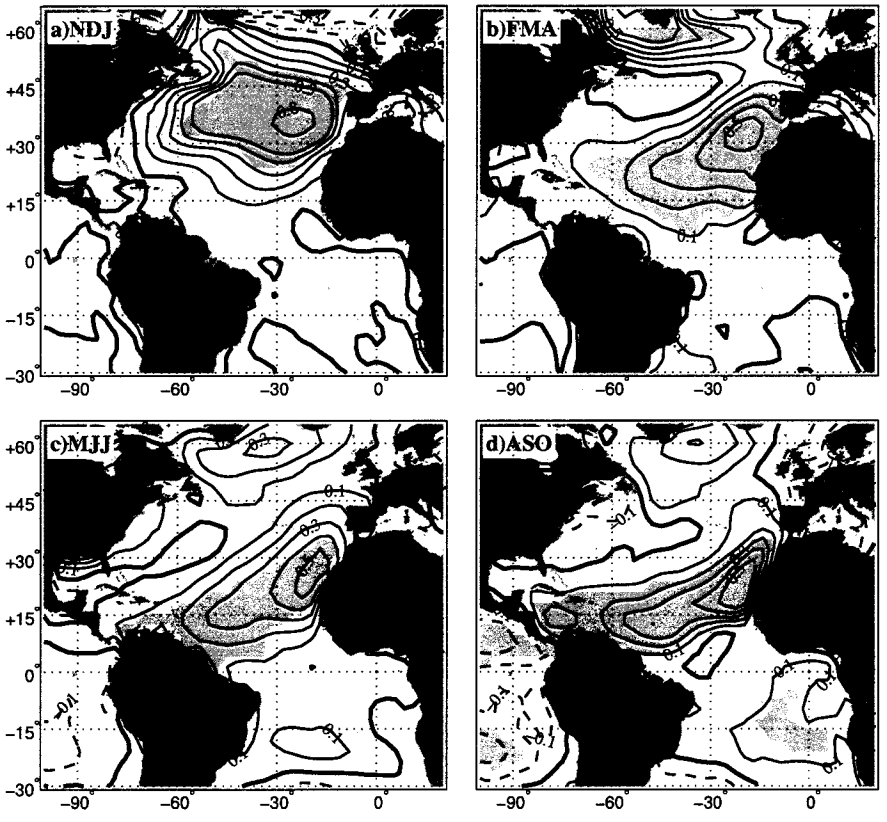

Figure 3.8: Mean SST difference between the warm and cold ensembles of the NCEP-based SOM.MID. The contour interval is 0.1^0C, negative contours are dashed and the zero contour is thickened. Shading indicates areas that are significant at the 95% confidence level.

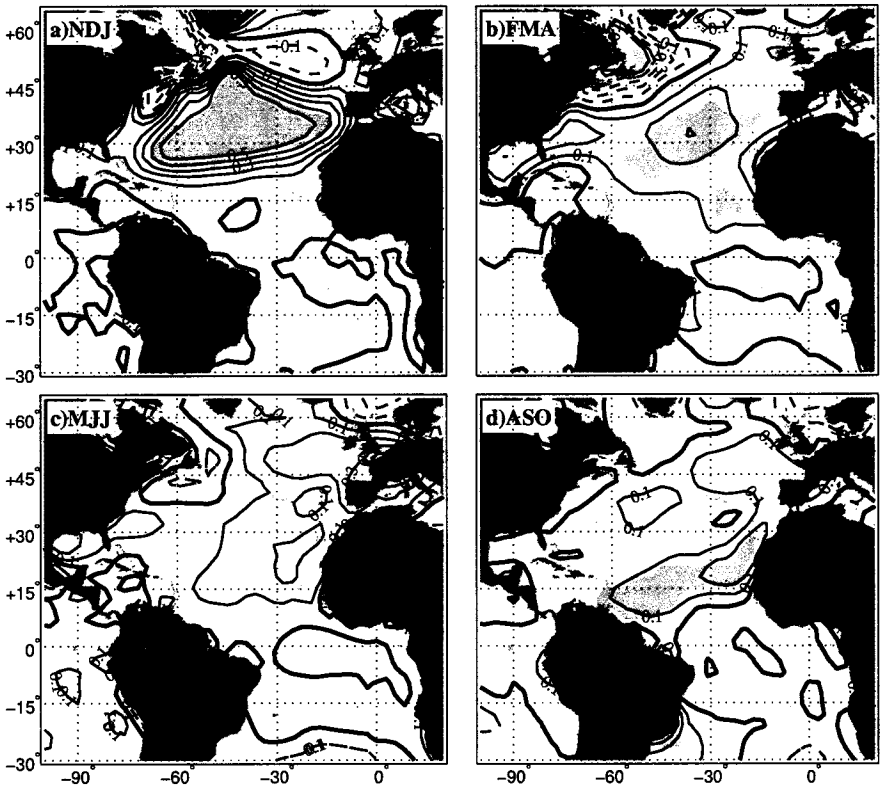

Figure 3.9: Mean SST difference for the Hadley-based SOM.MID.

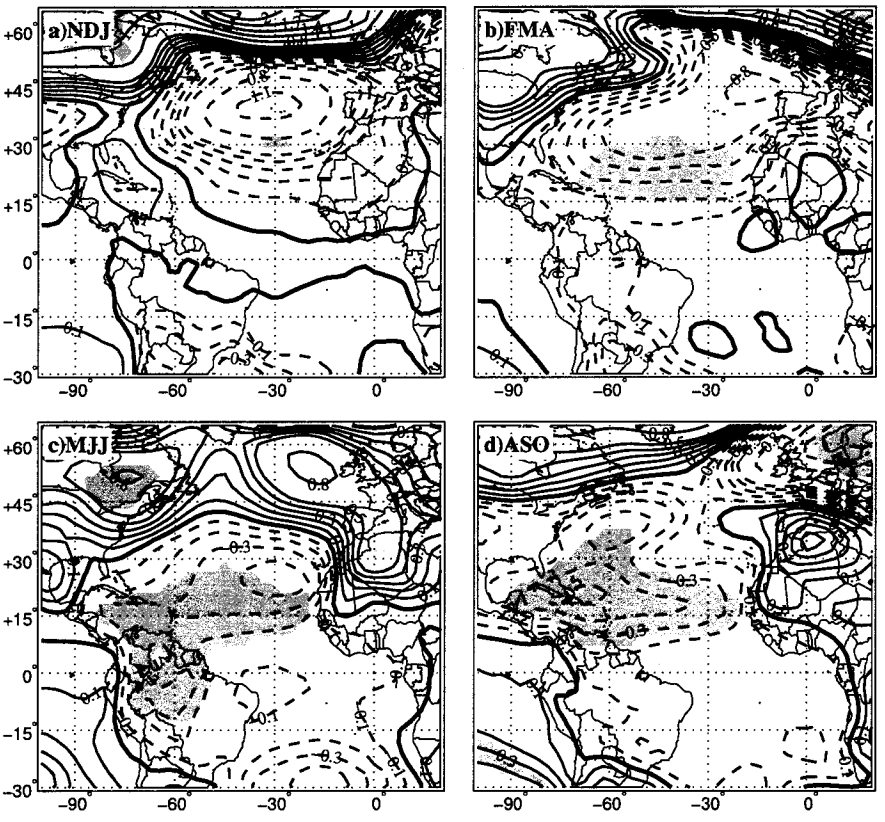

Figure 3.10: Mean SLP difference in the NCEP-based SOM.MID. Note that shading denotes the 90% confidence level.

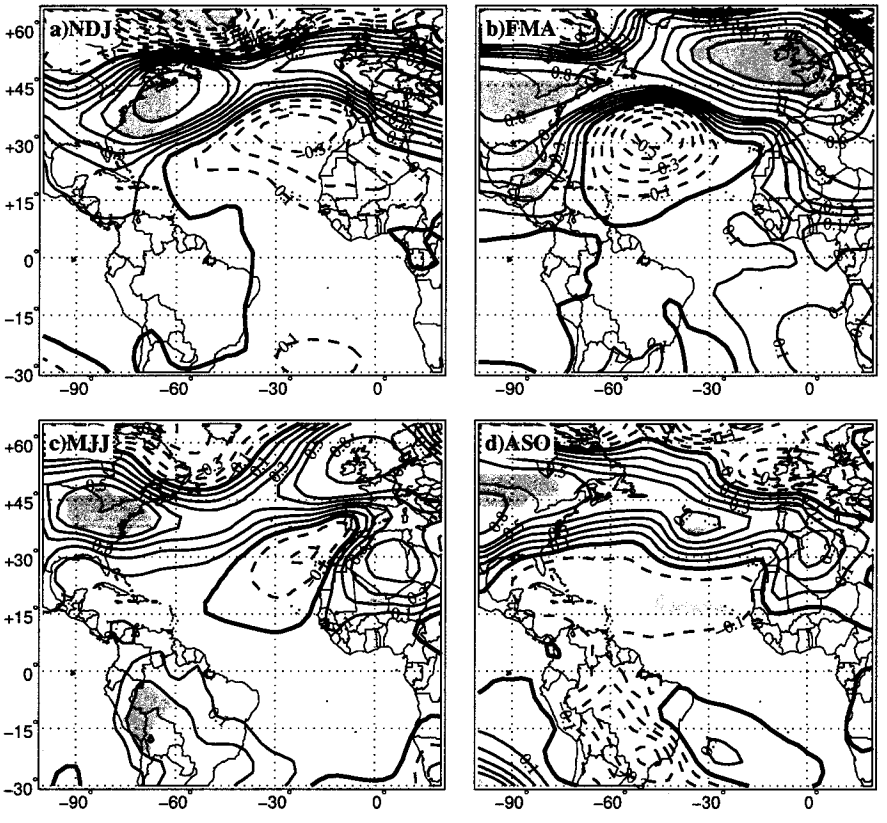

Figure 3.11: Mean SLP difference in the Hadley-based SOM.MID. Shading denotes the 90% confidence level.

(2003); Dahl et al. (2005)). The fast tropical response time and the use of a slab-ocean suggests the atmosphere is entirely capable of equatorward propagation of these extratropical thermal anomalies. To follow up on this, Fig. 3.12 shows the evolution of convective precipitation (hereafter, PRECC) in the NCEP-based SOM.MID experiment. The SOM.CLIMO reproduces the annual cycle of tropical and extratropical Atlantic PRECC well and two climatologically important areas of PRECC (values exceeding 4 mm day^{-1}) are denoted by the thick contour. Note the meridional movement of the ITCZ as well as the wintertime storm track regions are evident. During NDJ, a large swath of PRECC anomalies exceeding 0.2 mm day^{-1} are nearly perfectly collocated with the initial SST anomaly (see Fig. 3.8a). This also happens to coincide with the climatological storm track PRECC and later, we analyze the linearity of this response between the warm and cold ensembles.

During FMA, a lull in PRECC anomalies occurs, perhaps because the SST anomalies (Fig. 3.8b) are too far from either the north Atlantic storm track or ITCZ. Note that the ITCZ is at its southernmost climatological position during FMA. During MJJ, as the ITCZ position moves north with the seasonal cycle, the first tropical Atlantic PRECC anomalies appear in the eastern Caribbean Sea. Finally, by ASO, PRECC anomalies exceeding 0.2 mm day^{-1} flank the northern edge of the climatological ITCZ. Note that PRECC anomalies on the southern flank of the ITCZ are weaker and statistically insignificant. During ASO, PRECC anomalies also appear in the eastern Tropical Pacific, which has been seen in observational studies of the AMM (see Fig. 5 in Smirnov and Vimont (2011)).

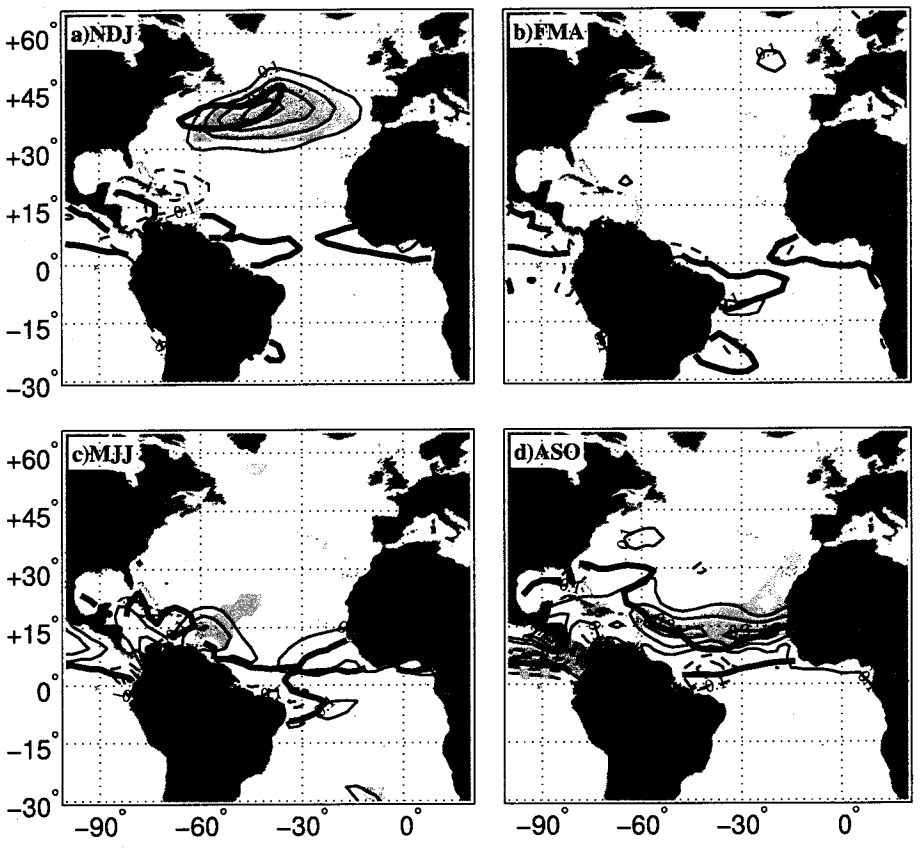

Figure 3.12: Mean difference for convective precipitation (in mm day^{-1}, contour interval 0.1) from the NCEP-based SOM.MID simulation. Shading denotes the 90% confidence level and the zero contour is omitted. The thick contour represents regions exceeding 4 mm day^{-1} from the control SOM.CLIMO simulation.

	SOM.Total[N]	SOM.Total[H]	SOM.Mid[N]	SOM.Mid[H]
$\Delta\overline{SST}$	**0.12**	**0.21**	**0.33**	**0.15**
$N_{w,sst} > N_{c,sst}$	17	21	23	20
$\Delta\overline{SLP}$	-0.08	-0.07	**-0.38**	**-0.16**
$N_{c,slp} > N_{w,slp}$	17	15	22	18

Table 3.1: Comparison of the mean difference in Main Development Region (MDR, 10-23°N, 60-15°W) SST and SLP anomalies from the NCEP (N) and Hadley (H) based SOM.MID and SOM.TOTAL simulations. Also shown is the number of instances, out of 30 total members, where the warm ensemble exceed the cold for SST, vice versa for SLP. Recall that SST and SLP anomalies are expected to be negatively correlated.

Since the tropical Atlantic response is of particular interest, further analysis is done by considering the intra-ensemble spread in SST and SLP in both the NCEP and Hadley-based SOM.MID simulations. Figure 3.13 shows the difference in SST (dark bars) and SLP (light bars) for each ensemble member during ASO, when the LIM indicates a AMM-like event. For now, it is sufficient to compare the warm and cold simulation (i.e. assume linearity); later, linearity is investigated by comparing each warm and cold ensemble to its respective SOM.CLIMO realization. When taken individually, 23 (22) out of the 30 ensembles show a higher (lower) SST (SLP) when the warm simulation is compared to the cold. If there were no difference between the ensembles, one would expect the warm ensemble to be higher than the cold 15 out of 30 times. A 1000-sample Monte Carlo test shows that for normally distributed populations (as the spread of ensembles is hypothesized to be), the 95% bounds on this value are 20 (or 10 for the case of SLP), showing the MDR SST anomalies are statistically significant. The mean difference between the warm and cold ensembles for the NCEP-based SOM.MID is 0.33 K and -0.38 hPa for SST and SLP, respectively. From the control SOM.CLIMO simulation, the interannual standard deviation of SST and SLP in the MDR during ASO is found to be 0.22 K and 0.38 hPa. Because these standard deviations are divided by $\sqrt{N}$ to obtain the "true" sample standard deviation,

where N is 30 realizations, the mean difference between the warm and cold ensembles is significant at the 99% level for both SST and SLP. Correlating each ensemble's SST difference with its SLP difference over the MDR yields an r^2 of -0.76 (significant at the 99% level), which signifies a strongly coupled process (Saravanan and Chang (1999)). Table 7 provides a summary of SST and SLP variations from the SOM.TOTAL and SOM.MID simulations.

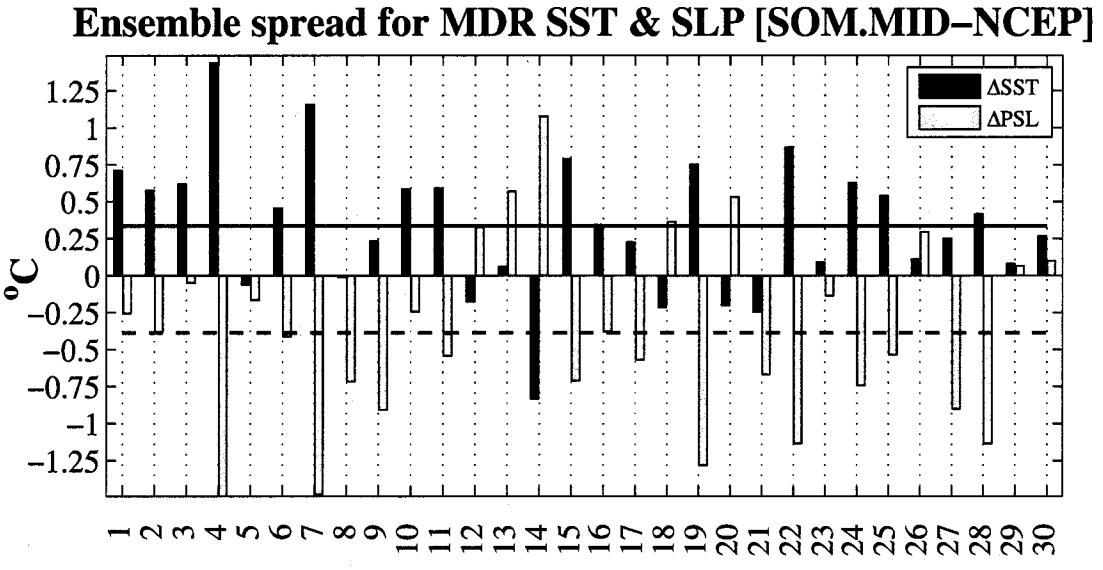

Figure 3.13: Individual ensemble spread (compared to SOM.CLIMO) for SOM.MID simulation for (a) SST and (b) SLP over the main-development region ($10-23$°N, $60-20$°W). The solid (dashed) line denotes the warm (cold) inter-ensemble mean.

Recall that one of the motivations to study AMM variability during ASO is the strong link to Atlantic hurricane activity. Past studies have shown that warming in the MDR coincides with reduced shear, both of which favor hurricane formation (Gray (1984); Goldenberg et al. (2001)). VK07 and KV07 showed that the AMM is also linked with key atmospheric variables like shear, vorticity and boundary-layer moisture. Smirnov and Vimont (2011) showed that the atmospheric anomalies can be well explained by the response of the atmospheric to AMM-like SST anomalies in

a CAM+SOM framework. With the SOM.MID simulation showing a strong AMM structure, we expect the associated baroclinic atmospheric anomalies to reduce shear. In accord, Fig. 3.14 shows the shear amplitude (calculated as the the difference in wind speed between 250- and 850-hPa) response in the NCEP-based SOM.MID simulation. Associated with the (+) SST during ASO is a statistically significant reduction of shear amplitude by nearly 0.5 - 1.0 m s^{-1} in the western portion of the MDR. Given that ASO is roughly 9 months into the simulation, the similarity between Fig. 3.14 and past observational studies (e.g. Fig. 7 in Smirnov and Vimont (2011)) is remarkable and suggests that the LIM can indirectly act as a tool for seasonal hurricane prediction. The robust, simultaneous increase in shear over the eastern tropical Pacific confirms past studies (e.g. Wang et al. (2007)) and is noteworthy because it is reproduced in a static ocean.

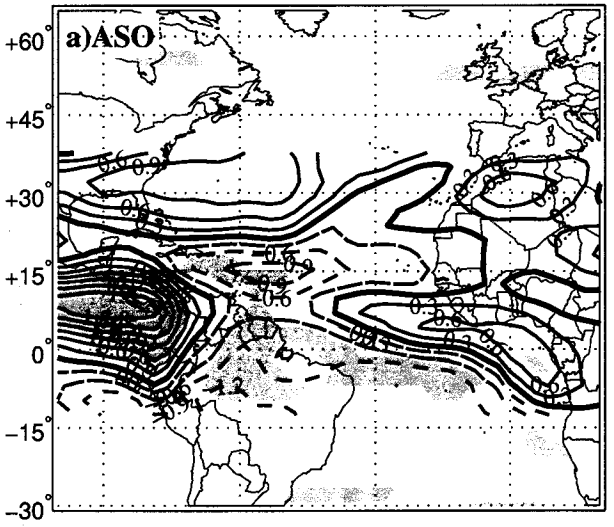

Figure 3.14: Same as Fig. 3.8 except for shear amplitude (SHRAMP: see text) during ASO. Shading denotes the 95% confidence level.

3.4 Physical Mechanism

The equatorward propagation of coupled air-sea thermal anomalies as shown by the NCEP-based SOM.MID in section 3.3 can be characterized by two processes. First is the extratropical atmospheric response to the initial SST anomaly. This response is very rapid and anomalies north of 35°N are lost within the first three months. Second is the gradual evolution of the SST anomalies from the subtropics into the tropics from FMA to ASO. The coupled response is discussed for the mid-latitudes in Section 3.4.1 and the for low-latitudes in Section 3.4.2.

3.4.1 Initial extratropical response

The initial period of the SOM.MID simulation characterizes the typical problem of the extratropical atmosphere's response to SST anomalies, which is amply found in literature due to several uncertainties that still remain. Unlike the tropics where positive SST anomalies are well correlated with a adjustment in localized deep convection (Gill (1980); Lindzen and Nigam (1987); Back and Bretherton (2009)), the mid-latitude situation is more complicated due to generally higher static stability that inhibits convection, as well as the periodic existence of unstable baroclinic transients with complex vertical structures (Held (1978); Hoskins and Karoly (1981)). Whereas a vast majority of past GCM experiments have prescribed Atlantic SST anomalies (Kushnir and Held (1996); Deser et al. (2004)), our coupled experiment is unique due to the surprisingly long persistence time of SST anomalies (though the signal transfers into the tropics). To investigate the initial atmospheric response, Fig. 3.15 shows the mean difference in the *net* surface energy flux (hereafter F_{NET} from eqn. 2) and its components; the radiative fluxes (shortwave and longwave) are combined. Although there is quiet a bit of scatter (not shown), the SOM.MID experiment suggests the mid-latitude atmosphere is damping SST anomalies between 30-40°N at an average rate of 25-40 W m^{-2},

which is consistent with previous GCM findings (Lau and Nath (1990); Power et al. (1995); Frankignoul et al. (1998)) and observations (Haney (1985)). By far the biggest contribution to F_{NET} is from the latent heat flux (F_{LH}), which is consistent with observations (Cayan (1992)), though off the east coast of North America, the sensible heat flux (F_{SH}) also contributes 5-10 W m^{-2} of damping due to the proximity of the large temperature gradient anchored by the Gulf Stream. The radiative flux anomalies (F_{SW} and F_{LW}) are generally positive due to less incoming shortwave from an increase in clouds (not shown).

Collectively, the sensitivity of the atmosphere to the SST anomaly during November is shown in Fig. 3.16 as the ratio, κ, of F_{NET} to SST, following Power et al. (1995)). In Fig. 3.16, κ is only calculated where $|\Delta SST| > 0.4$ K. Values of κ are between 10-25 W m^{-2} K^{-1} over the mid-latitude Atlantic, but there is large heterogeneity characterized by an overall increase towards the west. Note that southeast portions of the SST anomaly experience reduced or even negative damping (implying a positive feedback), which is significant for equatorward propagation during boreal spring, as discussed next.

Recall from Section 3.3 that, initially, the only statistically significant atmospheric response is an anomalous cyclonic circulation near 30°N and 30°W. Due to the anticyclonic background flow, this anomalous circulation simultaneously decreases the mean westerly winds to the north and easterly winds to the south. The thick dashed contour in Fig. 3.15a denotes the transition from mean easterlies to mean westerlies; thus, the anomalously weak F_{LH} due to the cyclonic circulation should cause warming SST in the region of mean easterlies. This is of critical importance to the rest of the simulation, and a simple thought experiment proves that this response would provide a much different result for domain-wide westerly flow. As many of the ensuing arguments are based off the the sensitivity of F_{LH}, it is appropriate to introduce the F_{LH} bulk

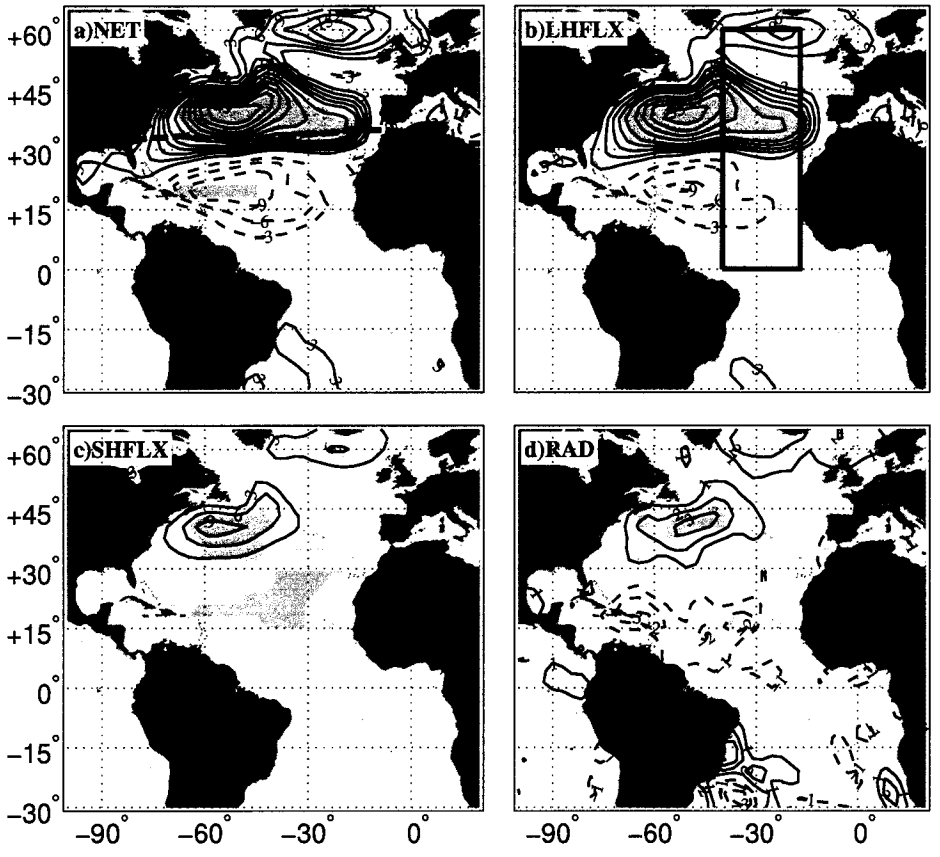

Figure 3.15: Mean difference in fluxes of (a) F_{NET}, (b) F_{LH}, (c) F_{SH} and (d) $F_{SW}+F_{LW}$ during November. Contour interval is 3 W m^{-2}, positive (negative) values are in solid (dashed) contours and shaded regions are significant at the 90% level. In (a), the thick dashed line indicates the boundary between mean surface easterlies and westerlies. In (b), the rectangular box is the averaging region for Fig. 3.19.

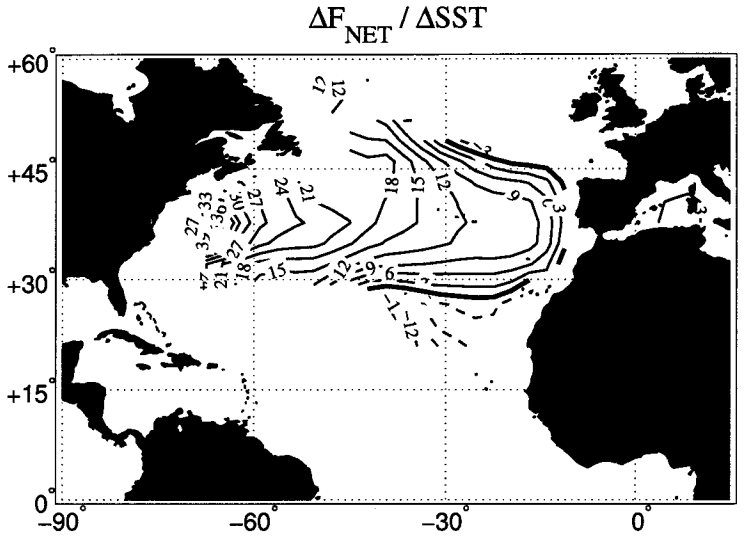

Figure 3.16: Mean ratio of $\frac{\Delta F_{NET}}{\Delta SST}$ for the NCEP-based SOM.MID simulations during November. The ratio is only calculated for SST differences exceed 0.4 K. Contour interval is 3 W m^{-2} K^{-1}, negative values are dashed and the zero contour is thickened.

formula used by CAM3:

$$F_{LH} = \rho_A C_E L_V W[q_s(SST) - RH \times q_s(T_{AIR})] \tag{11}$$

where ρ_A is the air density, C_E is a stability-dependent unitless surface drag coefficient and L_V is the latent heat of vaporization (2.5×10^3 J g^{-1}). W is the derived from the 10-m wind, $W = \sqrt{(u^2 + v^2 + w^2)}$, where the zonal, meridional and vertical wind speed values are used. More specifically, W, is the friction velocity that depends on the stability at the air-sea interface (Ban et al. (2010)). However, over most of the tropical Atlantic, the stability is fairly constrained because $SST - T_{AIR}$ does not vary appreciably. Notable exceptions occur in the stratiform cloud regions off the northwest coast of Africa and also near the coast of Angola and Namibia. The last term is the specific humidity gradient between the ocean surface and the lowest model level. In this final term, q_s is the saturated specific humidity evaluated for a given SST,

while RH and T_{AIR} are the relative humidity and air temperature at the lowest model level, respectively. The first three terms can approximately be assumed constant, $K = \rho_A C_E L_V \approx 3$, though in CAM3, these slightly vary with temperature, pressure and boundary-layer stability. Clearly, F_{LH} is mainly dependent on the variability in wind-speed and specific humidity gradient, $\Delta q = q_s(SST) - RH \times q_s(T_{AIR})$, and may contain non-linear interactions provided $W = W(\Delta q)$ or $\Delta q = \Delta q(W)$ which is shown to be the case by Mahajan (2008). However, in a linear sense, we can gauge the importance of the moisture and wind contribution to F_{LH} by separately constraining each one to climatological values taken from the control SOM.CLIMO simulation. In this "decomposition", the wind contribution to F_{LH} becomes:

$$F_{LH,W} = \rho_A C_E L_V W \Delta q_{CLIM} \tag{12}$$

which can be done for both the zonal ($F_{LH,u}$) and meridional winds ($F_{LH,v}$), while the moisture contribution is:

$$F_{LH,q} = \rho_A C_E L_V W_{CLIM} \Delta q. \tag{13}$$

Figure 3.17 shows the $F_{LH,u}$ and $F_{LH,q}$ components of F_{LH} during NDJ. Note that total F_{LH} (Fig. 3.17a) is *not* from the raw model output, but has been recreated using monthly-averaged values of wind and specific humidity. The fact that this calculation is very close to the model-calculated F_{LH} (not shown), which is averaged for every 20-min timestep, suggests that the use of monthly data is appropriate. The total F_{LH} is positive (negative) in regions of mean westerlies (easterlies) implying damping (generation) of SST anomalies. The wind component is responsible for most of the negative F_{LH} anomalies in the subtropics, while the increase in Δq leads to enhanced evaporation over the initially (+) SST anomalies in the mid-latitudes. To quantify the

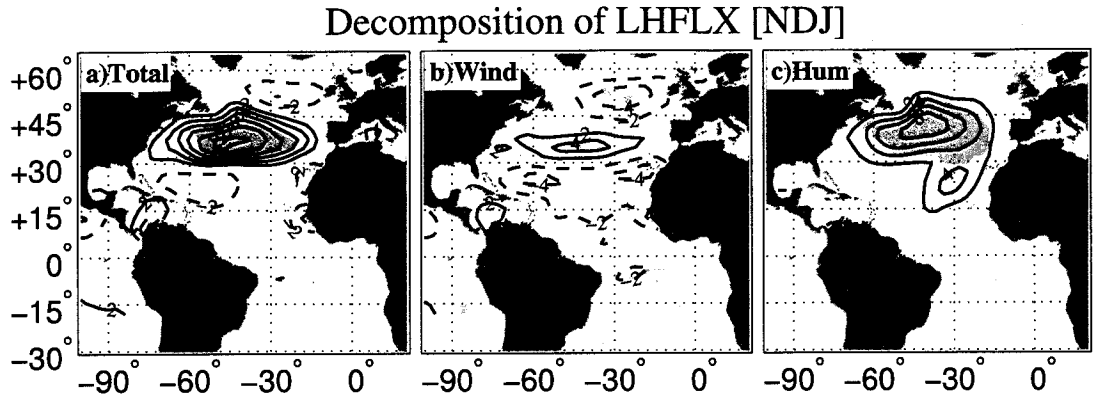

Figure 3.17: Decomposition of (a) F_{LH} into a (b) *zonal* wind contribution and (c) humidity contribution. Positive (negative) contours are solid (dashed) and imply upward (downward) heat transfer; the contour interval is 2 W m^{-2} and the zero contour is omitted. Shading indicates significance at the 90% confidence level.

impact of the latter, linearizing the Clausius-Clayperon equation around 298 K yields a sensitivity of $\frac{\delta F_{LH}}{\delta \mathrm{SST}} \approx 6$ W m^2 K^{-1}, assuming a constant relative humidity and a fixed value of $SST - T_{\mathrm{AIR}} = 1$K. Given such a large sensitivity, the temperature anomaly in a 50-m mixed layer can change by roughly 0.1 K within only one month.

To examine the atmospheric response over the full troposphere, Fig. 3.18 shows a longitude-pressure cross section of temperature (hereafter, T) and geopotential height (hereafter, Z) meridionally averaged from 30-40° to include the highest initial SST anomalies during NDJ. A local (implying directly overhead the SST anomaly that is between 25-55°W) baroclinic low and a downstream equivalent barotropic high characterize the response in the Z field. The local, low-level Z response is 8 m K^{-1}, or 1 hPa K^{-1}, which is on the low end of past studies, but recall that nearly all of those were uncoupled, SST-forced experiments. About 30° downstream (east) of the SST anomaly is a warm-core, equivalent barotropic high with a sensitivity of 10-15 m K^{-1} at 500-hPa, also in the lower range of previous experiments (e.g. Palmer and Sun (1985), found 20 m K^{-1} which is representative of similar other studies). The lon-

gitudinal position of the downstream high is also about 10° farther east than past studies, which could be due to our use of a coupled model. Although the combined baroclinic, equivalent barotropic response is remarkably similar to the linear model of (Hoskins and Karoly (1981), see their Fig. 4 and 5), it is likely a time-averaged picture that does not capture what occurred at any given time. For example, doing similar vertical cross-sections on monthly data leads to more emphasis of the baroclinic low during November, but also more scatter. This idea of a rapidly evolving atmospheric response is strongly supported by previous work with an SST-forced AGCM showing an initially intense baroclinic response giving way to an equivalent barotropic response within several weeks (Li and Conil (2003); Ferreira and Frankignoul (2005); Deser et al. (2007)). Regardless, the extratropical atmospheric anomalies decay within the first 2 to 3 months of the simulation, though leaving behind an important footprint in the subtropics, similar to the ENSO footprinting mechanism described by Vimont et al. (2001). The evolution of SST anomalies in the tropics starting in spring is described next.

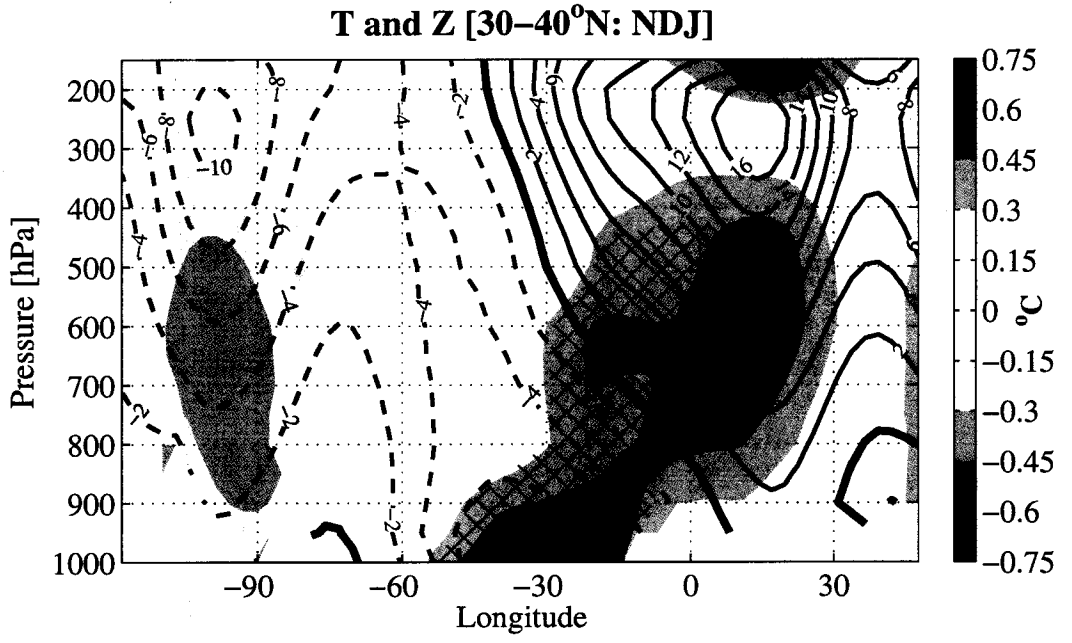

Figure 3.18: Longitude-pressure cross-section of the temperature (shaded) and geopotential height (Z, contoured, interval 2 m) from the NCEP-based SOM.MID simulation. Values indicate the mean difference between the warm and cold ensembles. Hatched regions are significant at the 90% confidence level. Positive (negative) values of Z are solid (dashed) and the zero contour is thickened.

3.4.2 Evolution into the tropical Atlantic

In the previous section, anomalies of F_{LH} are shown to be the main culprit in both eroding extratropical SST anomalies through enhanced evaporation and developing anomalies in the subtropics due to reduced easterly winds. To further explore this evolution, a Hovmöller diagram of SST and F_{NET} anomalies is shown in Fig. 3.19a. All anomalies were zonally averaged across the rectangular box shown in Fig. 3.15 in order to capture both the extratropical and tropical processes. Shown in Fig. 3.19b is the same F_{NET} as in (a) but also just the F_{LH} component (shaded). A quick inspection of panel (b) suggests that F_{LH} anomalies are indeed the largest contributor to the F_{NET} anomalies in this region. Notice the large negative F_{LH} anomalies of 4-8 W m^{-2} that originate in the subtropics starting in January. The same Hovmöller diagrams are shown for the Hadley-based SOM.MID simulation in Fig. 3.19c, d. Although there is also negative F_{LH} in the subtropics in the Hadley simulation, these develop one to two months later and only persist for one to two months. The differences between the two simulations highlights the importance of the southward extent of initial SST anomalies, which is roughly 3-5° latitude farther south in the NCEP-based initial conditions. However, this does not diminish the role of the mid-latitude SST anomalies, which are responsible for generating the anomalous circulation.

Next, F_{LH} is decomposed during the FMA period, a time when the bulk of the anomalous energy is delivered in the tropics as shown by the Hovmöller plots. Figure 3.20 shows that it is almost entirely the role of the wind in controlling the anomalous F_{LH}, implying an active WES feedback due to the presence of (+) SST anomalies during this time. However, a surprising finding is the lack of damping from the moisture component of F_{LH}, implying that the increase in Δq due to the Clausius-Clayperon relationship is being counterbalanced by the decrease expected due to the

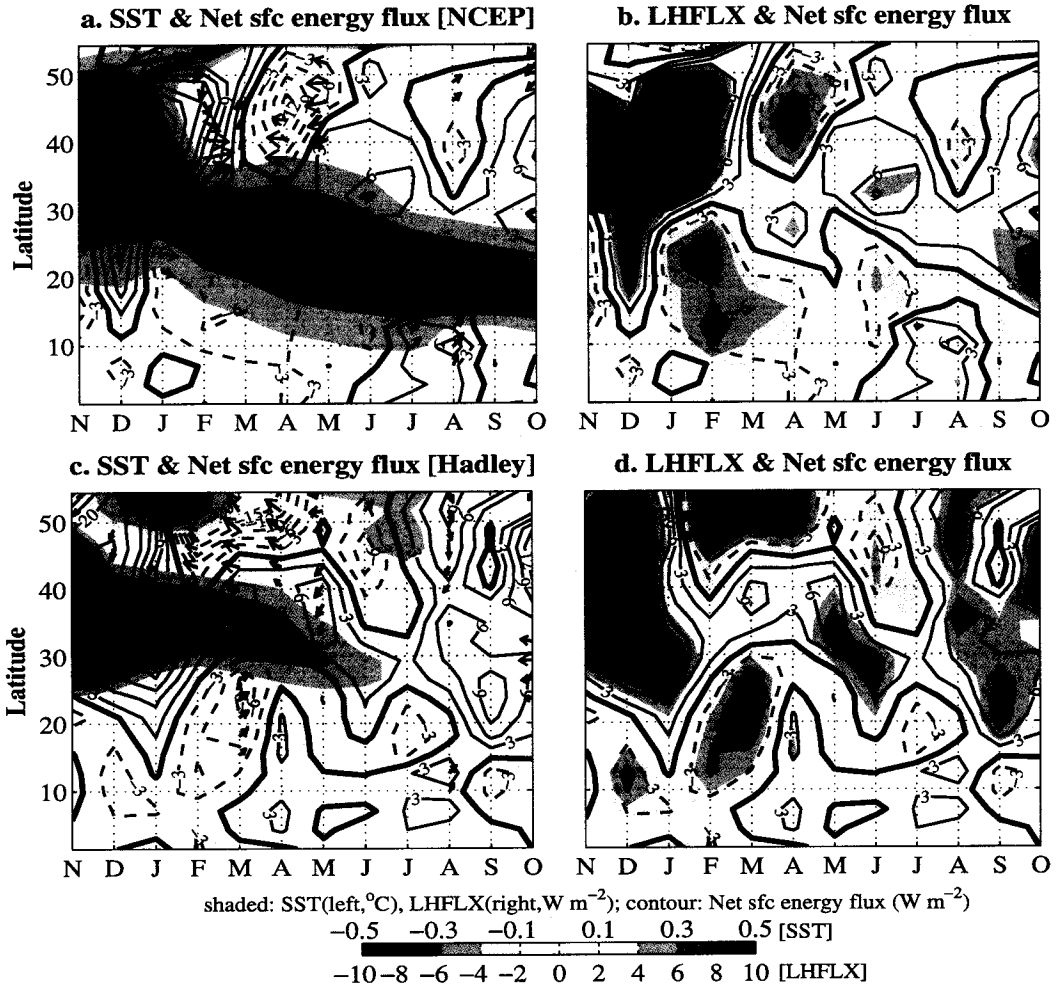

Figure 3.19: Hovmöller diagram (latitude vs. time) showing the evolution of (a) the mean difference in net surface energy flux (contoured) and SST (shaded) and (b) the mean difference in the net surface energy flux (contoured) and the latent heat flux (shaded) between the warm and cold ensembles of NCEP-based SOM.MID and. Panels (c) and (d) show the same Hovmöller diagrams, except for the Hadley-based SOM.MID. Also shown is the anomalous wind speed and direction, if significant at the 90% level. The values were zonally averaged from 60°W to 15°W.

advection of moister air northward by the anomalous low-level wind. The basis for the latter argument is shown in Fig. 3.21, where climatological Δq ranges from 8-11 g kg^{-1} over the northern Tropical Atlantic. Due to the lagged response of SST to anomalous F_{LH}, the anomalous wind affects the $q_s(T_{AIR})$ portion of Δq much faster than $q_s(SST)$.

Although the values of anomalous F_{LH} in the tropics are only -2 to -4 W m^{-2}, note that in our 50-m mixed layer, the forcing of SST can be re-written $\Delta SST = k\Delta t F_{NET}$, where $k = 0.012$. Thus, a 4 W m^{-2} anomaly can generate a ΔSST of 0.05°C within only 1 month. By late winter, the combination of SST (Fig. 3.8), SLP (Fig. 3.10) and F_{LH} anomalies collectively suggest that the WES feedback is active in the sustainment and further equatorward propagation of SST anomalies. It is notable that boreal spring is when the WES is most active in the tropical Atlantic due to its symmetric position with respect to the equator, which has been shown in observations (Xie and Carton (2004)) and models (Liu and Xie (1994); Vimont (2010)). Although the presence of the WES preliminarily corroborates past findings of extratopical forcing of tropical SST (e.g. Chiang et al. (2003); Chiang and Bitz (2005); Zhang and Delworth (2005); Mahajan et al. (2009)), it does not quantify the role of the WES in equatoward SST propagation, nor does it prove that no propagation would occur in the absence of the WES, which was shown by Mahajan et al. (2011) not to be the case. Later, we conduct a tailored experiment to remove the WES feedback to elaborate on this point.

Referring back to Hovmöller diagram of the NCEP-based SOM.MID simulation (Fig. 3.19, note the abatement of F_{LH} starting in April, though F_{NET} is still negative (into the ocean). A closer inspection of the individual components of F_{NET} shows that radiative fluxes become important, with the shortwave radiative flux (F_{SW}) generally dominating the longwave radiative flux (F_{LW}), consistent with the reduction of mainly low-clouds over (+) SST anomalies in CAM. This kind of relationship is not unexpected for low-cloud dominated regions, such as the eastern subtropical North Atlantic. We

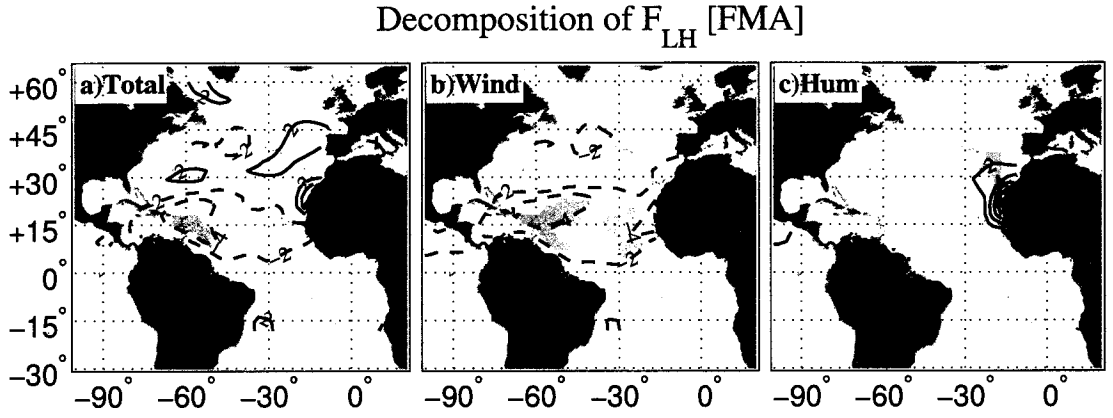

Figure 3.20: Decomposition of (a) total F_{LH} into a (b) wind contribution and (c) moisture contribution, as in Fig. 3.17 but for FMA.

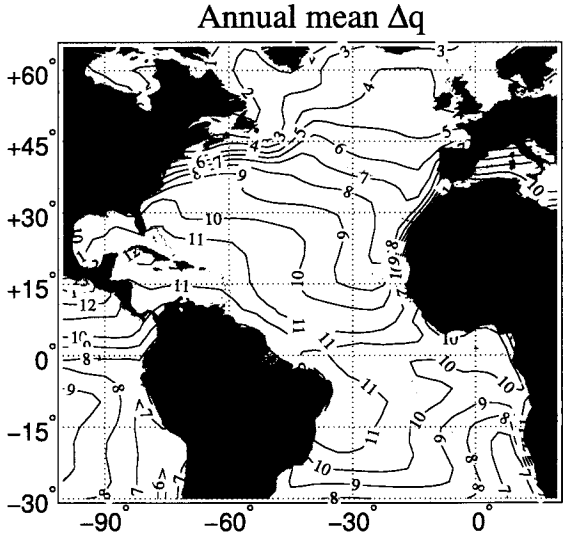

Figure 3.21: Annual mean Δq from the control SOM.CLIMO simulation. Contour interval 1 g H_2O kg^{-1} air.

defer on further discussion of this topic until later in the manuscript.

Lastly, the atmospheric circulation is analyzed in the subtropics using a longitude-pressure cross-section, as in Fig. 3.18 except between 10-22°N, shown in Fig. 3.22a. A baroclinic circulation is seen with a low-level cyclone and upper-level anticyclone, which is consistent with past theory (e.g. Gill (1980)) for steady-state tropical circulation with an anomalous heat source. During FMA, the circulation is rather weak and is only significant below 900 hPa, as shown by the black sounding taken over the largest (+) SST between 60-25°W in Fig. 3.22b. However, the anomalous circulation grows in amplitude and becomes roughly three times stronger during ASO (blue sounding) compared to FMA, probably due to the presence of a convectively active background state in the former (compare the precipitation anomalies in Fig. 3.12b,d). In accord, the anomalous diabatic heating is maximized within the boundary layer during FMA, but in the mid-troposphere near 500-hPa during ASO (not shown). The increase in the amplitude of the anomalous circulation is unexpected given its occurrence is six months into the coupled simulation, and reiterates the importance of the evolving background state, which is later explored in further detail. In next chapter, we further explore critical aspects of the mechanism that has been proposed in this section in order to quantify the importance of the WES and radiative feedback, seasonality and linearity.

3.5 Discussion

The results of the SOM.TOTAL and SOM.MID experiments yield a rather unprecedented persistence of significant SST anomalies, especially given the use of a coupled model. The response to the OPT forcing pattern is characterized by a fast extratropical atmospheric excitation from November through February, followed by a more gradual equatorward propagation through the boreal spring and fall. Attention is focused on the NCEP-based SOM.MID ensembles due to the most vivid depiction of

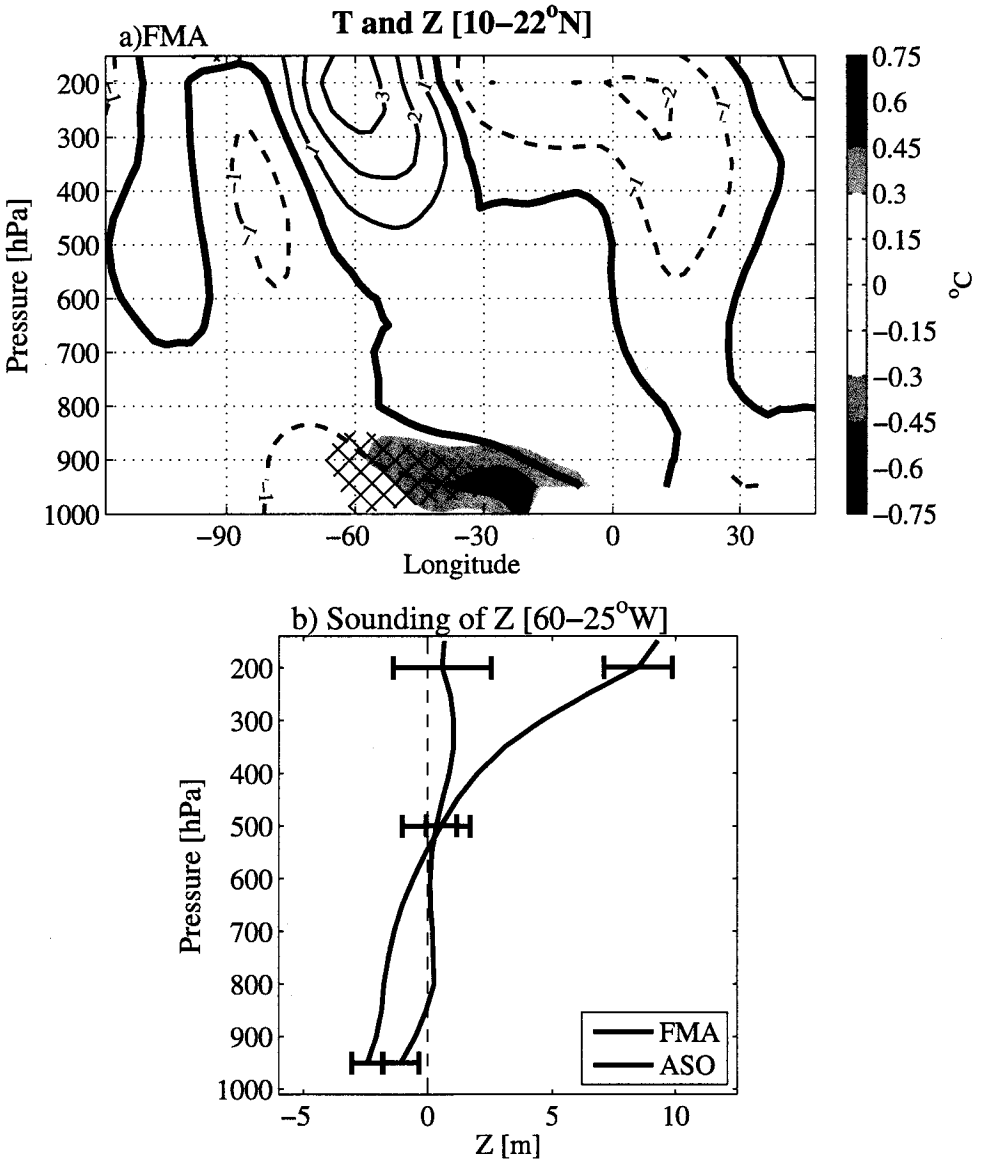

Figure 3.22: (a) Same as Fig. 3.18 but in the Tropical Atlantic [10-22°N]. Also contour interval for Z is 1 m. (b) Sounding of Z zonally averaged between 60-30°W from (a) during FMA (black) and ASO (blue). A inter-ensemble standard deviation is shown as the bars at 950, 500 and 200-hPa.

an AMM-like event; however, all SOM.TOTAL and SOM.MID experiments yielded some positive SST anomalies in the tropical Atlantic with statistical significance. The SOM.LOW experiments are discarded with relatively high confidence due to uncertainty in the LIM initial condition and the robust result by SOM.MID. However, it may be worth repeating a SOM.MID experiment that contains a dynamically coupled equatorial Atlantic Ocean, such as the Zebiak and Cane (1987) type model to see if the AMM can indeed be forced by Atlantic Nino variability, as discussed in Okumura and Xie (2006).

While the confirmation of Vimont's (2011) LIM result in a coupled model is certainly an accomplishment, it must be remembered that the CAM+SOM framework, by design, tends to accentuate thermodynamically coupled modes such as the AMM. Thus, it still remains to be seen whether our result can withstand several additions to bring the conclusion closer to reality. First is the impact of ENSO and its teleconnections into the Atlantic Ocean (Trenberth et al. (1998); Alexander et al. (2002)), especially given the overlapping seasonality of ENSO forcing which peaks in the winter. Second is the inclusion of oceanic dynamics, notably Ekman advection, which may be important on the time scales considered here (Lee et al. (2008)). The omission of sub-mixed layer oceanic dynamics may be acceptable given the relatively fast, seasonal evolution. For example, "freshwater hosing" experiments require at least several years before a robust change in the ITCZ (Dong and Sutton (2002); Dahl et al. (2005)). Ocean dynamics aside, the rest of this manuscript is dedicated to scrutinizing the mechanism presented in the previous section.

4 SENSITIVITY EXPERIMENTS

The SOM.MID experiment answered the critical question posed within this manuscript: the signal suggested by the LIM experiment appears legitimate and is unlikely to be a statistical artifact. Thus, the hypothesis can be modified accordingly to state: given that the SOM.MID simulation portrays a realistic depiction of extratropical-tropical interaction, what are the processes that play a central role in the excitation of tropical Atlantic variability? Based on various aspects of the SOM.MID experiment along with past literature, we can design several sensitivity tests. First, several studies (Mahajan (2008); Chiang and Bitz (2005); Chiang et al. (2008)) have proposed the WES feedback to serve as the main player in communicating extratropical SST anomalies equatorward. Yet, close inspection of Chang et al. (1997) and Xie (1999) suggests that the WES may only act within 15-20° of the equator and eventually succumbs to the overwhelming role of damping due to enhanced evaporation associated with a warmer SST. *Thus, one test is to remove the WES feedback to see in the result in SOM.MID can be reproduced.* Second, we focus on seasonality, both because it is found to be important in the LIM result of Vimont (2011) and that there is uncertainty in the GCM-dependence of extratropical air-sea experiments (e.g. Kushnir et al. (2002)). *Can we obtain the same AMM excitation given forcing in other seasons besides boreal fall?* Thirdly, early GCM simulations with prescribed extratropical SST anomalies suggest very large non-linearities (Pitcher et al. (1988); Kushnir and Lau (1992)), yet more recent studies (Deser et al. (2004)) show a modest adherence to linearity. *Does the development of the AMM during boreal fall show a bias when warm or cold ensembles are analyzed separately?.* Finally, the last experiment stems from the lack of F_{LH} anomalies during early boreal summer in the SOM.MID experiment. *Is there an alternate forcing of tropical SSTs during this time, or is it simply a lack of damping*

that sustains the AMM through boreal fall? The ensuing four sections target these issues in their respective order.

4.1 Shutting off the WES feedback

In discussing the physical mechanism of the SOM.MID simulation, a great deal of emphasis was placed on the anomalous F_{LH} which generated a WES-feedback beginning in early spring. Due to the relative simplicity of the CAM+SOM mixed layer heat budget equation and based on prior work of Mahajan (2008) and Mahajan et al. (2011), one test for the robustness of the SOM.MID result is to run a separate experiment where wind speed variability is eliminated. This is done by fixing W in eqn. 11 to seasonally varying climatology in the calculation of the the turbulent heat fluxes over the tropical Atlantic Ocean (between 30°S-30°N). If the WES is indeed the main culprit in the equatorward propagation and generation of an AMM event, then removing the WES feedback should preclude SST anomalies in sensitive regions. A discussion of the details of how the WES is removed is found in Appendix 7.2, but generally follows the steps outline by Mahajan (2008). In generating a stable, WES-deprived climate, the Q-flux must be recalculated based on a new CAM+DOM experiment (DOM.WES-OFF in Table 2.3) simulation with prescribed winds as in the CAM+SOM. To first order, the climates of the DOM.CLIMO and DOM.WES-OFF are similar, though as expected, the DOM.WES-OFF suppresses SST, F_{LH} and consequently precipitation variance in WES-sensitive regions, in some cases by 50%. This is consistent with a similar experiment by Mahajan (2008) and suggests that the suppression of the WES feedback is working properly, though the reduced variability must be kept in mind when directly comparing the WES-OFF results to the unperturbed GCM. With the new Q-flux obtained, we now turn to the results of the coupled SOM.WES-OFF simulation.

Shown in Fig. 4.1 and 4.2 is the evolution of the mean difference in SST and

SLP, respectively, between the warm and cold simulations of NCEP-based SOM.WES-OFF (see Table 2.3; note that a Hadley-based SOM.WES-OFF was not conducted). During NDJ and FMA, the evolution of the SOM.WES-OFF is nearly identical to the SOM.MID, with a quick reduction of SST anomalies north of 40°N by FMA. The atmospheric response is a similar downstream (-) SLP anomaly, though it is more (less) significant during NDJ (FMA); the difference perhaps attributed to intrinsic atmospheric variability. By ASO, the SST anomaly pattern modestly resembles the AMM, though the amplitude, as measured over the MDR, is reduced by 70% compared to SOM.MID (see Fig 3.8). Similarly, the SLP response still features a downstream (-) SLP anomaly and (+) upper-level height anomaly (not shown), but that amplitude is reduced by 55%. A comparison of SOM.WES-OFF to SOM.MID during ASO is provided in Table 4.1. Note that the SST and SLP differences are lower in SOM.WES-OFF, but still significant due to the reduced variance of SST, F_{LH}, etc., in the SOM.WES-OFF framework (see Fig. 7.7 in Appendix 6.2). Notably, 26 out of 30 "warm" ensembles in SOM.WES-OFF are warmer than their "cold" counterpart, compared to 22 in the SOM.MID. Yet, off the northwest coast of Africa, there are virtually no SST anomalies in the SOM.WES-OFF, where SOM.MID shows its maximum signal of anywhere in the Tropical Atlantic, at roughly 0.5°C. Thus, the WES feedback is extremely important to maintaining the *amplitude* and *structure* of an AMM-like response. However, the fact that robust tropical SST and SST anomalies are obtained implies that the WES feedback cannot be a critical factor to the excitation of the AMM, only an amplifier. This same conclusion was reached by Mahajan et al. (2011) and strongly suggests the need to further analyze the cause of SST anomalies in the SOM.WES-OFF simulation.

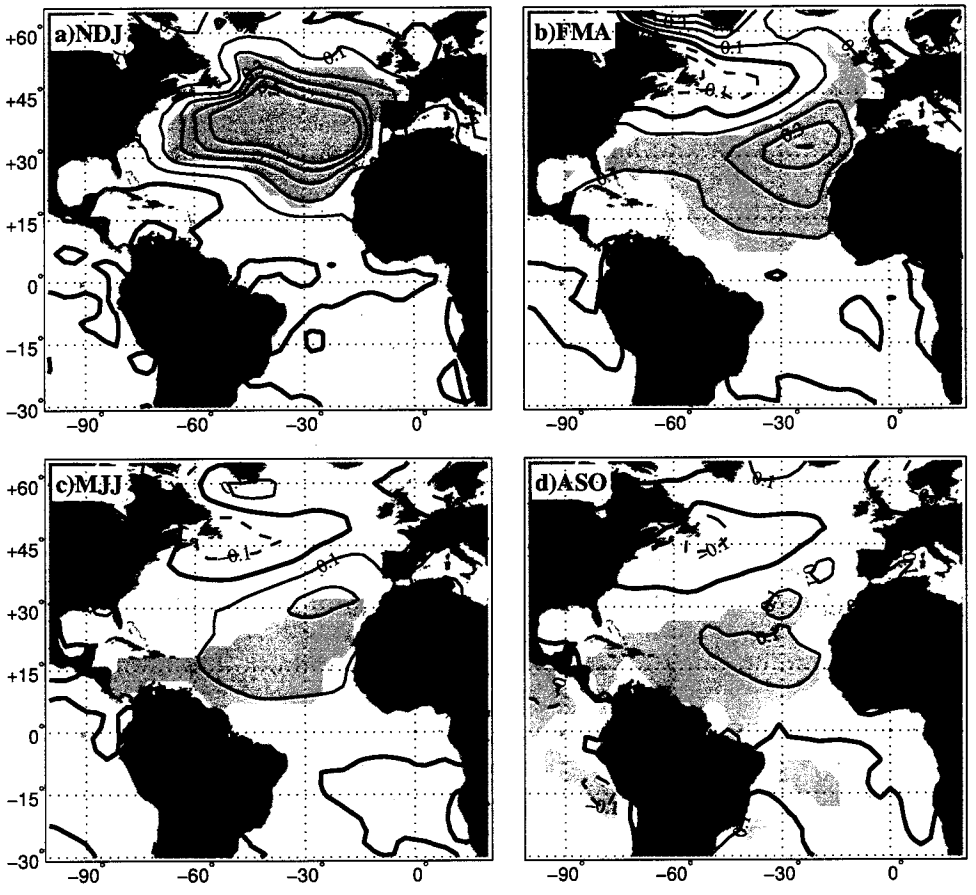

Figure 4.1: Evolution of SST in the SOM.WES-OFF experiment.

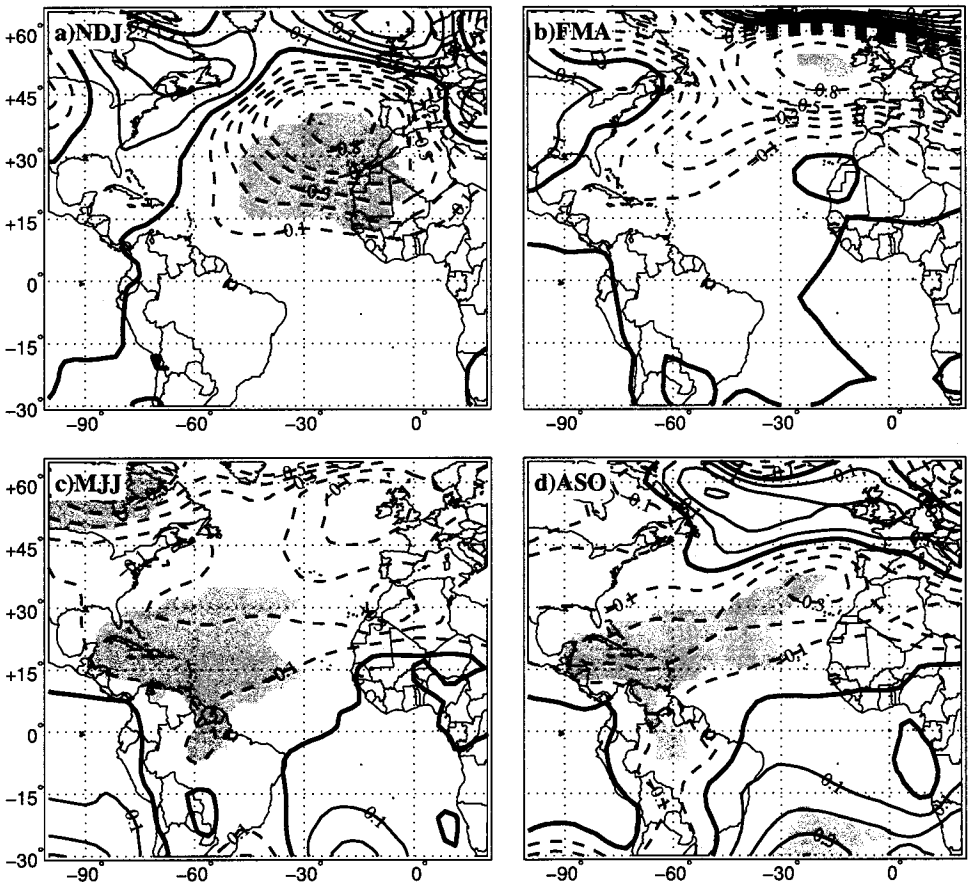

Figure 4.2: Evolution of SLP in the SOM.WES-OFF experiment.

	SOM.MID	SOM.WES – OFF
$\Delta\overline{SST}$	**0.33**	**0.10**
$\Delta\overline{SLP}$	**-0.38**	**-0.16**
$N_{w,sst} > N_{c,sst}$	23	26
$N_{c,slp} > N_{w,slp}$	22	22
$r\{SST_i, SLP_i\}$	**-0.76**	**-0.79**

Table 4.1: Comparison of the mean difference in Main Development Region (MDR, 10-23°N, 60-15°W) SST and SLP anomalies from the NCEP-based SOM.MID and SOM.WES-OFF simulations. Also shown is the number of instances, out of 30 total members, where the warm ensemble exceed the cold for SST, vice versa for SLP. Recall that SST and SLP anomalies are expected to be negatively correlated.

As with the analysis of the SOM.MID simulation, a latitude-time Hovmöller was created to show the equatorward propagation of SST anomalies and the net surface energy flux that causes them, shown in Fig. 4.3a. The extratropical portion of the Hovmöller is very similar to the SOM.MID (see Fig. 3.19), which is reassuring given that the WES-OFF modifications are restricted to north of 30°C. Interestingly, the region between 5-18°N is experiencing (-) F_{NET} anomalies through February, implying warming SST. Figure 4.3b compares F_{NET} with only the F_{LH} component, showing that nearly all of this warming is due to F_{LH}. Given that the wind speed is imposed in the F_{LH} calculation, it is peculiar that F_{LH} anomalies are still observed. Obviously this leaves the specific humidity portion of F_{LH} as the culprit as suggested by Chiang and Bitz (2005) and Mahajan et al. (2011). It is plausible to envision a scenario where the initial extratropical SST anomaly moistens the boundary layer (in terms of *specific*, not *relative* humidity) and this moisture anomaly is advected south and west by the *mean* easterly winds. This deserves some further attention.

It is not clear how the role of Δq fits into the WES feedback, though humidity changes were argued to be important in past experiments of extratropical-tropical interaction (Chiang et al. (2003); Chiang and Bitz (2005); Mahajan et al. (2011)). In

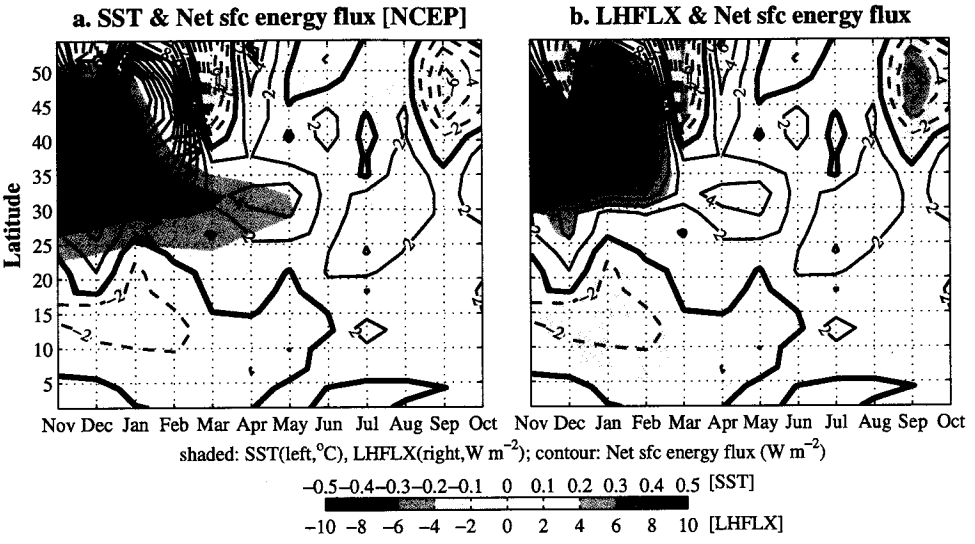

Figure 4.3: Hovmöller diagram (latitude vs. time) showing the evolution of the mean difference in net surface energy flux (contoured) and SST between the warm and cold ensembles of NCEP-based SOM.MID. The values were zonally averaged from 60°W to 15°W.

the WES feedback paradigm (Xie and Philander (1994); Liu and Xie (1994); Vimont (2010)), a seemingly passive role for Δq is implied in the following manner. Given SST anomalies in the tropical Atlantic, the anomalous atmospheric circulation acts to reinforce the SST anomalies through the wind-induced component of F_{LH}, consistent with the high correlations between anomalies of wind and F_{LH} (e.g. Fig. 8 in Mahajan (2008); also Vimont (2010)). With a purely passive role for Δq ($\Delta q \neq \Delta q(W)$), this implies *negative* correlations between anomalies of wind (W from eqn. 11) and Δq as the wind-induced SST anomalies enhance the evaporation (damping) rate through the Clausius-Clayperon equation. This correlation is shown in Fig. 4.4 for the SOM.MID and SOM.WES-OFF simulations. In the SOM.MID simulation, large areas of negative anomalies exist, consistent with the WES feedback argument. However, several areas of positive correlations are present namely near 20-25°N, 30°W. However, in the SOM.WES-OFF simulation, the near-absence of negative anomalies suggests that no

WES feedback is present, which seems reasonable given the goal of the experiment. Yet, the presence of large areas of positive correlations suggests that *substantial secondary effects of W anomalies have not been removed.* Through the non-linear advection terms, $\vec{W} \cdot \nabla(\Delta q)$, anomalies of W can still generate SST anomalies through anomalous advection up the gradient of Δq, which was already shown to have large *spatial* gradients in Fig. 3.21.

Another secondary complication seems to be that the anomalous wind will quickly advect boundary layer moisture, but only slowly impact the SST, thus decreasing Δq. This may explain why the anomalies of F_{LH} occur earlier in the SOM.WES-OFF compared to the SOM.MID simulations (compare the Hovmöller plots in Fig. 3.19 and4.3 during the boreal winter and early spring). The importance of humidity gradients is currently being investigated by prescribing the specific humidity gradient, much the same as prescribing surface wind for the WES-OFF experiments. Thus, the WES-OFF experiment and the WES feedback argument motivates additional sensitivity studies where Δq is constrained, which is an active area of research presently.

4.2 Impact of seasonality

The importance of seasonality in extratropical air-sea interaction cannot be overemphasized. Past modeling studies (e.g. Peng et al. (1995), Peng et al. (1997)) have shown that forcing with SST anomalies during late boreal fall results in a nearly opposite atmospheric response compared to winter. While there is a growing body of observational evidence suggesting that the extratropical atmosphere in the Atlantic is most sensitive to underlying SST anomalies during late fall and early winter (Czaja and Frankignoul (2002); Wu et al. (2004); Cassou et al. (2004); Wang et al. (2004)), this has yet to be proven in coupled GCMs. The aforementioned studies are mostly concerned with the large-scale impact of SSTs, for example, how they relate to NAO variability;

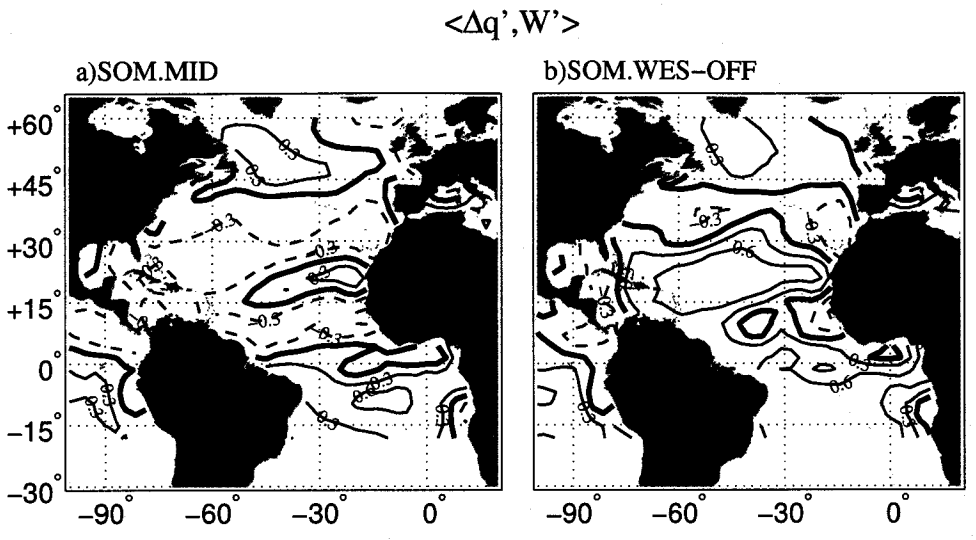

Figure 4.4: Correlation between anomalies of W and Δq in the (a) SOM.MID and (b) SOM.WES-OFF simulations. Positive values are solid, negative dashed and the contour interval 0.3. The zero contour is thickened.

the local atmospheric response is somewhat overlooked. Also, the LIM in KV07 and Vimont (2011) is seasonally invariant (though it is possible to roughly determine the role of seasonality through the amplitude of the "noise" term, ζ, in eqn. 4). However, as shown in Vimont (2011), there is distinct seasonality in the skill of forecasting the AMM based on the LIM which peaks when the forecast is made for boreal fall AMM. This suggests the need to test whether the AMM can be excited when forcing during seasons other than boreal fall.

To investigate the role of seasonality, the DOM.MID simulation (see Table 2.3) is conducted by forcing the uncoupled CAM3 with the boundary conditions of the LIM-based OPT superimposed onto the climatological SST. As in the coupled experiments, both a warm and cold simulation is conducted. The simulation is run for 10 years and each month of any given year is assumed independent of the same month a year before and after, leading to 10 "ensemble members". Figure 4.5 shows the difference

in F_{LH} and SLP between the warm and cold simulations averaged for early (a) and late winter (b) forcing. First, note that the structure of SLP during NDJ looks similar to the coupled simulation (Fig. 3.10a), which is a good reaffirmation that SST anomalies are driving the atmosphere. During NDJ, both DOM.MID and SOM.MID show a lowering of SLP over warmer SSTs between $30^o - 40^o$N. As one may expect, this results in negative F_{LH} anomalies, as seen in the DOM.MID experiment (Fig. 4.5a) due to a relaxation of trade winds. The subtropical F_{LH} anomaly is more substantial in the uncoupled versus coupled simulation during NDJ, though by FMA, the coupled simulation also has 10-15 W m^2 F_{LH} anomalies. However, during FMA, the DOM.MID shows a much different scenario where there is an absence of negative SLP anomalies and consequently, F_{LH} is upward over most of the North Atlantic, indicating a damping of the prescribed SST anomalies at roughly 15-20 W m^{-2} °C, which is on the low end of the range seen in past uncoupled experiments (Frankignoul et al. (1998)).

The main point of the DOM.MID experiment is to show that forcing with the OPT during February (rather than November) results in a very different tropical forcing. While this preliminary finding may partially explain why the LIM-based forecasting of the AMM is strongly seasonally dependent, it remains to be seen why this is the case, in the mechanistic sense. Past studies have suggested that the difference in the mean and transient atmospheric states between early and late winter should be the main controlling feature of the atmospheric response (Lau and Nath (1990); Kushnir and Held (1996); Kushnir et al. (2002)). An in-depth analysis of this, as in LAU and Nath (1991), requires higher temporal resolution than our experiments and is beyond the scope of our main conclusions. One important revelation, however, is the necessity to consider the localized atmospheric response to SST, rather than the projection onto the large-scale anomalies.

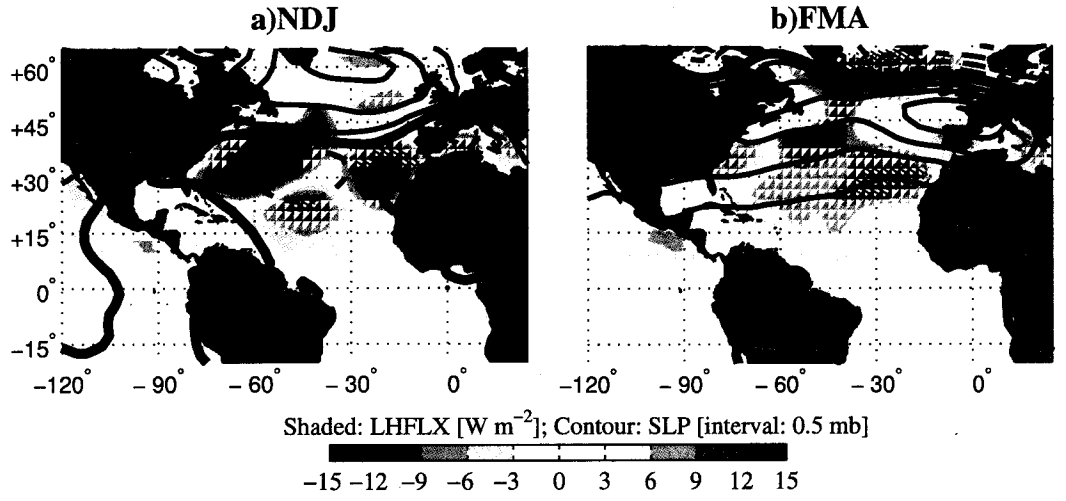

Figure 4.5: The mean difference in the F_{LH} (shaded) and SLP (contoured, interval 0.5mb) between the warm and cold polarity simulations of DOM.MID averaged over (a) NDJ and (b) FMA for the 10 years of the simulation. The hatching denotes areas of F_{LH} significantly different from zero at the 90% confidence level. For SLP, the zero contour is thickened.

4.3 Linearity of response

By construction, the LIM cannot provide much insight into the linearity of the geophysical system that it models, at least not through the dynamical matrix, **B**. Past modeling studies of extratropical air-sea interaction (e.g. Pitcher et al. (1988); Kushnir and Lau (1992)) have found large non-linearities, though the extent to which this is GCM-dependent remains to be seen. One simple and illustrative example of how a non-linear response can occur is through convection: if a perturbed system is normally convectively active, then a warm and cold SST anomaly should have roughly the opposite effect. If the system does not normally experience convection, a cold SST anomaly cannot produce negative precipitation anomalies.

To investigate linearity in our coupled system, we individually compare the warm and cold simulations to the control SOM.CLIMO simulation. For interpretation, the

cold response (hereafter, CLIM-C) is multiplied by -1 so that it would be identical to the warm response (hereafter, W-CLIM) if linearity is obeyed. The linearity test is shown in Fig. 4.6 for SST and in Fig. 4.7 for SLP. In both the SST and SLP field, it may appear that the response is initially strongly non-linear because during NDJ, both the warm and cold responses project onto the (-) NAO (compare 4.6a and b) though the warm response projects much more strongly). However, given the relatively limited ensemble size and large amount of internal atmospheric dynamics, investigating the projection onto the large-scale atmospheric modes may not be all that useful. Instead, it is worthwhile to closely inspect the *local* atmospheric response to the SST anomaly, which would be more comparable to the arguments by Hoskins and Karoly (1981). In Fig. 4.6a and b, note that the only region to respond linearly is over and just downstream of the original SST anomaly (inspect the region around 35°N and $25 - 30$°W), though the cold response is notably more significant than the warm. In Fig. 4.7a and b, it is seen that this same region also has a linear response in the SLP fields, even though the NAO projections are wildly different. These arguments reiterate the earlier conclusion that it is the local atmospheric response just downstream of the SST anomaly that is essential for the ensuing equatorward propagation. By MJJ and ASO, both the SST and SLP fields resemble a (+) AMM and linearity is obeyed to first-order.

Another important atmospheric metric to investigate linearity is the role of precipitation. The SOM.CLIMO reproduces the mean precipitation in the Atlantic "storm-track" region well compared to a satellite-based reanalysis from 1979-2008 (Xie and Arkin (1997); not shown). Fig. 4.8 shows the warm and cold responses in convective precipitation (stratiform precipitation was much weaker except towards the higher latitudes, not shown) during NDJ. For reference, the climatological storm track precipitation during the winter months can be found in Fig. 3.12a. It is clear that the

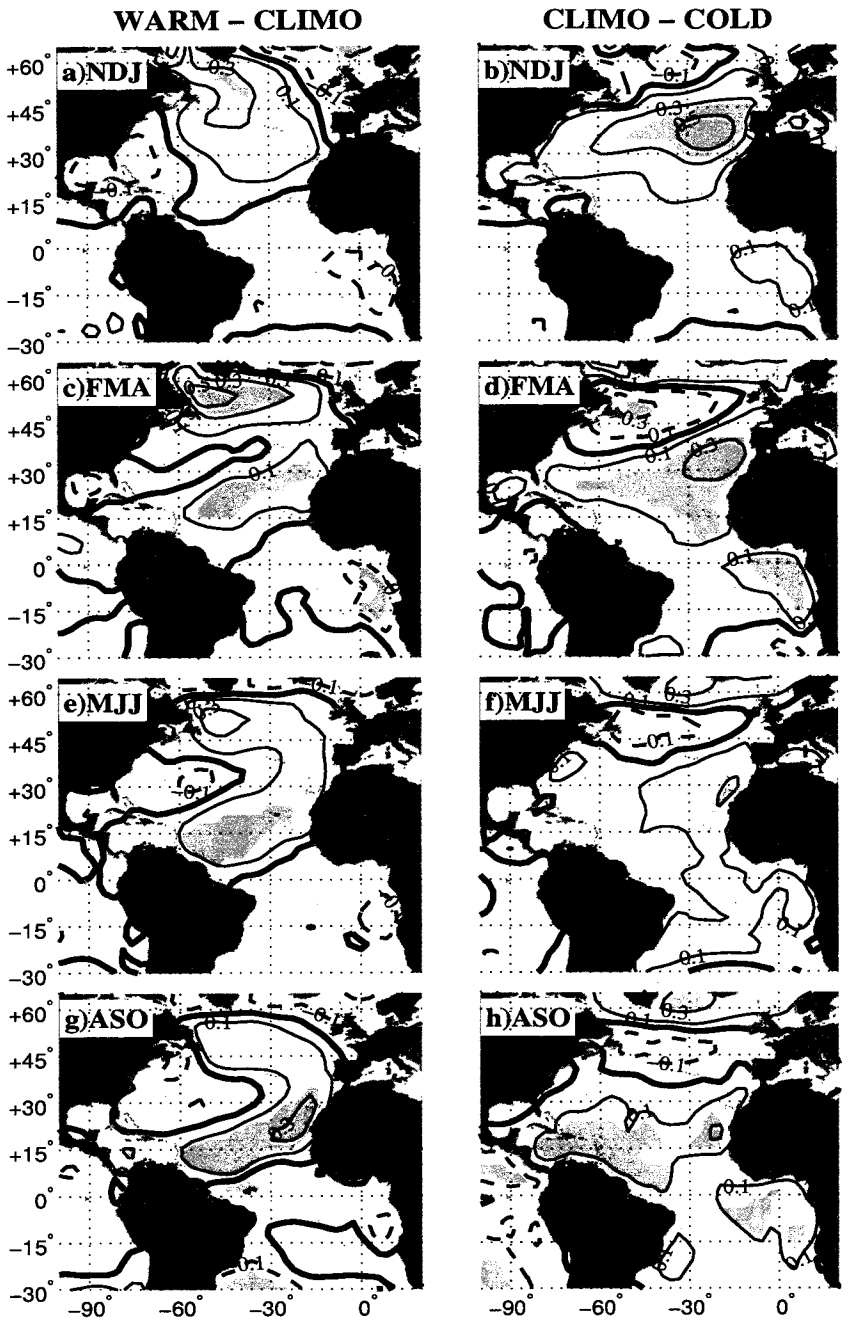

Figure 4.6: The mean difference in SST between the (left column) SOM.MID warm ensembles and SOM.CLIMO and (right panel) SOM.CLIMO and the SOM.MID cold ensembles. Contour interval is 0.2°C, starting with +/- 0.1°C, with the zero contour thickened. Shading denotes significance at the 90% confidence level.

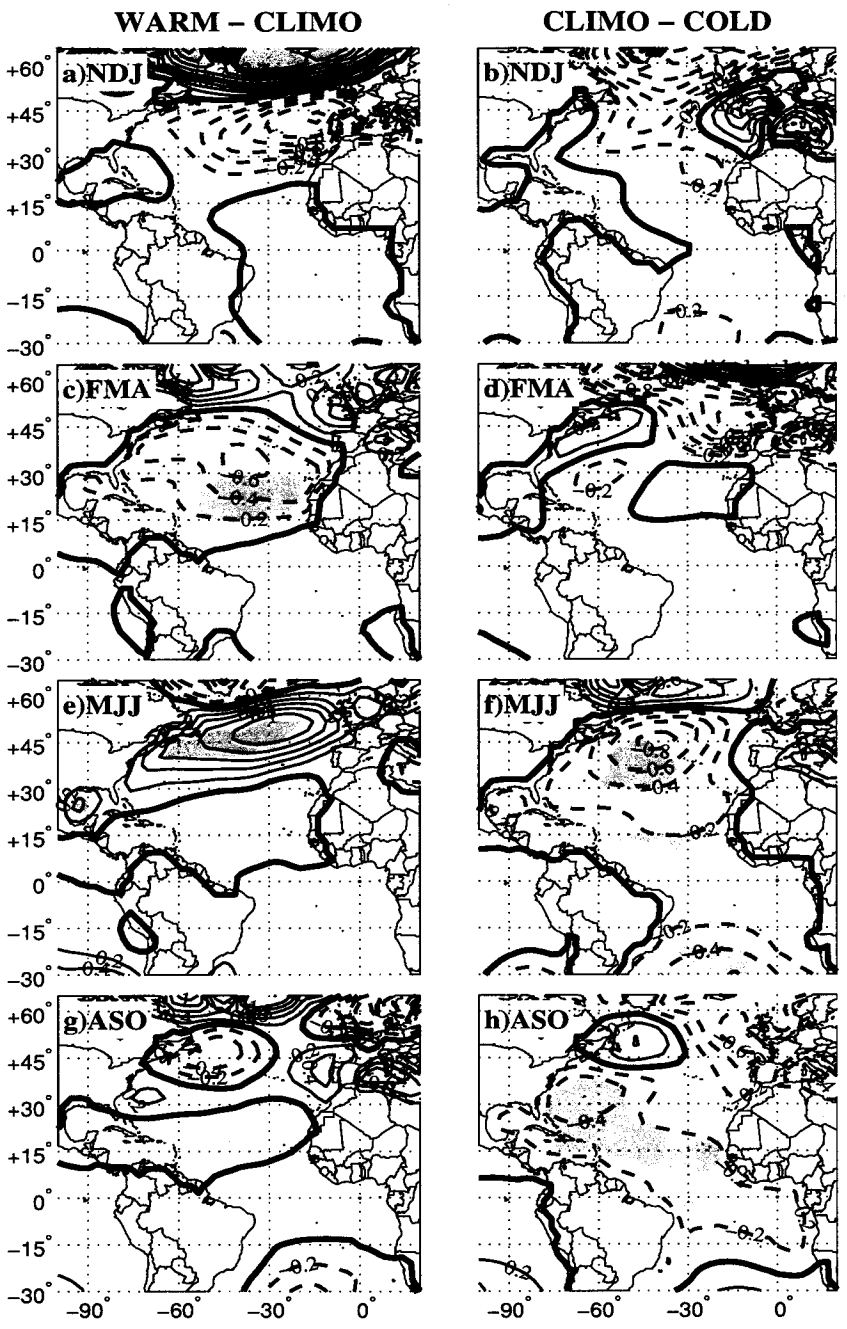

Figure 4.7: Same as 4.6 except for sea-level pressure. The contour interval is 0.2mb until +/- 1mb, and 0.3mb for higher values.

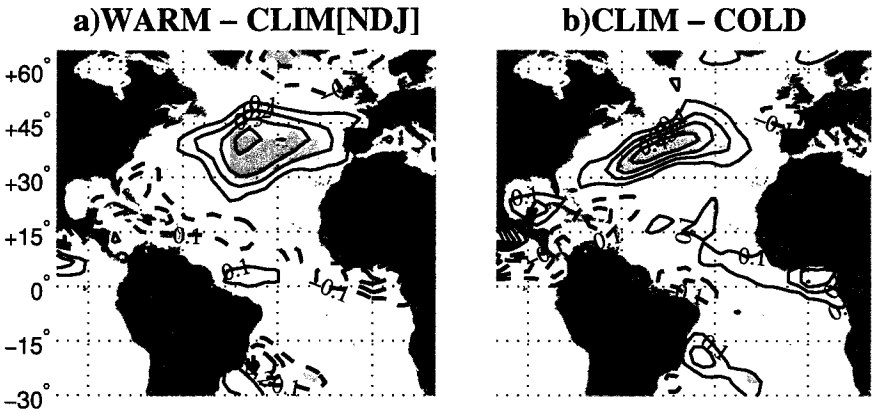

Figure 4.8: The response of convective precipitation for (a) Warm-SOM.CLIMO and (b) SOM.CLIMO-Cold. The contour interval is 0.1 mm day^{-1}. The zero contour is omitted. Compare to Fig. 3.12 for climatologically important areas of precipitation.

magnitude and, to a lesser extent, the position of convective precipitation responds linearly because this region experiences roughly 3 to 5 mm day^{-1} of precipitation during the wintertime. If precipitation was climatologically more scarce, we may expect non-linearities to become important. Furthermore, a close comparison of the warm and cold responses compared to the mean wintertime convective precipitation from SOM.CLIMO (thick contour in Fig. 3.12) indicates that the warm response generates an eastward extension of the storm track, while the cold response attenuates the climatological storm track precipitation without modifying the location. These modest non-linearities are also found by diagnosing other metrics of storm track activity, such as 500-mb eddy momentum and eddy heat flux anomalies (not shown). A complete investigation of the role of eddies in the SOM.MID result requires daily or sub-daily resolution output, which was not available and likely much beyond the scope of our goal (LAU and Nath (1991); Kushnir et al. (2002); Deser et al. (2007)). However, this seems like an appropriate next step in diagnosing our result and extratropical air-sea interaction in general.

Because precipitation anomalies are associated with anomalous atmospheric dia-

batic heating, it is useful to determine how this heating differs between the warm and cold responses. To view this, Fig. 4.9 shows the linearity of the diabatic heating rate (Q_{DIAB}; units of °C day^{-1}) during NDJ as a pressure-longitude cross-section averaged meridionally from 32-40°N. Q_{DIAB} in CAM3.1 is the sum of DTH + DTV + QRS + QRL + DTCOND, where the DTH (DTV) is the horizontal (vertical) diffusion rate, QRS (QRL) is the heating from shortwave (longwave) radiative forcing, and DTCOND is the heating from "adjustment physics", which collectively incorporates cloud physics and condensation processes . Away from the near-surface, it is the DTCOND (which includes the effects latent heat release) term that accounts for most of the differences seen in Fig. 4.9 (not shown). Though the magnitude of the Q_{DIAB} is roughly similar between the warm and cold responses (a maximum of 0.25°C day^{-1}), there are notable differences. First, the warm response extends to a slightly higher level in the troposphere, 300mb, compared to 400mb in the cold response, which is very consistent with Deser et al. (2004) and makes intuitive sense because convection can extend higher given an low-level heat anomaly. Second, the cold response shows large anomalous diabatic heating in the boundary layer, which is partially from shallow convection, but also partially from an increase in outgoing longwave radiation due to a reduction in cloud cover. It is difficult to diagnose the importance of clouds given the crude parameterization of low-clouds in CAM, but Kang et al. (2008) have shown that radiative anomalies can influence extratropical-tropical interaction.

Finally, to investigate the role of linearity in the overall atmospheric response, Fig. 4.10 shows the same cross-section as Fig. 3.18 except for the W-CLIM and CLIM-C components separately during NDJ. There are immense non-linear components in the geopotential height field, as see that the CLIM-C portion contributes most of the signal seen in the WARM-COLD difference in Fig. 3.18. However, given the large projection of the WARM component onto the NAO, as seen by the SST and SLP

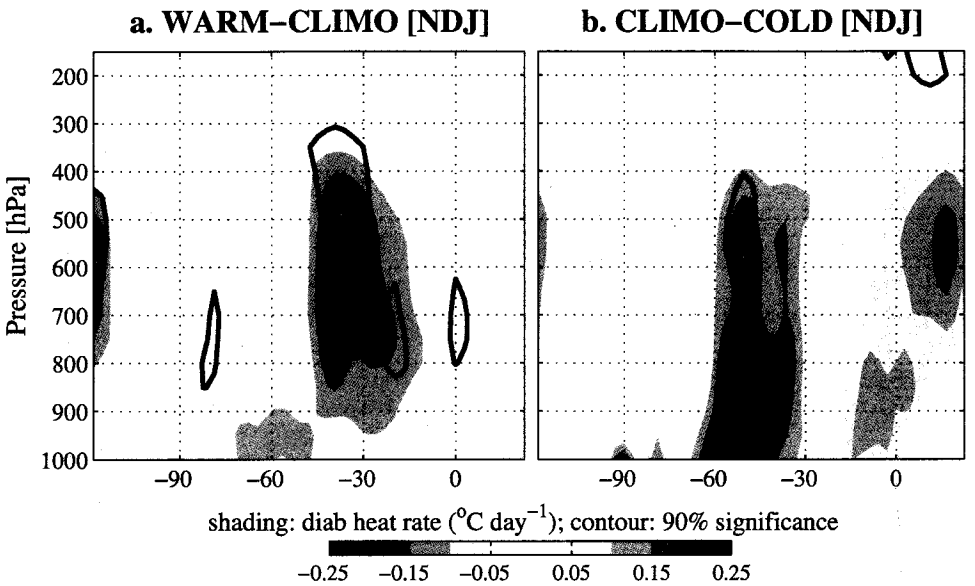

Figure 4.9: Linearity test for diabatic heating rate, Q_{DIAB} during NDJ for (a) the warm response and (b) the cold response. The contour indicates significance at the 90% confidence level.

fields in Fig. 4.6 and 4.7, this result is not entirely surprising. In essence, the WARM ensembles are projecting largely onto the internal dominant mode of variability, the "indirect" response in Deser et al. (2004), leaving a very shallow and weak localized projection and vice versa for the COLD ensembles. The reason for this non-linearity is not clear and requires further investigation. However, the limited number of ensembles (we use 30 compared to 200+ used by other studies looking at air-sea interaction, e.g. Li and Conil, 2003; Deser et al., 2007) may be a constraint. Regardless, during FMA, both components show an overhead and downstream equivalent barotropic high in the mid-latitudes, regaining some semblance of linearity.

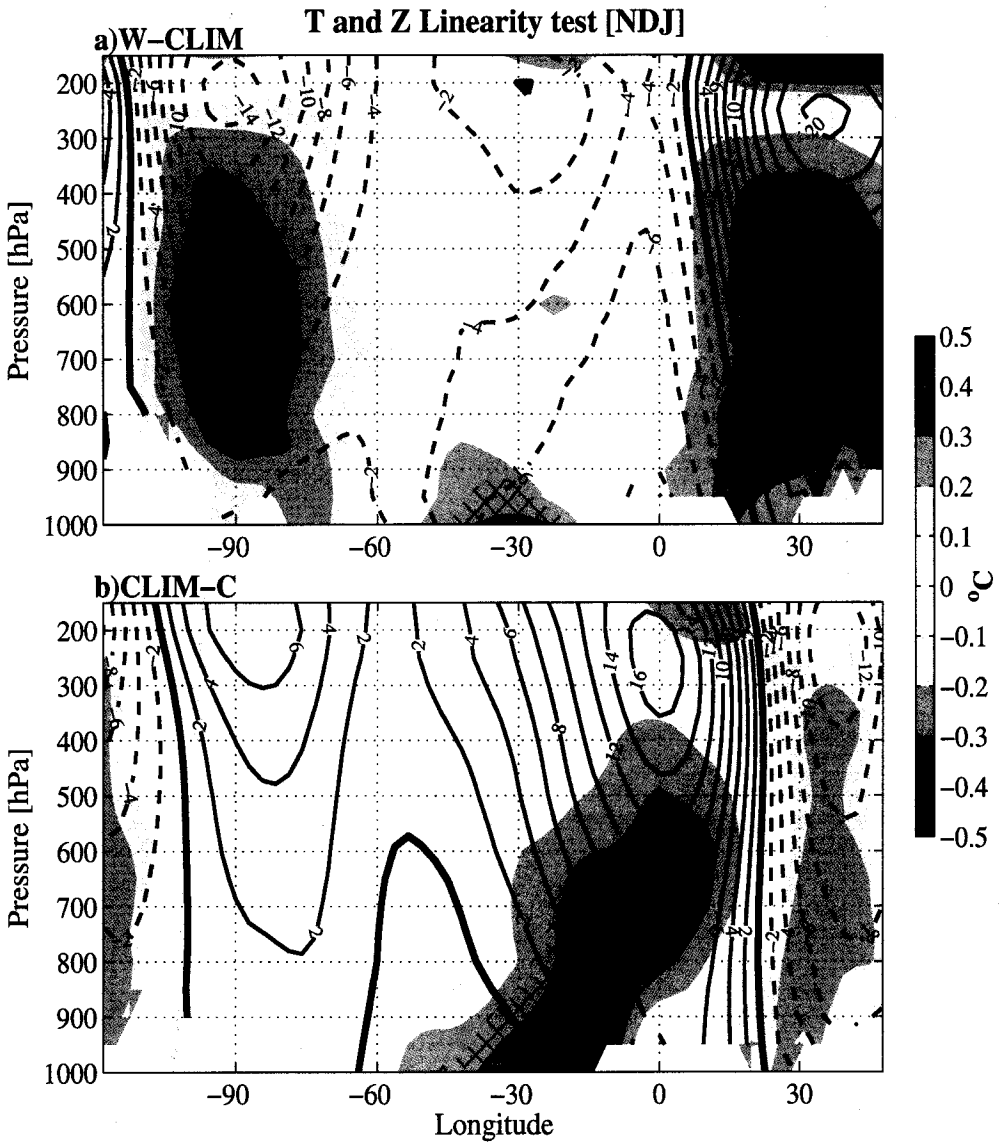

Figure 4.10: Longitude-pressure cross-section of the temperature (shaded) and geopotential height (Z, contoured) from the NCEP-based SOM.MID simulation. Values indicate the mean difference between the warm and cold ensembles. The hatched regions indicate significance of Positive (negative) values of Z are solid (dashed) and the zero contour is thickened.

4.4 Eliminating low-cloud-SST feedback

The last sensitivity test is based on two aspects of the SOM.MID, which can be seen in the Hovmöller plot in Fig. 3.19b. First, note that during May through July, F_{LH} is weak or absent in the tropical Atlantic, while there is still a (-) net surface energy flux (F_{NET}) acting to warm the SST, leaving the radiative fluxes to assume the dominant role in SST forcing (the sensible heat flux is negligible). Figure 4.11 shows the (F_{NET}), the shortwave radiative flux (F_{SW}) and F_{LH}. As suggested in the Hovmöller diagram, F_{LH} is zero to weakly positive (damping) while F_{SW} strongly resembles F_{NET} over the tropical Atlantic between 0-30°N.

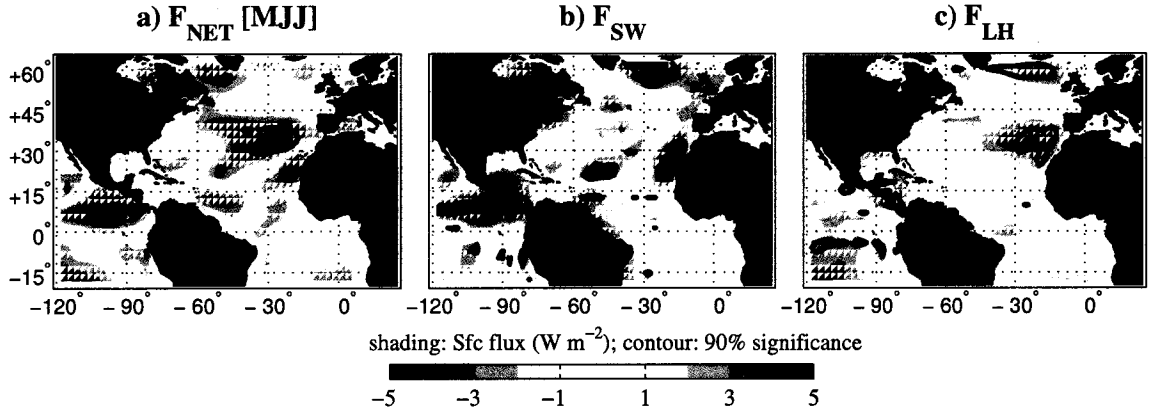

Figure 4.11: The mean difference in (a) F_{NET}, (b) F_{SW} and (c)F_{LH} in the NCEP-based SOM.MID simulation. Positive values imply upward heat transfer. The contour indicates areas significant at the 90% confidence level.

Figure 4.11 highlights the region off the Northwest African coast, near 25°N, 20°W, which experiences F_{SW} anomalies of greater than 5 W m^{-2}. Figure 4.12 shows the inter-ensemble scatter of the F_{LH} and F_{SW} components in this region (averaged over 15-30°N, 15-25°W) as a function of the SST difference. Note that F_{SW} is acting opposite to F_{LH} and the latter is actually damping SST anomalies during MJJ, quite different from FMA. The large negative slope of $\Delta F_{SW}/\Delta SST$ suggests that this region may be

experiencing a positive radiative-SST feedback. This is not entirely unexpected given that there is a large seasonal cycle of low-level cloud cover, with a maximum during the boreal summer months. Furthermore, the low-cloud-SST feedback has already been described using observations by Klein et al. (1995). The feedback is postulated to occur in the following manner: F_{LH}-induced SST anomalies propagate southward from the mid-latitude Atlantic during FMA, causing negative low-cloud anomalies due to a decrease in boundary layer stability. In accord, SOM.MID shows a signficant 2-4% reduction in low cloud fraction in the warm ensembles, compared to the cold (95% confidence level, not shown). During MJJ, when the seasonal stratus deck peaks off the northwest African coast, the initial reduction in clouds causes excess shortwave radiation to reach the surface and maintain or even amplify the already (+) SST anomalies. Finally, the feedback is complete when (+) SST anomalies cause a further decrease in boundary layer stability, amplifying the decrease in low-cloud cover.

Although the proposed low-cloud-SST feedback is physically plausible, one complicating factor is that the CAM3, like many GCMs, uses SST in the calculation of marine low-cloud fraction, based on an empirical relationship (Klein and Hartmann (1993)). A second complicating factor is that low-cloud cover during MJJ is grossly overestimated by CAM3. Figure 4.13 shows the observed low-cloud cover during MJJ from ISCCP climatology; also shown is the difference between ISCCP and SOM.CLIMO, as ISCCP-SOM.CLIMO. Although ICCSP shows a tongue of low-cloud cover that approaches 40%, CAM3 generates low-clouds too close to the African coast and overestimates observations by a 20-40%. This suggests the low-cloud-SST feedback may be largely exaggerated, causing uncertainty as to the maintenance of SST anomalies during the summer months. To investigate this, we designed an experiment where F_{SW} is prescribed to it's climatological values over the box shown in Fig. 4.13 (hereafter, SOM.SW-CLIM, see Table 2.3). The climatological values are obtained

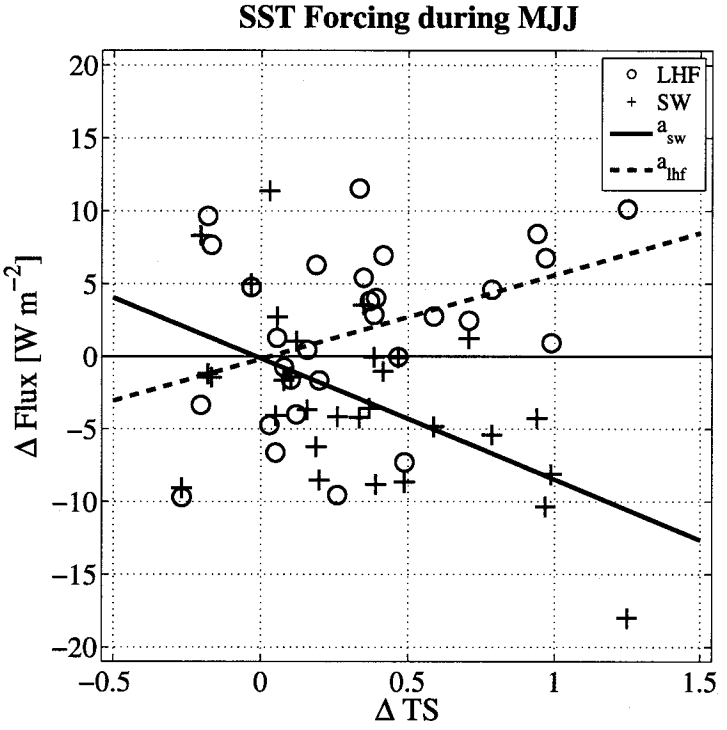

Figure 4.12: Scatter plot of the mean difference in SST between the warm and cold ensembles of the NCEP-based SOM.MID and the differences in LH flux (gray circles) and shortwave radiative fluxes (crosses). Values have been averaged over 15-30°N, 15-25°W. Also shown are best fit lines based on a least-square error regression for the shortwave (solid) and latent heat (dashed) fluxes.

from the control SOM.CLIMO simulation and only prescribed from May to August, when the bias is largest in CAM3. Prescribed values are monthly averages that are linearly interpolated to daily values by the CAM3 code.

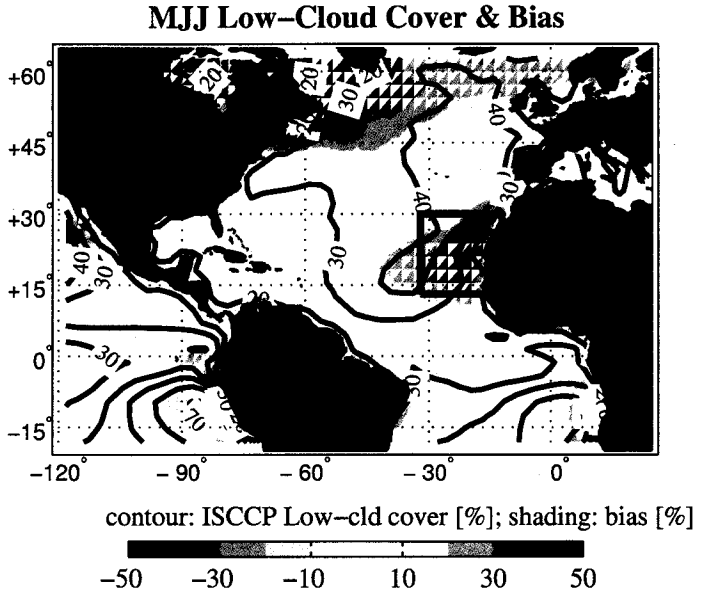

Figure 4.13: In contours, the climatological low-cloud cover (%, contour interval 10) from ISCCP (1981-2008). The shading shows the bias in low-cloud cover from SOM.CLIMO, as ISCCP-SOM.CLIMO. Positive values indicate when CAM3 is over-estimating low-clouds. The thick box indicates where F_{SW} is prescribed.

Figure 4.14 and 4.15 show the evolution of SST and SLP, respectively, during the last 6 months of the SOM.SW-CLIM simulation. Note that 20 ensembles are used, as opposed to 30 in SOM.MID. Although SST anomalies are reduced by roughly 0.2 K (40% reduction from SOM.MID) immediately off the African coast where shortwave insolation is prescribed, the SST and SLP evolution still maintains a strong AMM-like structure. Thus, while there may actually be a positive low-cloud-SST feedback (it is difficult to assess from observations alone), the effect is likely *local* in nature and does not affect the large-scale structure of the AMM, which operates on much larger spatial scales.

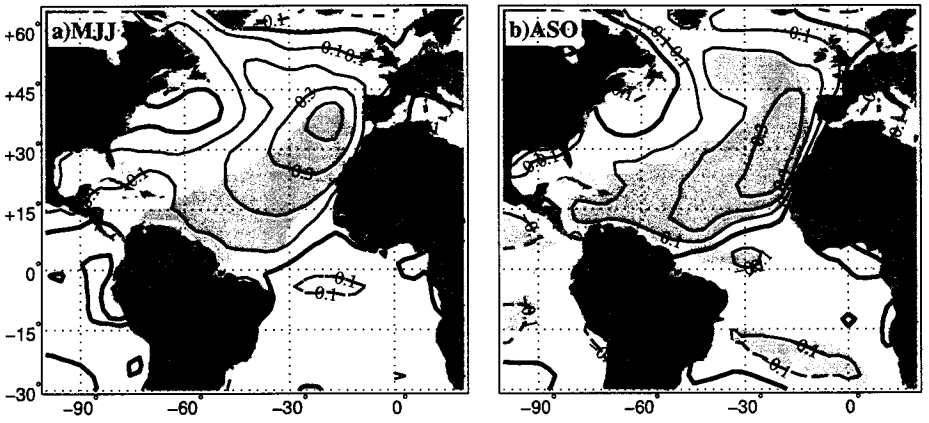

Figure 4.14: Evolution of mean SST difference between warm and cold ensembles for SOM.SW-CLIM simulation during (a) MJJ and (b) ASO. The 95% confidence level is shaded.

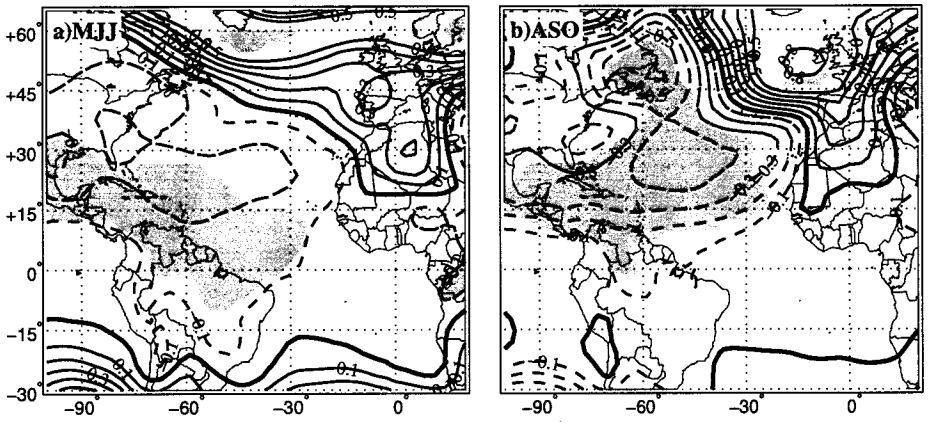

Figure 4.15: Same as Fig. 4.14 except for sea-level pressure. The 90% confidence level is shaded.

5 CONCLUSION

Extratropical forcing of tropical Atlantic air-sea variability has been investigated on inter-seasonal timescales. The motivation for this work came from a finding by KV07 and Vimont (2011) that used a LIM to show that the AMM may be predictable up to a year in advance, with a bias towards higher forecast skill during boreal fall. To corroborate this finding, a set of ensembles using CAM+SOM are forced based on the optimal pattern found by the LIM (Fig. 2.1). The GCM simulations, notably the SOM.MID, reproduce the LIM finding that initial mid-latitude Atlantic SST anomalies in November generate an AMM-like response in the tropical Atlantic by the following boreal summer and fall. First, the mid-latitude atmosphere responds to the positive SST anomalies by developing a downstream surface low-pressure, which is consistent with past theoretical arguments using linear theory (Hoskins and Karoly, 1981). This anomalous cyclonic circulation quickly erodes the northern edge of the initial SST anomalies through an enhanced F_{LH}. Due to the anticyclonic background flow, the same circulation also develops SST anomalies in the subtropical north Atlantic due to a relaxation of the mean easterly winds.

The WES feedback appears to play a dominant role in subtropical SST anomaly generation and maintenance as the wind-induced F_{LH} continually reinforces the SST anomalies. This occurs predominantly during boreal spring, as deduced from the Hovmöller plots in Fig. 3.19. Whether coincidence or not, this matches the seasonality when WES is argued to be most active due to its proximity to the equator (Liu, 1996). Due to the large role of the wind component F_{LH}, CAM is modified by prescribing surface wind speed in order to suppress the WES feedback, as in Mahajan et al. (2011). In the SOM.WES-OFF simulation, tropical SST anomalies only reach 25% of their values from the original simulation. However, the presence of significant SST

anomalies suggests an active role for the indirect forcing of wind on the background gradient in specific humidity, as alluded to in Chiang and Bitz (2005). Note that the direct role of humidity should be damping due to the Clausius-Clayperon exponential relationship, yet past studies (e.g. Saravanan and Chang, 2000; Chiang et al., 2003) have shown that the moisture component of F_{LH} actually aids in developing SST anomalies. This topic is still unsettled and would benefit from further investigation, due to a complex effect of specific humidity on F_{LH}.

During late boreal spring and early summer a positive feedback between stratiform low clouds and SST maintains the tropical SST anomalies. Observational evidence for this feedback has been shown over global stratiform regions by Klein and Hartmann (1993) and over the Atlantic by Okumura et al. (2001), yet the main uncertainty with this feedback is due to the large bias shown by the GCM in low cloud cover during boreal summer (Fig. 4.13). By prescribing the incoming shortwave radiation in bias-sensitive areas of the tropical Atlantic, the SOM.SW-CLIM simulation largely reproduces the SST and SLP response from the SOM.MID, signaling a strong AMM. However, locally near the northwest coast of Africa, the SST anomalies are reduced by 30-40%, suggesting that the low-cloud SST feedback is likely too short and spatially constrained to significantly impede the generation of an AMM event from extratropical SST forcing.

In addition to the two sensitivity studies, repeating our experiment with prescribed (uncoupled) SSTs, we showed that seasonality plays a vital role in our main finding. When forcing with the same optimal SST anomaly during February, no equatorward propagation is seen. We attribute the strong impact of seasonality to the evolving background state in the north Atlantic, which features a southward shift of the jet stream from November to February. The drastic role of seasonality confirms past observational studies (Czaja and Frankignoul, 2002; Cassou et al., 2004) high-

lighting boreal fall as the most active season for SST forcing of the atmosphere in the mid-Atlantic.

We have investigated the linearity of the response by running both warm and cold simulations in addition to a control CAM+SOM simulation. Our results compare well with the result of Deser et al. (2004), who showed that the warm ensembles project strongly onto the NAO while the cold ensembles do not. In accord with Deser et al. (2004), we find that diabatic heating in the warm ensembles extends to a higher level in the troposphere compared with the cold simulations. This suggests the importance of deep convection in the atmospheric response; however, this is not a simple task given the crudeness of the convective parameterization in a GCM. Even though our SST anomaly is in the vicinity of the warm Gulf Stream extension region of the Atlantic Ocean, which is a climatologically favored area for deep convection (Minobe et al. (2010)), it may be presumptuous to make conclusions regarding the non-linear response of deep-convection to the SST anomaly (Kang et al. (2008)).

Comparing the results herein with past studies of mid-latitude forcing of tropical variability shows consistency with Chiang and Bitz (2005) that extratropical thermal forcing can affect the ITCZ position through thermodynamic processes alone, even though our anomaly was 15 further south. Our results support those of Mahajan (2008) because we have demonstrated that the WES feedback is very important to the propagation of SST anomalies into the subtropics and tropics, south of 25N. However, our results from the SOM.WES-OFF experiment are also similar to the recent work of Mahajan et al. (2011), which shows that extratropical excitation of tropical SST anomalies can occur in the absence of the WES feedback, albeit with greatly reduced amplitude. Additionally, we have showed that seasonality has a large impact on whether or not tropical excitation occurs, which has been omitted in past studies that focused on longer time-scales. Although we focus on inter-seasonal timescales and

our model does not have ocean dynamics and thus cannot be directly compared to the study by Zhang and Delworth (2005), we believe it is highly unlikely that a change in the strength of the AMOC can propagate SST anomalies into the tropics via oceanic processes in the short time scales that we have considered. Thus, we can conclude that oceanic dynamics are not essential in extratropical-to-tropical climate interactions in the North Atlantic.

As a whole, this study provided the necessary evidence to accept the LIM result by Vimont (2011), which was somewhat constrained by the use of only SST anomalies. The fact that extratropical forcing can produce such a fast and strong tropical response seems to be an innovative finding, especially due to the prior evidence that ENSO appears to be the most dominant forcing of Atlantic SST anomalies on seasonal timescales (Enfield and Mayer (1997)). Yet, our omission of oceanic dynamics, which includes ENSO, seems to be the most severe obstacle to the addition of the LIM as a seasonal forecasting tool at the present moment. In the final section, the importance of oceanic dynamics is discussed, along with other limitations that may or may not be significant to our main result. We also comment on several routes for future research that have arisen directly from our results thus far.

6 FUTURE RESEARCH

There are several limitations arising from our neglect of oceanic dynamics. First, note that the seasonality shown by the LIM and DOM.MID experiments suggest that boreal fall is the optimal time for extratropical forcing. However, the evolution of air-sea anomalies shown by the SOM.MID experiment in Section 3.4 also coincides with the seasonality of ENSO forcing. Because ENSO is not captured by a CAM+SOM setup, an unanswered, though crucial question is: can our mechanism still occur given the remote impact of a large El Nino or La Nina event. To address this, we used NCEP-Reanalysis observations and calculated lagged regression coefficients of SST and SLP anomalies onto the AMM_{ASO} time series, shown in Fig. 6.1 for lags of 0 to 8 months in increments of 2. Beginning in DJF, Fig. 6.1 shows a very similar equatorward propagation of SLP and SST anomalies, though the SLP signal is insignificant until boreal spring, FMA (panel c). To test the contribution of ENSO, the same lagged regression is repeated except each strong ENSO year, defined where the Nino3.4 SST index (NOAA, Climate Prediction Center) exceeds 1.5 standard deviations, and the subsequent year is removed. This ensures that lagged ENSO effects are removed, to first order. Removal of ENSO only acts to change the amplitude, not the structure of the regressions shown in Fig. 6.1. Most notably, the (-) SLP during FMA becomes slightly weaker and statistically significant areas shrink modestly (not shown). However, the fact that an SLP signal is observed in the extratropics strongly suggests that our mechanism can still operate, even in the presence of ENSO.

Second, note that we have not explained the high-latitude differences between the GCM simulations and the LIM final structure (compare Fig. 3.8 and Fig. 3.9 with Fig. 2.1). Although both the NCEP- and Hadley-based SOM.MID simulations generate SST anomalies north of 50N, these are very weak and misplaced compared to

the LIM, preventing us from making any conclusions in this area, though providing a direction for future research. One hypothesis for the difference is that lack of a fully coupled sea-ice model that can generate oceanic convection through ice processes, thus largely impacting SST. Once again, this can be grouped into to a broader category of issues arising from neglecting oceanic dynamics. Another such limitation is the use of a constant (50m) mixed-layer depth, compared to the large mixed-layer depths found in the mid-latitude oceans, especially during winter time (Alexander and Deser (1995). Using a 50-m seasonally and spatially invariant mixed layer may be somewhat unrealistic, yet it is also a safe strategy because the climatological mixed layer depth during November in the mid-Atlantic basin is between 75 and 100 m. Thus, the heat content anomaly that we impose is fairly conservative and certainly within the realm of natural variability, especially in comparison with early GCM studies (Chervin et al. (1980)).

Discussion of the origin of the LIM-based OPT initial condition has largely been avoided so far, in favor of corroborating the LIM result. Eventually, the initial condition must be investigated in further detail, especially if predictability is sought; here, several preliminary findings are presented. Recall that the OPT is the second right singular vector, in eqn. 10, representing a superposition of the dynamical modes contained in **B**. Although the structure of the dynamical modes themselves are quite noisy when varying the lag in the LIM calculation (e.g. Penland and Sardeshmukh (1995a)), the

Figure 6.1 *(following page)*: Lagged regressions of (left column) SLP and (right column) SST onto the boreal fall AMM, AMM_{ASO}. Three month averages are used centered on the middle month denoted in the captions, from top to bottom, DJF, FMA, AMJ, JJA and ASO. Thus, these represent lags of 8, 6, 4, 2 and 0 months, respectively. Positive (negative) regression coefficients are solid (dashed) and represent anomalies per standard deviation of AMM_{ASO}. Shaded regions denote significance at the 95 (90) % level for SST (SLP). SST and SLP data is from NCEP-Reanalysis over the period 1950-2008.

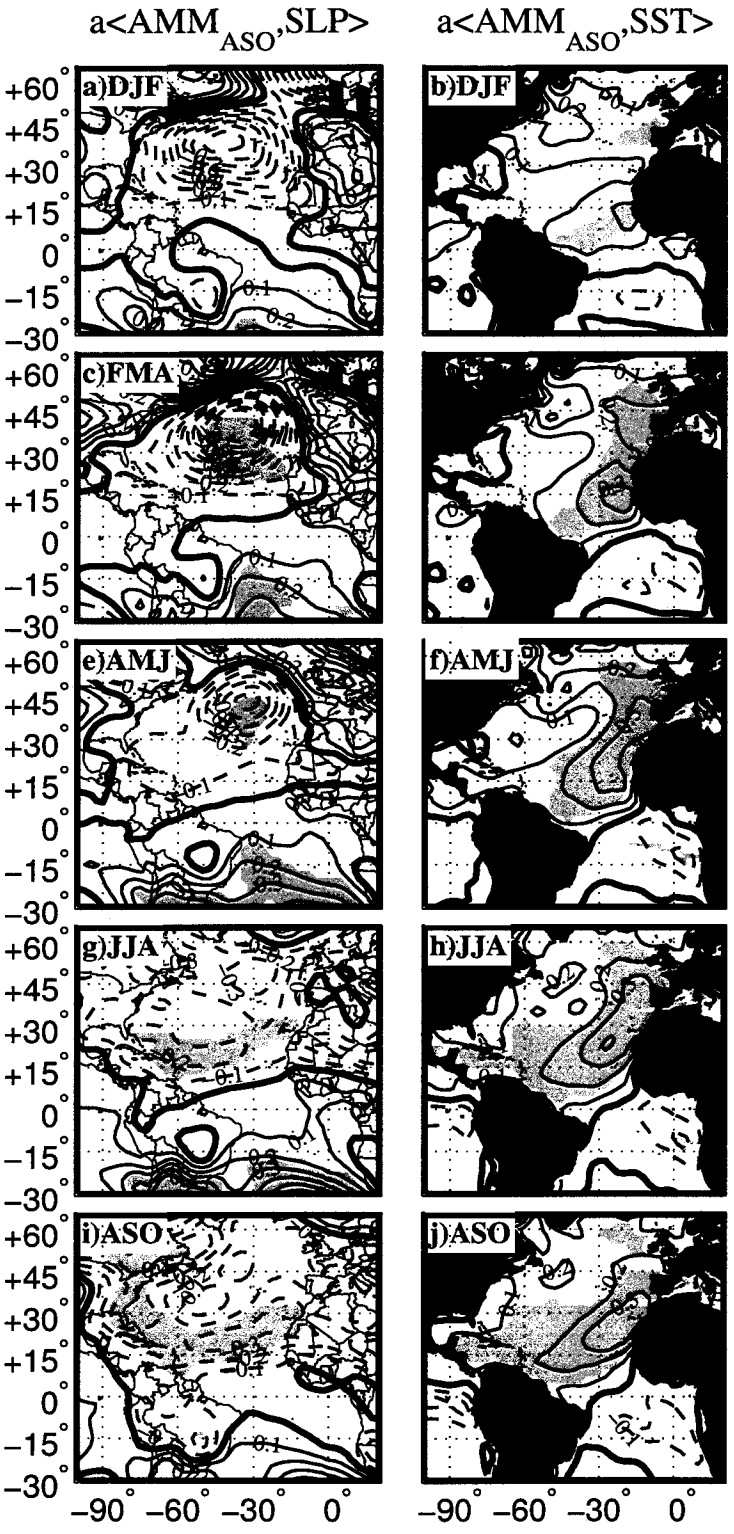

leading columns of V are stable, as is calculated by the important "tau test" (Vimont, 2011). Given the long time-scale of the LIM OPT anomaly (see Vimont, 2011, for OPT time series) , it is worth asking whether OPT SST anomalies are forced by oceanic processes, as opposed to the null hypothesis of atmospheric forcing as in FH77.Thermal memory in the ocean is long and does seem to provide substantial forecast skill (Sutton and Allen (1997)), especially near the Gulf Stream and Gulf Stream extension regions, where OPT has large loadings. It is also in these regions that the oceanic forcing of the atmosphere is particularly robust (Minobe et al. (2008); Kwon et al. (2010)).

To investigate the cause of OPT SST anomalies, we calculate the correlation (hereafter, $R_{dSST,F}$) between anomalous net surface heat flux (F_{NET}) and SST tendency (hereafter, $dSST$) over the region where OPT shows large loadings (55-25°W, 30-43°N). This is shown in Fig. 6.2 using monthly averaged anomalies from three different observational data sets: NCEP-Reanalysis (Kalnay et al., 1996), the Coupled Forecast System Reanalysis (CFSR, Saha and co authors (2010)) and the Modern-Era Retrospective Analysis for Research and Applications (MERRA, Rienecker and co authors (2011)). Because seasonality is important, data is stratified into 3-month bins centered on each month. Note that CFSR and MERRA only span the satellite era (1980-present); thus the longer NCEP dataset was also divided into a satellite era subset for direct comparison. Based on FH77 and previous observational studies (Davis (1976); Cayan (1992)), we expect large absolute values of $R_{dSST,F}$ (note that F_{NET} is negative when heat goes into the ocean, implying a negative $R_{dSST,F}$ if the atmosphere is forcing). Indeed, averaging Fig. 6.2 across all months shows that $|R_{dSST,F}|$ is substantial, around 0.6. However, there is also a distinct seasonal cycle where during the boreal winter, $|R_{dSST,F}|$ is very high, near 0.8, but in the late summer, correlations drop to insignificant levels, though the exact timing depends on the data set. Recall that the seasonality of AMM forecast skill peaked for boreal fall OPT forcing. Thus,

Fig. 6.2 suggests atmospheric processes may not be the dominant forcing of the OPT SST pattern.

To follow up on Fig. 6.2, spatial plots of $R_{dSST,F}$ are shown in Fig. 6.3 for boreal winter (JFM) and late boreal summer/fall (ASO) based on the highest and lowest values of $|R_{dSST,F}|$ in Fig. 6.2, respectively. During JFM, vast areas of the Atlantic Ocean experience large $|R_{dSST,F}|$, exceeding 0.6, indicating that the atmosphere is driving SST anomalies, as expected from FH77. Notable exceptions include areas immediately near the Gulf Stream, where oceanic heat advection is large and high-latitude areas, where ice thermodynamics are crucial. However, during ASO, $|R_{dSST,F}|$ is near zero over major portions of the western mid-latitude Atlantic Ocean, which overlaps with the OPT initial condition. Although it is tempting to conclude that SST anomalies are being forced by the ocean during this time, it is difficult to do so using only observations. Attempts to deduce the oceanic heat flux convergence as a residual in the mixed-layer heat budget equation (essentially Q in eqn. 2) yielded low correlations with $dSST$ for several reasons. First, due to lack of observations, the mixed-layer depth is fixed to seasonally varying climatology from Monterey and Levitus (1997), even though mixed-layer depth variability is large in the mid-latitude oceans, especially during winter (Alexander (1992a)). Second, there could be biases in the atmospheric flux data resulting in a lack of closure in the surface energy budget (e.g. Foken (2008)).

Finally, one relevant observational finding that has not been explained is the long persistence time of SST anomalies during the boreal fall. Figure. 6.4 shows the lagged autocorrelation of SST anomalies (MERRA SST data) averaged over the OPT region (55-30°W and 30-43°N) as a function of month. The thick dashed line is the e-folding decay time, as would be expected from an exponential decay of SST anomalies, as suggested by FH77 in the absence of forcing. As shown by Frankignoul (1985), mid-

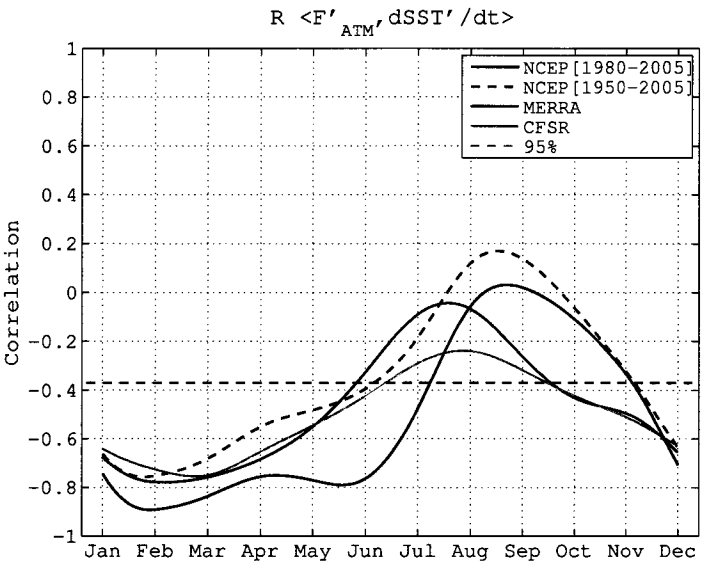

Figure 6.2: Correlation between anomalies of F_{NET} and $dSST$ averaged over the OPT region (55-25°W, 30-43°N) for each 3-month period centered on the month given by the x-axis. The red dashed line shows the 95% confidence level.

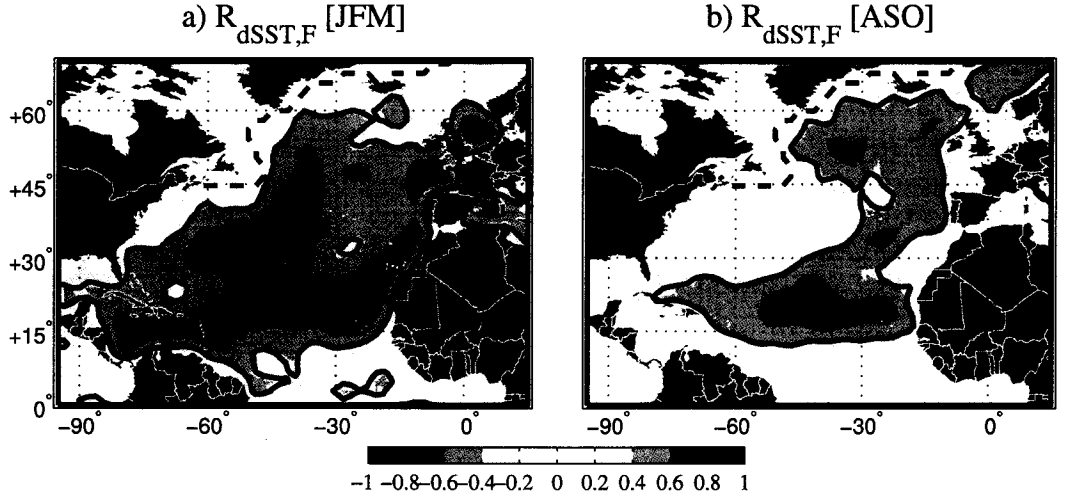

Figure 6.3: Correlation (shading, interval 0.2) between anomalies in F_{NET} and $dSST$ for boreal winter (left) and boreal summer/fall (right). The solid contour denotes region exceeding the 95% confidence level. The dashed line indicates regions that experience ice at some point during the annual cycle and thus have been omitted from the calculation.

latitude SST anomalies follow an AR1 process with a nearly constant damping from the atmosphere. Past observational and modeling studies have incorporated e-folding decay times of 1-3 months (Frankignoul et al., 1998). Figure 6.4 suggests that these decay times exist only between February and July. However, the most interesting aspect of Fig. 6.4 is the large seasonality in the rate of SST anomaly decay. Note that the e-folding decay time during June is 2 mo., but drastically increases to 7 mo. just two months later, in August. Although purely speculative, the interesting maximum is summertime SST anomaly persistence does not appear to be related to re-emergence process (the mixed layer depth does not deepen until September), but seems to corroborate observational studies that find the mid-latitude Atlantic atmosphere is particularly sensitive to SST anomalies during boreal fall (Czaja and Frankignoul (2002); Cassou et al. (2004); Wang et al. (2004)). One would expect long-lasting SST anomalies to leave a stronger footprint on the atmosphere, though the dynamics of this phenomenon have yet to be determined. Collectively, preliminary evidence illuminates the importance of oceanic processes in developing the optimal initial condition suggested by LIM. However, there are clearly several hurdles to clear before implementation of the LIM in an operational setting.

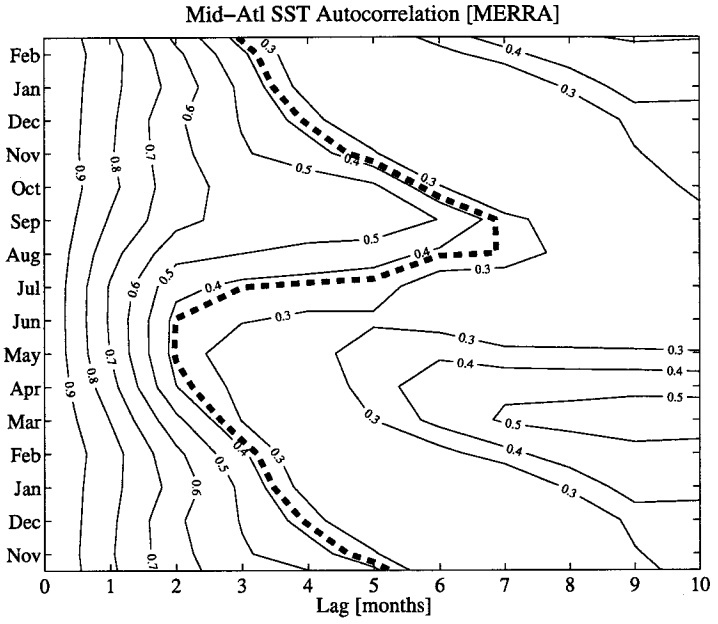

Figure 6.4: Lagged correlation values of SST anomalies averaged from 55-30°W and 30-43°N. Values are obtained based on 3-month bins center on the month shown on the y-axis. The x-axis indicates the lag based on an initial condition of the month shown on the y-axis. For example, the y-value of January and lag of 4 months shows the correlation between SST anomalies during DJF and the following AMJ. The thick dashed line shows the e-folding decay-time using the eqn.1 paradigm.

7 APPENDIX

7.1 Mixed layer heat tendency equation for an AGCM coupled to a slab ocean

The use of a 50-m fixed mixed layer depth in our "slab" ocean necessitates the parameterization of thermodynamic processes internal to the ocean, such as Ekman pumping and advection, advection by oceanic currents and sub mixed-layer entrainment (Frankignoul, 1985; Alexander et al. (2000)). The way this is achieved in the CAM+SOM framework is by first conducting a CAM+DOM experiment with prescribed, seasonally varying climatological SST, which is done in the DOM.CLIMO experiment (see Table 2.3). After running DOM.CLIMO for 40 years, the oceanic heat flux convergence, Q, in eqn. 2 is found as a residual between the difference in the SST tendency and net atmospheric heat flux, averaged for each month. Figure 7.5 shows the mean boreal winter and boreal summer Q obtained from the DOM.CLIMO simulation. Positive values denote regions where heat flows from the ocean to the atmosphere, and vice versa. Important regions of Q variability that cannot be captured by the CAM+SOM are in the mid-latitude storm tracks and along the equator.

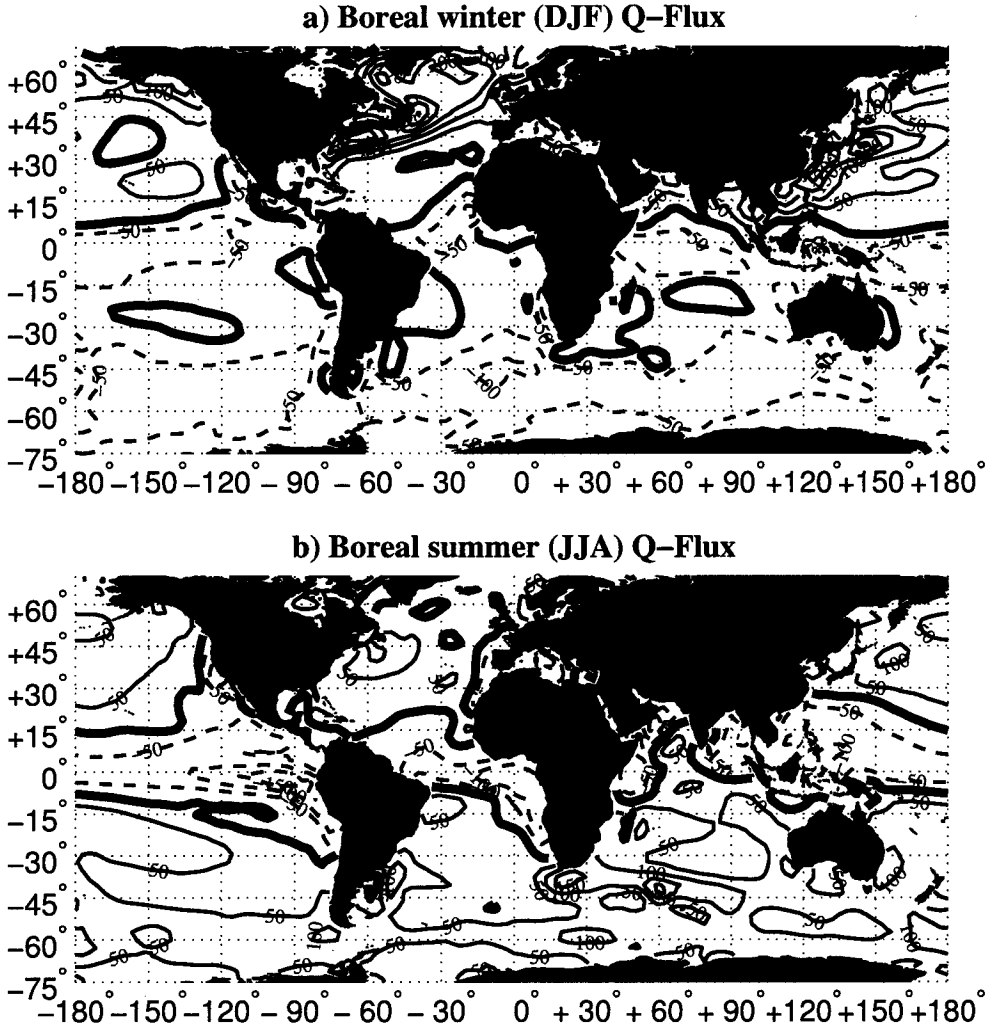

Figure 7.5: Q-flux term derived from the DOM.CLIMO simulation, used in all unmodified CAM+SOM experiments in Table 2.3. Values are shown for (a) boreal winter and (b) boreal summer. Contour interval is 50 W m^{-2} and the zero contour is thickened.

7.2 Shutting off the WES feedback

In order to remove the WES feedback over the tropical Atlantic Ocean, a similar methodology is followed as described by Mahajan et al. (2008). There are three steps:

1. Run a uncoupled simulation (DOM.WES-OFF) using CAM where surface wind speed is prescribed to climatological values taken from the SOM.CLIMO simulation. The prescribed SST boundary condition is the climatological seasonal cycle.

2. Calculate a new Q-flux (using eqn. 2) by running the uncoupled simulation until stable statistics are found (10-15 years is enough in this case).

3. Run a coupled simulation where wind speed is prescribed and calculate the SST-tendency using the Q obtained from the uncoupled DOM.WES-OFF simulation.

To first order, the mean climates between the SOM.CLIMO and SOM.WES-OFF are be similar (not shown). However, there are regions where modest differences occur, which can be shown by finding the difference between the Q in the SOM.CLIMO and SOM.WES-OFF simulation, seen in Fig. 7.6 for the boreal winter and summer seasons. During boreal winter, notable areas where Q changes occur in the northern Atlantic. Also, by fixing the surface wind speed, the amount of SST variability the coupled model can produce is greatly reduced, especially in regions where the wind speed contribution dominants the F_{LH} anomalies. This is seen in Fig. 7.7 which compares the standard deviation of SST anomalies as a ratio of the SOM.WES-OFF versus SOM.CLIMO simulation.

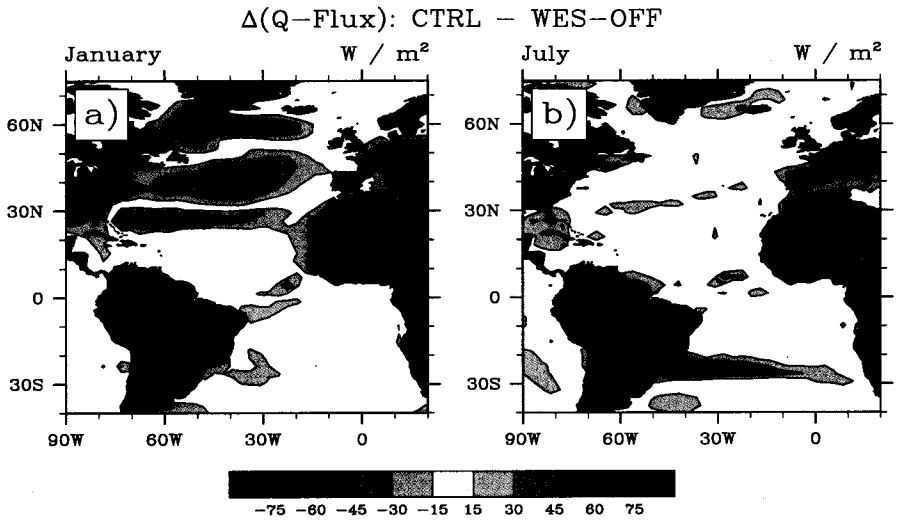

Figure 7.6: Difference in Q between the SOM.CLIMO simulation and the modified SOM.WES-OFF simulation for (left) boreal winter and (right) boreal summer

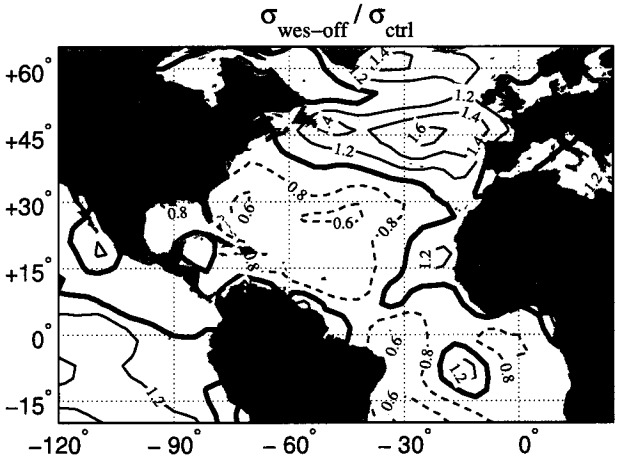

Figure 7.7: Ratio of $\sigma_{SST'}$ between the SOM.WES-OFF and SOM.CLIMO simulations. The contour interval is 0.2 and the contour where the ratio = 1 is thickened.

References

Alexander, M., 1992a: Midlatitude atmosphere–ocean interaction during El Niño. Part I: The North Pacific Ocean. *J. Climate*, **5**, 944–958.

Alexander, M., 1992b: Midlatitude atmosphere–ocean interaction during El Niño. Part II: the Northern Hemisphere atmosphere. *J. Climate*, **5**, 959–972.

Alexander, M., 2010: Extratropical air-sea interaction, SST Variability and the Pacific Decadal Oscillation. *Climate Dynamics: Why Does Climate Vary?*, **189**, 123–148.

Alexander, M., I. Bladé, M. Newman, J. Lanzante, N. Lau, and J. Scott, 2002: The atmospheric bridge: The influence of ENSO teleconnections on air-sea interaction over the global oceans. *J. Climate*, **15**, 2205–2232.

Alexander, M. and C. Deser, 1995: A mechanism for the recurrence of wintertime midlatitude SST anomalies. *J. Phys. Oceanogr.*, **25**, 122–137.

Alexander, M., L. Matrosova, C. Penland, J. Scott, and P. Chang, 2008: Forecasting Pacific SSTs: Linear inverse model predictions of the PDO. *J. Climate*, **21**, 385–402.

Alexander, M. and C. Penland, 1996: Variability in a mixed layer ocean model driven by stochastic atmospheric forcing. *J. Climate*, **9**, 2424–2442.

Alexander, M., J. Scott, and C. Deser, 2000: Processes that influence sea surface temperature and ocean mixed layer depth variability in a coupled model. *J. Geophys. Res.*, **105**, 16.

Alexander, M., et al., 2006: Extratropical atmosphere-ocean variability in CCSM3. *J. Climate*, **19**, 2496–2525.

Back, L. and C. Bretherton, 2009: On the relationship between SST gradients, boundary layer winds, and convergence over the tropical oceans. *J. Climate*, **22**, 4182–4196.

Ban, J., Z. Gao, and D. Lenschow, 2010: Climate simulations with a new air-sea turbulent flux parameterization in the National Center for Atmospheric Research Community Atmosphere Model (CAM3). *J. Geophys. Res.*, **115**, D01 106.

Barsugli, J. and D. Battisti, 1998: The Basic Effects of Atmosphere-Ocean Thermal Coupling on Midlatitude Variability. *J. Atmos. Sci*, **55**, 477–493.

Battisti, D., U. Bhatt, and M. Alexander, 1995: A modeling study of the interannual variability in the wintertime North Atlantic Ocean. *J. Climate*, **8**, 3067–3083.

Bhatt, U., E. Schneider, and D. Dewitt, 2003: Influence of North American land processes on North Atlantic Ocean variability. *Global and Planetary Change*, **37**, 33–56.

Bretherton, C. and D. Battisti, 2000: Interpretation of the results from atmospheric general circulation models forced by the time history of the observed sea surface temperature distribution. *Geophys. Res. Lett*, **27**, 767–770.

Broccoli, A., K. Dahl, and R. Stouffer, 2006: Response of the ITCZ to Northern Hemisphere cooling. *Geophys. Res. Lett.*, **33 (1)**.

Brunet, G. and R. Vautard, 1996: Empirical normal modes versus empirical orthogonal functions for statistical prediction. *J. Atmos. Sci.*, **53**, 3468–3489.

Carton, J. and B. Huang, 1994: Warm events in the tropical Atlantic. *J. Phys. Oceanogr.*, **24**, 888–903.

Cassou, C., C. Deser, L. Terray, J. Hurrell, and M. Drévillon, 2004: Summer sea surface temperature conditions in the North Atlantic and their impact upon the atmospheric circulation in early winter. *J. Climate*, **17**, 3349–3363.

Cayan, D., 1992: Latent and sensible heat flux anomalies over the northern oceans: Driving the sea surface temperature. *J. Phys. Oceanogr.*, **22**, 859–881.

Chan, J. and K. Liu, 2004: Global warming and western North Pacific typhoon activity from an observational perspective. *J. Climate*, **17**, 4590–4602.

Chang, P., L. Ji, and H. Li, 1997: A decadal climate variation in the tropical Atlantic Ocean from thermodynamic air-sea interactions. *Nature*, **385**, 516–518.

Chang, P., L. Ji, H. Li, C. Penland, and L. Matrosova, 1998: Prediction of tropical Atlantic sea surface temperature. *Geophys. Res. Lett.*, **25**, 1193–1196.

Chang, P., R. Saravanan, L. Ji, and G. Hegerl, 2000: The effect of local sea surface temperatures on atmospheric circulation over the tropical Atlantic sector. *J. Climate*, **13**, 2195–2216.

Chervin, R., J. Kutzbach, D. Houghton, and R. Gallimore, 1980: Response of the NCAR general circulation model to prescribed changes in ocean surface temperature. Part II: Midlatitude and subtropical changes. *J. Atmos. Sci.*, **37**, 308–332.

Chiang, J., M. Biasutti, and D. Battisti, 2003: Sensitivity of the Atlantic intertropical convergence zone to last glacial maximum boundary conditions. *Paleoceanography*, **18**.

Chiang, J. and C. Bitz, 2005: Influence of high latitude ice cover on the marine Intertropical Convergence Zone. *Climate Dynamics*, **25**, 477–496.

Chiang, J., W. Cheng, and C. Bitz, 2008: Fast teleconnections to the tropical Atlantic sector from Atlantic thermohaline adjustment. *Geophys. Res. Lett.*, **35**, L07 704.

Chiang, J. and D. Vimont, 2004: Analogous Pacific and Atlantic Meridional Modes of Tropical Atmosphere–Ocean Variability*. *J. Climate*, **17**, 4143–4158.

Collins, W., et al., 2006: The community climate system model version 3 (CCSM3). *J. Climate*, **19**, 2122–2143.

Curtis, S. and S. Hastenrath, 1995: Forcing of anomalous sea surface temperature evolution in the tropical Atlantic during Pacific warm events. *J. Geophys. Res.*, **100**, 15 835–15 847.

Czaja, A., 2004: Why is north tropical Atlantic SST variability stronger in boreal spring? *J. Climate*, **17**, 3017–3025.

Czaja, A. and C. Frankignoul, 1999: Influence of the North Atlantic SST on the atmospheric circulation. *Geophys. Res. Lett.*, **26**, 2969–2972.

Czaja, A. and C. Frankignoul, 2002: Observed impact of Atlantic SST anomalies on the North Atlantic Oscillation. *J. Climate*, **15**, 606–623.

Czaja, A., P. van der Vaart, and J. Marshall, 2002: A diagnostic study of the role of remote forcing in tropical Atlantic variability. *J. Climate*, **15**, 3280–3290.

Dahl, K., A. Broccoli, and R. Stouffer, 2005: Assessing the role of North Atlantic freshwater forcing in millennial scale climate variability: A tropical Atlantic perspective. *Climate Dynamics*, **24**, 325–346.

Davis, R., 1976: Predictability of sea surface temperature and sea level pressure anomalies over the North Pacific Ocean. *J. Phys. Oceanogr.*, **6**, 249–266.

Deser, C. and M. Blackmon, 1993: Surface climate variations over the North Atlantic Ocean during winter: 1900–1989. *J. Climate*, **6**, 1743–1753.

Deser, C., G. Magnusdottir, R. Saravanan, and A. Phillips, 2004: The effects of North Atlantic SST and sea ice anomalies on the winter circulation in CCM3. Part II: Direct and indirect components of the response. *J. Climate*, **17**, 877–889.

Deser, C., R. Tomas, and S. Peng, 2007: The transient atmospheric circulation response to North Atlantic SST and sea ice anomalies. *J. Climate*, **20**, 4751–4767.

Dong, B. and R. Sutton, 2002: Adjustment of the coupled ocean–atmosphere system to a sudden change in the thermohaline circulation. *Geophys. Res. Lett.*, **29**, 1728.

Enfield, D. and D. Mayer, 1997: Tropical Atlantic sea surface temperature variability and its relation to El Niño-Southern Oscillation. *J. Geophys. Res.*, **102**, 929–945.

Enfield, D., A. Mestas-Nuñez, D. Mayer, and L. Cid-Cerrano, 1999: How ubiquitous is the dipole relationship in tropical Atlantic sea surface temperatures? *J. Geophys. Res.*, **104**, 7841–7848.

Ferranti, L., F. Molteni, and T. Palmer, 1994: Impact of localized tropical and extratropical SST anomalies in ensembles of seasonal GCM integrations. *Quart. J. Roy. Met. Soc.*, **120**, 1613–1645.

Ferreira, D. and C. Frankignoul, 2005: The transient atmospheric response to midlatitude SST anomalies. *J. Climate*, **18**, 1049–1067.

Foken, T., 2008: The energy balance closure problem: an overview. *Ecological Applications*, **18**, 1351–1367.

Frankignoul, C., 1985: Sea surface temperature anomalies, planetary waves, and air-sea feedback in the middle latitudes. *Reviews of geophysics*, **23**, 357–390.

Frankignoul, C., A. Czaja, and B. L'Heveder, 1998: Air-sea feedback in the North Atlantic and surface boundary conditions for ocean models. *J. Climate*, **11**, 2310–2324.

Frankignoul, C. and K. Hasselmann, 1977: Stochastic climate models, part II: Application to sea-surface temperature anomalies and thermocline variability. *Tellus*, **29**, 289–305.

Frankignoul, C. and E. Kestenare, 2005: Observed Atlantic SST anomaly impact on the NAO: An update. *J. Climate*, **18**, 4089–4094.

Gill, A., 1980: Some simple solutions for heat-induced tropical circulation. *Quart. J. Roy. Met. Soc.*, **106 (449)**, 447–462.

Goldenberg, S., C. Landsea, A. Mestas-Nuñez, and W. Gray, 2001: The recent increase in Atlantic hurricane activity: Causes and implications. *Science*, **293 (5529)**, 474479.

Gray, W., 1984: Atlantic seasonal hurricane frequency. Part I: El Niño and 30 mb quasi-biennial oscillation influences. *Mon. Wea. Rev*, **112 (9)**, 1649–1668.

Haney, R., 1985: Midlatitude sea surface temperature anomalies: A numerical hindcast. *J. Phys. Oceanogr.*, **15**, 787–799.

Hasselmann, K., 1988: PIPs and POPs: The reduction of complex dynamical systems using principal interaction and oscillation patterns. *J. Geophys. Res.*, **93 (11)**, 11,015–11,021.

Hastenrath, S., 1976: Variations in low-latitude circulation and extreme climatic events in the tropical Americas. *J. Atmos. Sci.*, **33**, 202–215.

Hastenrath, S., 1978: On modes of tropical circulation and climate anomalies. *J. Atmos. Sci.*, **35**, 2222–2231.

Hastenrath, S. and L. Heller, 1977: Dynamics of climatic hazards in northeast Brazil. *Quart. J. Roy. Met. Soc.*, **103 (435)**, 77–92.

Held, I., 1978: The Vertical Scale of an Unstable Baroclinic Wave and Its Importance for Eddy Heat Flux Parameterizations. *J. Atmos. Sci.*, **35**, 572–576.

Holton, J. R., 2004: *An introduction to dynamic meteorology.* 4th ed., Elsevier Academic Press.

Hoskins, B. and D. Karoly, 1981: The steady linear response of a spherical atmosphere to thermal and orographic forcing. *J. Atmos. Sci.*, **38 (6)**, 1179–1196.

Houghton, R. Q. and Y. M. Tourre, 1992: Characteristics of Low-Frequency Sea Surface Temperature Fluctuations in the North Atlantic. *J. Climate*, **5**, 765–771.

Hurrell, J., 1995: Decadal trends in the North Atlantic Oscillation: regional temperatures and precipitation. *Science*, **269 (5224)**, 676–679.

Hurrell, J., et al., 2006: Atlantic climate variability and predictability: A CLIVAR perspective. *J. Climate*, **19 (20)**, 5100–5121.

Kalnay, E. and co authors, 1996: The NCEP/NCAR 40-year reanalysis project. *Bull. Amer. Met. Soc.*, **77**, 437–471.

Kang, S., D. Frierson, and I. Held, 2008: The response of the ITCZ to extratropical thermal forcing in an idealized GCM: The importance of radiative feedbacks and convective parameterization. *J. Atmos. Sci*, **66**, 2812–2827.

Kerr, R., 2000: A North Atlantic climate pacemaker for the centuries. *Science*, **288 (5473)**, 1984–1986.

Klein, S. and D. Hartmann, 1993: The seasonal cycle of low stratiform clouds. *J. Climate*, **6 (8)**, 1587–1606.

Kossin, J. and D. Vimont, 2007: A more general framework for understanding Atlantic hurricane variability and trends. *Bulletin of the American Meteorological Society*, **88 (11)**, 1767–1782.

Kushnir, Y. and I. Held, 1996: Equilibrium atmospheric response to North Atlantic SST anomalies. *J. Climate*, **9 (6)**, 1208–1220.

Kushnir, Y. and N. Lau, 1992: The General-Circulation Model Response to a North Pacific SST Anomaly - Dependence on Time Scale and Pattern Polarity. *J. Climate*, **5**, 271–283.

Kushnir, Y., W. Robinson, I. Bladé, N. Hall, S. Peng, and R. Sutton, 2002: Atmospheric GCM Response to Extratropical SST Anomalies: Synthesis and Evaluation*. *J. Climate*, **15**, 2233–2256.

Kushnir, Y., W. Robinson, P. Chang, and A. Robertson, 2006: The Physical Basis for Predicting Atlantic Sector Seasonal-to-Interannual Climate Variability*. *J. Climate*, **19 (23)**, 5949–5970.

Kwon, Y., M. Alexander, N. Bond, C. Frankignoul, H. Nakamura, B. Qiu, and L. Thompson, 2010: Role of the Gulf Stream and Kuroshio-Oyashio Systems in Large-Scale Atmosphere-Ocean Interaction: A Review. *J. Climate*, **23 (12)**, 3249–3281.

Latif, M. and T. Barnett, 1996: Decadal climate variability over the North Pacific and North America: Dynamics and predictability. *J. Climate*, **9 (10)**, 2407–2423.

Lau, N., 1997: Interactions between global SST anomalies and the midlatitude atmospheric circulation. *Bull. Amer. Met. Soc.*, **78 (1)**, 21–34.

Lau, N. and M. Nath, 1990: A general circulation model study of the atmospheric response to extratropical SST anomalies observed in 1950-79. *J. Climate*, **3**, 965–989.

LAU, N. and M. Nath, 1991: Variability of the baroclinic and barotropic transient eddy forcing associated with monthly changes in the midlatitude storm tracks. *J. Atmos. Sci.*, **48 (24)**, 2589–2613.

Lee, D., Z. Liu, and Y. Liu, 2008: Beyond Thermal Interaction between Ocean and Atmosphere: On the Extratropical Climate Variability due to the Wind-Induced SST*. *J. Climate*, **21 (10)**, 2001–2018.

Li, Z. and S. Conil, 2003: Transient response of an atmospheric GCM to North Atlantic SST anomalies. *J. Climate*, **16**, 3993–3998.

Lindzen, R. and S. Nigam, 1987: On the role of sea surface temperature gradients in forcing low-level winds and convergence in the tropics. *J. Atmos. Sci.*, **44 (17)**, 2418–2436.

Liu, Z., 1996: Modeling equatorial annual cycle with a linear coupled model. *J. Climate*, **9**, 2376–2385.

Liu, Z. and L. Wu, 2004: Atmospheric Response to North Pacific SST: The Role of Ocean-Atmosphere Coupling. *J. Climate*, **17**, 1859–1882.

Liu, Z. and S. Xie, 1994: Equatorward propagation of coupled air-sea disturbances with application to the annual cycle of the eastern tropical Pacific. *J. Atmos. Sci.*, **51 (24)**, 3807–3822.

Liu, Z., Q. Zhang, and L. Wu, 2004: Remote Impact on Tropical Atlantic Climate Variability: Statistical Assessment and Dynamic Assessment*. *J. Climate*, **17 (7)**, 1529–1549.

Mahajan, S., 2008: Free and Forced Tropical Variability: Role of the Wind-Evaporation-Sea Surface Temperature (WES) Feedback. Ph.D. thesis, Texas A M University.

Mahajan, S., R. Saravanan, and P. Chang, 2009: The role of the wind-evaporation-sea surface temperature (WES) feedback in air-sea coupled tropical variability. *Atmospheric Research*, **94 (1)**, 19–36.

Mahajan, S., R. Saravanan, and P. Chang, 2011: The Role of the Wind–Evaporation–Sea Surface Temperature (WES) Feedback as a Thermodynamic Pathway for the Equatorward Propagation of High-Latitude Sea Ice–Induced Cold Anomalies. *Journal of Climate*, **24**, 1350–1361.

Manabe, S. and R. Stouffer, 1996: Low-frequency variability of surface air temperature in a 1000-year integration of a coupled atmosphere-ocean-land surface model. *J. Climate*, **9 (2)**, 376–393.

Marshall, J., et al., 2001: North Atlantic climate variability: phenomena, impacts and mechanisms. *International Journal of Climatology*, **21 (15)**, 1863–1898.

Mehta, V., M. Suarez, J. Manganello, and T. Delworth, 2000: Oceanic influence on the North Atlantic Oscillation and associated Northern Hemisphere climate variations: 1959–1993. *Geophysical Research Letters*, **27 (1)**, 121–124.

Minobe, S., A. Kuwano-Yoshida, N. Komori, S. Xie, and R. Small, 2008: Influence of the Gulf Stream on the troposphere. *Nature*, **452 (7184)**, 206–209.

Minobe, S., M. Miyashita, A. Kuwano-Yoshida, H. Tokinaga, and S. Xie, 2010: Atmospheric Response to the Gulf Stream: Seasonal Variations*. *Journal of Climate*, **23 (13)**, 3699–3719.

Mitchell, T. and J. Wallace, 1992: The Annual Cycle in Equatorial Convection and Sea Surface Temperature. *J. Climate*, **5**, 1140–1156.

Monterey, G. and S. Levitus, 1997: Climatological cycle of mixed layer depth in the world ocean. Tech. rep., NOAA.

Moura, A. D. and J. Shukla, 1981: On the dynamics of droughts in northeast Brazil: Observations, theory and numerical experiments with a general circulation model. *J. Atmos. Sci.*, **38**, 2653–1675.

Muller, W. A., C. Frankignoul, and N. Chouaib, 2008: Observed decadal tropical Pacific-North Atlantic teleconnections. *Geophys. Res. Lett.*, **35**, GL035 901.

Namias, J., 1972: Influence of northern hemisphere general circulation on drought in northeast Brazil1. *Tellus*, **24**, 336–343.

Newman, M., P. Sardeshmukh, C. R. Winkler, and J. S. Whitaker, 2003: A Study of Subseasonal Predictability. *Mon. Wea. Rev.*, **131**, 1715–1732.

North, G., T. Bell, R. Cahalan, and F. Moeng, 1982: Sampling errors in the estimation of empirical orthogonal functions. *Mon. Wea. Rev.*, **110**, 699–706.

Okumura, Y. and S. Xie, 2006: Some overlooked features of Tropical Atlantic climate leading to new Nino-like Phenomenon. *J. Climate*, **19**, 5859–5874.

Okumura, Y., S. Xie, A. Numaguti, and Y. Tanimoto, 2001: Tropical Atlantic air-sea interaction and its influence on the NAO. *Geophys. Res. Lett.*, **28**, 1507–1510.

Palmer, T. and Z. Sun, 1985: A modeling and observational study of the relationship between sea surface temperature in the northwest Atlantic and the atmospheric general circulation. *Quart. J. Roy. Met. Soc.*, **111**, 947–975.

Peng, S., L. Mysak, H. Ritchie, J. Derome, and B. Dugas, 1995: The Differences between Early and Midwinter Atmospheric Responses to Sea Surface Temperature Anomalies in the Northwest Atlantic. *J. Climate*, **8**, 137–157.

Peng, S. and W. Robinson, 2001: Relationships between Atmospheric Internal Variability and the Responses to an Extratropical SST Anomaly. *J. Climate*, **14**, 2943–2959.

Peng, S., W. Robinson, and M. Hoerling, 1997: The Modeled Atomspheric Response to Midlatitude SST Anomalies and Its Dependence on Background Circulation States. *J. Climate*, **10**, 971–987.

Peng, S., W. Robinson, and S. Li, 2002: North Atlantic SST Forcing of the NAO and Relationships with Intrinsic Hemispheric Variability. *Geophys. Res. Lett.*, **29**, GL014 043.

Penland, C., 1989: Random forcing and forecasting using principal oscillation pattern analysis. *Monthly Weather Review*, **117 (10)**, 2165–2185.

Penland, C. and L. Matrosova, 1998: Prediction of tropical Atlantic sea surface temperatures using linear inverse modeling. *J. Climate*, **11**, 483–496.

Penland, C. and P. Sardeshmukh, 1995a: Error and sensitivity analysis of geophysical eigensystems. *Journal of climate*, **8 (8)**, 1988–1998.

Penland, C. and P. Sardeshmukh, 1995b: The optimal growth of tropical sea surface temperature anomalies. *Journal of climate*, **8 (8)**, 1999–2024.

Peterson, L., G. Haug, K. Hughen, and U. R
"ohl, 2000: Rapid changes in the hydrologic cycle of the tropical Atlantic during the last glacial. *Science*, **290**, 1947–1951.

Pitcher, E., M. Blackmon, G. Bates, and S. Munoz, 1988: The effect of North Pacific sea surface temperature anomalies on the January climate of a general circulation model. *J. Atmos. Sci.*, **45**, 173–188.

Power, S., R. Kleeman, R. Colman, and B. McAvaney, 1995: Modeling the surface heat flux response to long-lived SST anomalies in the North Atlantic. *J. Climate*, **8**, 2161–2180.

Rajagopalan, B., Y. Kushnir, and Y. Tourre, 1998: Observed decadal midlatitude and tropical Atlantic climate variability. *Geophys. Res. Lett.*, **25**, 3967–3970.

Rayner, N., D. Parker, E. Horton, C. Folland, L. Alexander, D. Rowell, E. Kent, and A. Kaplan, 2003: Global analyses of sea surface temperature, sea ice, and night marine air temperature since the late nineteenth century. *J. Geophys. Res.*, **108**, D002 670.

Repelli, C. and P. Nobre, 2004: Statistical prediction of sea-surface temperature over the tropical Atlantic. *Int. J. Climatology*, **24**, 45–55.

Rienecker, M. and co authors, 2011: MERRA - NASA's Modern-Era Retrospective Analysis for Research and Applications. *J. Climate*, **24**, 3624–3648.

Riviere, G. and I. Orlanski, 2007: Characteristics of the Atlantic storm-track eddy activity and its relation with the North Atlantic Oscillation. *J. Atmos. Sci.*, **64**, 241–266.

Rodwell, M., D. Rowell, and C. Folland, 1999: Oceanic forcing of the wintertime North Atlantic Oscillation and European climate. *Nature*, **398**, 320–323.

Ruiz-Barradas, A., J. Carton, and S. Nigam, 2000: Structure of interannual-to-decadal climate variability in the tropical Atlantic sector. *J. Climate*, **13**, 3285–3297.

Saha, S. and co authors, 2010: The NCEP climate forecast system reanalysis. *Bull. Amer. Met. Soc.*, **91**, 1015–1057.

Saravanan, R., 1998: Atmospheric low-frequency variability and its relationship to midlatitude SST variability: Studies using the NCAR Climate System Model. *J. Climate*, **11 (6)**, 1386–1404.

Saravanan, R. and P. Chang, 1999: Oceanic mixed layer feedback and tropical Atlantic variability. *Geophys. Res. Lett.*, **26**, 3629–3632.

Sardeshmukh, P. and P. Sura, 2009: Reconciling non-Gaussian climate statistics with linear dynamics. *J. Climate*, **22 (5)**, 1193–1207.

Servain, J., 1991: Simple Indices for the Tropical Atlantic Ocean and Some Applications. *Geophys. Res. Lett.*, **96**, 15 137–15 146.

Servain, J., A. Busalacchi, M. McPhaden, A. Moura, G. Reverdin, M. Vianna, and S. Zebiak, 1998: A pilot research moored array in the tropical Atlantic (PIRATA). *Bull. Amer. Met. Soc.*, **79**, 2019–2032.

Servain, J., I. Wainer, J. McCreary Jr, and A. Dessier, 1999: Relationship between the equatorial and meridional modes of climatic variability in the tropical Atlantic. *Geophys. Res. Lett.*, **26**, 485–488.

Smagorinsky, J., 1953: The dynamical influence of large-scale heat sources and sinks on the quasi-stationary mean motions of the atmosphere. *Quart. J. Roy. Met. Soc.*, **79**, 342–266.

Smirnov, D. and D. Vimont, 2011: Variability of the Atlantic Meridional Mode during the Atlantic Hurricane season. *J. Climate*, **24**, 1409–1424.

Sura, P., M. Newman, and M. Alexander, 2006: Daily to Decadal Sea Surface Temperature Variability Driven by State-Dependent Stochastic Heat Fluxes. *J. Phys. Oceanogr.*, **36**, 1940–1958.

Sutton, R. and M. Allen, 1997: Decadal predictability of North Atlantic sea surface temperature and climate. *Nature*, **388**, 563–567.

Tanimoto, Y. and S. Xie, 1999: Ocean-Atmosphere Variability over the Pan-Atlantic Basin. *J. Meteor. Soc. Japan*, **77**, 31–46.

Trenberth, K., G. Branstator, D. Karoly, A. Kumar, N. Lau, and C. Ropelewski, 1998: Progress during TOGA in understanding and modeling global teleconnections associated with tropical sea surface temperatures. *J. Geophys. Res.*, **103**, 14 291–14 324.

Vimont, D., 2010: Transient growth of thermodynamically coupled disturbances in the tropics under an equatorially symmetric mean state. *J. Climate*, **23**, 5771–5789.

Vimont, D., 2011: Regional and Seasonal Diagnosis of Tropical Atlantic Climate Predictability. *J. Climate*, accepted.

Vimont, D., D. Battisti, and A. Hirst, 2001: Footprinting: a seasonal link between the mid-latitudes and tropics. *Geophys. Res. Lett.*, **28**, 3923–3926.

von Storch, H., T. Bruns, I. Fischer-Bruns, and K. Hasselmann, 1988: Principal Oscillation Pattern Analysis of the 30- to 60-Day Oscillation in General Circulation Model Equatorial Troposphere. *J. Geophys. Res.*, **93**, 11 022–11 036.

Wang, C., S. Lee, and D. Enfield, 2007: Impact of the Atlantic Warm Pool on the Summer Climate of the Western Hemisphere. *J. Climate*, **20**, 5021–5040.

Wang, C., S. Lee, and D. Enfield, 2008: Atlantic Warm Pool acting as a link between Atlantic Multidecadal Oscillation and Atlantic tropical cyclone activity. *Geochem. Geophys. Geosyst.*, **9**, Q05V03.

Wang, W., B. Anderson, R. Kaufmann, and R. Myneni, 2004: The Relation between the North Atlantic Oscillation and SSTs in the North Atlantic Basin. *J. Climate*, **17**, 4752–4759.

Webster, P., 1981: Mechanisms Determining the Atmospheric Response to SST Anomalies. *J. Atmos. Sci.*, **38**, 554–571.

Wu, L. and Z. Liu, 2002: Is the Tropical Atlantic Variability driven by the North Atlantic Oscillation? *Geophys. Res. Lett.*, **29**, L014939.

Wu, P. and C. Gordon, 2002: Oceanic Influence on North Atlantic Climate Variability. *J. Climate*, **15**, 1911–1925.

Wu, Z., E. Schneider, and B. Kirtman, 2004: Causes of low frequency North Atlantic SST variability in a coupled GCM. *Geophys. Res. Lett.*, **31**, L019548.

Xie, P. and P. Arkin, 1997: Global precipitation: A 17-year monthly analysis based on gauge observations, satellite estimates and numerical model outputs. *Bull. Amer. Met. Soc.*, **78**, 2539–2558.

Xie, S., 1999: A Dynamic Ocean-atmosphere Model of the Tropical Atlantic Decadal Variability. *J. Climate*, **12**, 64–70.

Xie, S. and J. Carton, 2004: Tropical Atlantic Variability: Patterns, Mechanisms, and Impacts, Earth's Climate: The Ocean-Atmosphere Interaction. **Geophysical Monograph Series 147**, 121–142.

Xie, S. and S. Philander, 1994: A coupled ocean-atmosphere model of relevance to the ITCZ in the eastern Pacific. *Tellus*, **46A**, 340–350.

Zebiak, S., 1993: Air-Sea Interaction in the Equatorial Atlantic Region. *J. Climate*, **6**, 1567–1586.

Zebiak, S. and M. Cane, 1987: A Model El Nino-Southern Oscillation. *Mon. Wea. Rev.*, **115**, 2262–2278.

Zhang, R. and T. Delworth, 2005: Simulated Tropical Response to a Substantial Weakening of the Atlantic Thermohaline Circulation. *J. Climate*, **18**, 1853–1860.